The Use of Spontaneous Vestibular Response for Diagnosis of Meniere's Disease

by

Zeinab Alsadat Dastgheib

A thesis submitted to the Faculty of Graduate Studies of

The University of Manitoba

in partial fulfillment of the requirements for the degree of

Doctor of Philosophy

Biomedical Engineering

University of Manitoba

Winnipeg, Manitoba, Canada

Abstract

Meniere's disease is a common inner ear disorder that affects balance and hearing. Electrovestibulography (EVestG) is a relatively new vestibular driven test that measures spontaneous and driven field potential activity recorded in the external ear canal in response to various vestibular stimuli. The main objectives of this thesis were to record and analyze EVestG signals in order to 1) testify whether the EVestG technology is capable of classifying individuals with Meniere's from healthy ones, and if it is, then 2) identify the EVestG tilt stimulus providing the most informative response in relation to identifying Meniere's symptoms; thus, optimizing the EVestG experimental protocol as a Meniere's disease diagnostic aid.

EVestG signals of two groups of Meniere's and control individuals during seven different EVestG tilt stimuli were recorded and analyzed by linear and nonlinear signal processing techniques. Data of 14 with Meniere's disease and 16 healthy individuals were used as the training set, while additional data of 21 individuals with vertiginous disorders (and suspected of Meniere's disease) and 10 controls were used as the test set. An ad-hoc voting classifier built upon single-feature linear classifiers was designed, and used for classification of the two groups of both training and test datasets.

The results showed an overall accuracy of 87% and 84% for training and test datasets, respectively. Among the seven different tilts that each evokes a specific part of the inner ear organ, the side tilt which stimulates most of the labyrinth and particularly the utricle, was found to generate the best characteristic features for identifying Meniere's disease

from controls. Thus, one may simplify the EVestG protocol to only the side tilt stimulus for a quick screening of Meniere's disease.

The proposed method encourages the use of EVestG technology as a non-invasive and potentially reliable diagnostic/screening tool to aid clinical diagnosis of Meniere's diseases.

Acknowledgments

I would like to thank my advisors, Prof. Z. Moussavi and Prof. B. Lithgow, for their guidance and support during my Ph.D. study, for their patience and immense knowledge, and for the friendly behaviour they established with their students. Working with them and learning from them during my study was definitely a great opportunity to develop and improve my academic skills. Also, I thank my committee members, Prof. B. Blakley and Prof. W. Kinsner, for their time, support, and beneficial advices.

In addition, I would like to extend my deepest gratitude to my husband, Masoud. His sacrifices, patience, and motivational talks have made it possible for me to pursue this degree. I also want to thank my parents and my parents in law for their consistent prayers toward me and my lovely daughters, Houra and Zahra, who let me devote extra time and energy to my studies with their patience.

Zeinab Alsadat Dastgheib

August 2016

Table of Contents

List of Tables

List of Figures

List of Abbreviations

AAO-HNS	American Academy of Otolaryngology-Head and Neck Surgery
AC	Alternating current
ANOVA	Analysis of variance
AP	Action potential
BEAR	Brainstem-evoked acoustic response
BPPV	Benign paroxysmal positional vertigo
CD	Correlation dimension
CM	Cochlear microphonic
CNS	Central nervous system
CT	Contralateral tilt
DC	Direct current
ID	Information dimension
ECOG	Electrocochleography
ENG	Electronystagmography
EVestG	Electrovestibulography
FD	Fractal dimension
FP	Field potential
HFD	Higuchi fractal dimension
IAC	Internal acoustic canal
IAM	Internal acoustic meatus
IT	Ipsilateral tilt

LDA	Linear discriminant analysis
MADRS	Montgomery Asberg Depression Rating Scale
MoCA	Montreal Cognitive Assessment
MRI	Magnetic resonance imaging
mRMR	Minimal-redundancy-maximal-relevance
NEER	Neural Event Extraction Routine
PDF	Probability distribution function
RHC	Riverview Health Center
RTC	Return of chair to the center
SCC	Semicircular canal
SNR	Signal to noise ratio
SP	Summating potential
VCR	Vestibulo-cervical reflex
VN	Vestibular nuclei
VOR	Vestibulo-ocular reflex
VSR	Vestibulo-spinal reflex
VADL	Vestibular Disorders Activities of Daily Living Scale

CHAPTER 1 Introduction

1.1 Motivations and Objectives

Meniere's disease is an inner ear disorder that can cause severe episodes of vertigo, ringing in the ear (tinnitus), a feeling of fullness or pressure in the ear, and fluctuating hearing loss [1]. The prevalence of Meniere's disease varies around the world (about 0.2% in US [2]) but it increases with age in a linear fashion up to the age of 60 [3]. Meniere's disease is a persistent and recurrent problem for patients, and affects their quality of life especially during periods of acute symptomatology [4, 5]. Vertigo mainly influences the balance and physical movements, while tinnitus and hearing loss impact more the psychosocial aspects of patients' lives [6].

Despite the magnitude of the efforts in the field, diagnosis of Meniere's disease as well as its etiology has remained a challenge. Meniere's diagnosis is usually based on a combination of a set of clinical symptoms and test results. However, differential diagnosis may be extremely difficult as the tests are mostly subjective and not highly specific [7]. Thus, misdiagnosis is a common problem as some of the symptoms of the disease overlap with other vestibular diseases, such as Benign paroxysmal positional vertigo (BPPV), Vestibular Neuritis, and Labyrinthitis [8, 9].

The process of diagnosis usually includes a hearing test (audiometry), Electronystagmography (ENG) and several blood tests. Magnetic resonance imaging (MRI) scans of the head and/or Electrocochleography (ECOG) assessments are also often helpful [1]. Given the frequent reoccurring nature of the disease, efforts to avoid misdiagnosis and deficiencies of the treatments highlight the great need for an objective assessment leading to a reliable diagnosis. A novel technology called Electrovestibulography (EVestG) [10, 11], has the potential to be considered as an objective and reliable diagnostic tool for diagnosis of Meniere's disease from healthy subjects. This thesis investigates the application of EVestG signal analysis as a diagnostic aid for separating Meniere's from other forms of dizziness as well as healthy controls.

Electrovestibulography is a newly developed vestibular recording technique, which is able to detect specific background and driven vestibular field potentials (FPs) in response to passive tilt stimuli. It is believed that this technique can provide a quantitative and direct measure of activities of the vestibular system and associated neural pathways in the central nervous system (CNS) [3]. EVestG is fundamentally similar to ECOG but the acoustic stimuli are replaced by a series of vestibular stimuli (orthogonal tilts).

Currently, the EVestG experiment has a relatively lengthy experimental protocol: data is recorded during seven different tilt stimuli. However, all the seven stimuli may not be needed to be recorded or analyzed as some of them may carry redundant information for detection of a specific disease. Therefore, it might be possible to identify the optimum tilt(s) best selective of the classification of Meniere's from healthy subjects.

In this thesis we examine whether application of advanced signal processing techniques on EVestG signals obtained from Meniere's and healthy subjects leads to a reliable and

accurate diagnostic aid for separating Meniere's from other forms of dizziness as well as healthy controls. In addition, we investigate whether the EVestG experimental protocol can be optimized by identifying the most important stimulus among the seven current EVestG stimuli for Meniere's diagnosis.

Thus, the specific objectives are:

1. To record and analyze EVestG signals of different stimuli, extract the most significant bio- features of the recorded signals specific to Meniere's symptoms, and design a robust diagnostic classification algorithm. A classification algorithm, which its training and unbiased testing accuracies are close to each other and above 80%, is considered as a robust algorithm.

2. To evaluate classification accuracies of each tilt's data and investigate whether any tilt's data could be removed without hampering the final diagnostic classification; thus, optimizing the EVestG recording protocol.

1.2 Contribution of the Thesis

This is the very first study on the novel EVestG technology investigating whether EVestG signals analysis would lead to a reliable, robust and accurate diagnostic aid for separating Meniere's and healthy individuals; data used in this thesis were collected from two collaborating laboratories in Australia and Canada, with the similar equipment and the same protocol. The contributions of this thesis are listed in detailed as below:

1- Discovering EVestG signals biomarkers sensitive to Meniere's disease.

2- Designing a robust classification method for classification of Meniere's subjects from healthy controls.

3- Identification of the most informative EVestG stimulus in Meniere's/control classification.

4- Verification of superiority of suggested classification method versus a few structurally similar classifiers (specifically in dealing with missing data).

1.3 Organization of the Thesis

Chapter 2 provides background information on Meniere's disease, its symptoms, and some common vestibular testing methods, as well as introducing EVestG technology and the classification scheme of this thesis. Chapter 3 presents the methodology including the measurement setup, recording protocol, and study subjects preparation as well as details of signal analysis and classification methods. Chapter 4 displays the classification results and discussion of the results. Chapter 5 presents the conclusion of this study and suggests recommendations for future works.

CHAPTER 2 Background

2.1 Overview

In this chapter we present introductory information about Meniere's disease, anatomy of the vestibular system, and different common vestibular testing methods in relation to Meniere's disease. We also introduce EVestG, the technology used in this study, followed by a review of the biological data classification methods.

2.2 Meniere's Disease

In 1861 the French physician, Dr. Prosper Meniere's, theorized that attacks of vertigo, ringing in the ear (tinnitus) and hearing loss originate from the inner ear rather than the brain (which was generally believed to be the origin of the symptoms at the time). His hypothesis was confirmed [12]; thus the name of Dr. Prosper Meniere's began its long association with this inner ear disease and inner ear balance disorders in general.

A Meniere's episode is usually preceded by hearing fluctuations or tinnitus, and involves severe vertigo (spinning), imbalance, nausea and vomiting, which may last two to

four hours [13]. Meniere's episodes may occur in clusters; that means several attacks may happen within a short period of time, while years may pass between the acute attacks. This disease usually starts in one ear but often extends to both ears over time. In most cases, a progressive hearing loss occurs in the affected ear(s). The effect of the hearing loss first appears in the low frequencies but over time it can progress to either a peaked pattern with the peak in the frequency range of 250 Hz-8 kHz or to a flat loss over the entire frequency band [14].

The area affected by Meniere's disease is the entire labyrinth, which includes the semicircular canals (SCC), otolith organs, and the cochlea. It appears that the main problem in Meniere's disease is an increase of the volume and pressure of endolymph that can cause a dilation of the endolymph system (Figure 2-1) [15]; this is called "hydrops". This may happen when the drainage system, called the endolymphatic duct or sac, is blocked or too much endolymph fluid is secreted into the inner ear. The "hydrops" may be a marker for the Meniere's disease, rather than necessarily being responsible for the symptoms [8].

More recent researches on the origin of Meniere's disease show that hydrops is not found in all individuals with Meniere's disease; hydrops is also commonly (6%) found on autopsy studies of individuals with no Meniere's symptoms [16]. Because Meniere's disease occurs in roughly 0.2% of population, and hydrops is found in 6% of temporal bones, there is more than an order of magnitude of larger population with hydrops than those with Meniere's disease. Thus, logically, there must be something more than simply hydrops involved in Meniere's disease. Viral infection, autoimmune disease, head injury, hereditary predisposition, and allergy are considered as the precipitating factors of Meniere's disease [17].

To have a better insight of the Meniere's disease's cause and effect the anatomy of the inner ear is briefly reviewed in the next section.

2.3 Anatomy of the Vestibular System

The human vestibular system is built upon three main components: a peripheral sensory apparatus, a central processor, and the (vestibular) motor outputs (Figure 2-2). There are a set of motion sensors within the peripheral apparatus, which send the vestibular information to the central nervous system (CNS), specifically to the vestibular nuclei and the cerebellum. The CNS receives these signals along with other sensory information (such as visual and proprioceptive sensory inputs) and estimates head and body orientation.

The output of the CNS is sent to the ocular muscles and spinal cord to provide three important reflexes: the vestibulo-ocular reflex (VOR), the vestibulo-cervical reflex (VCR) and the vestibulo-spinal reflex (VSR). The VOR generates and controls eye movements in order to enable clear vision, while the head is in motion. The VCR works on the neck musculature to stabilize the head. The VSR generates compensatory body movement that preserves head and postural stability, and therefore prevents falling. The performance of the vestibular reflexes is monitored by the CNS, readjusted or controlled as necessary by the cerebellum, and completed by slower higher cortical processes.

The following sub-sections describe the anatomy and the physiology of the vestibular system in the periphery and CNS as well as the clinical presentation of common peripheral vestibular disorders.

2.3.1 **The Peripheral Sensory Apparatus**

The following overview of the peripheral vestibular system is extracted from reviews [1, 9, 18]. The peripheral vestibular system consists of: 1) the bony labyrinth, 2) the membranous labyrinth, and 3) the motion sensors of the vestibular system (hair cells) that are the end-organs of the SCCs and the otolith organs. The peripheral vestibular system (Figure 2-3) lies within the inner ear. It is extended laterally by the air-filled middle ear and medially by the temporal bone. It is located posterior to the cochlea [8]. The external ear (the pinna and ear canal) and middle ear (the tympanic cavity which includes the three ear bones or ossicles: the malleus, incus, and stapes, the Eustachian tube, and the mastoid air cell system) are auditory organs, which do not directly affect the vestibular function; t, disease or infection related to these parts, particularly the middle ear can affect the inner ear. The tympanic membrane or ear drum separates the external and middle ear. It has a diameter of 8.5 to 10 mm and a thickness of 0.1 mm [8].

The bony labyrinth consists of the bones of three SCCs, the cochlea, and otolith organs, which consist of the utricle and saccule (Figure 2-4). Note that one end of each SCC is widened in diameter to form an ampulla. The bony labyrinth is filled with perilymphatic fluid, in which the membranous labyrinth is suspended (by perilymphatic fluid and supportive connective tissue). The membranous labyrinth is filled with endolymphatic fluid. Under normal circumstances, there is no direct communication between the endolymph and perilymph compartments.

Specialized hair cells contained in each ampulla of SCCs and in otolith organs are the biological sensors that convert the mechanical shearing forces generated by head motion into neural discharges or neural firings. Each hair cell is innervated by an afferent neuron

located in the vestibular ganglion (Figure 2-3), which is located close to the ampulla. When the hair cells (stereocilia) are bent toward or away from the longest one (kinocilium), firing rate increases or decreases in the vestibular nerve respectively (see Figure 2-5). The neural discharges will then be directed to specific areas of the brainstem and the cerebellum. Because of the orientation of the SCCs and otolith organs and due to the differences in their fluid mechanics, they are able to respond selectively to head motions in particular directions such that the SCCs respond to angular velocity, and the otolith organs to linear acceleration.

The SCCs and their hair cells: In each ear there are three SCCs oriented approximately at right angles to each other as shown in Figure 2-3. One canal (the lateral) is located in a plane that forms a 30 degree angle with the horizontal plane. The other two canals (the posterior and anterior) are almost orthogonal with each other and with respect to the lateral canal plane.

The hair cells in the ampullae rest on a tuft of blood vessels, nerve fibers, and supporting cellular tissue called cristae ampullaris. Within each crista, all hair cells are oriented in the same direction and a flexible and gelatinous membrane, called the cupula, covers them. When an angular head motion occurs, the inertial lag of the endolymph fluid causes the cupula to bend back or forth, which stimulates the hair cells (Figure 2-5) [19]. Neural firing in the vestibular nerve is proportional to the head velocity over the range of frequencies, in which the head commonly moves (0.5–7 Hz) [8].

The semicircular canals are only able to detect the start and end of rotation but not the velocity during a prolonged rotation. They respond well in the first seconds of the initiation and termination of the rotation as they act like accelerometers. As the head rotates the duct

moves, but the endolymph resists and lags behind. This deflects the cupula, and bends the cilia within. Over time, the endolymph catches up to the movement of the duct, and the cupula is no longer affected [20]. However, when the rotation stops, the endolymph continues to move while the duct has stopped; hence, it stimulates the hair cells in the opposite direction.

Each SCC co-works very closely as a pair with a SCC located on the same plane but in the other side of the head (see Figure 2-6). The individual SCCs make the following three coplanar pairs: (1) right and left lateral, (2) left anterior and right posterior, and (3) left posterior and right anterior. The hair cells within two SCCs of the same plane aligned oppositely. Thus, when an angular head motion occurs, the endolymph of the coplanar pair is displaced in opposite directions; consequently, neural firing increases in one vestibular nerve, and decreases on the other side.

There are advantages due to the arrangement of coplanar pairing. First, it provides sensory redundant information, which is useful when a disease (such as vestibular neuritis, or benign paroxysmal positional vertigo) or ear surgery affects the SCC on one side. In that case, CNS will still receive vestibular information about head velocity within that plane from the contralateral SCC of the coplanar pair. Second, pairing allows the brain to ignore changes in neural firing that occurs without head motion and on both sides simultaneously (such as changes in body temperature or chemistry).

The otolith organs and their hair cells: The otolith organs include structures that are similar to the cupulae. The otolith organs consist of utricle and saccule, which are located between the cochlea and the semicircular canals. Inside the utricle and saccule, there is a

layer of hair cells called macula. The macula of the utricle lies mainly in the horizontal plane, whereas the macula of the saccule is located mainly in the vertical plane.

The hair cells of the macula are covered by a gelatinous layer, in which are embedded otoconia. The otoconia are calcium carbonate crystals, which have more mass than cupulae (Figure 2-7). The sensitivity to gravity and linear acceleration is obtained due to the mass of the otoconia inside the otolith organs. Therefore, when the head tilts or linearly accelerates, gravity causes the gelatinous layer to shift relatively to the hair cells, and bend them. In contrast with the macula, the cupulae (inside the SCC) normally have the same density as the surrounding endolymphatic fluid, and are insensitive to gravity [1].

The otolith organs distinguish forces related to linear acceleration such as linear motions and static head tilts with respect to gravity. Their function is different from the SCCs in two main ways: 1) they respond to linear motion instead of angular motion, and 2) they respond to acceleration rather than to velocity [21]. Overall, the otolith organs have a simpler function than the SCCs. Unlike the SCCs that must convert head velocity into displacement to properly activate the hair cells of the cristae, the otolith organs need no special hydrodynamic system.

Although the otolith organs have only two sensors for three axes of linear motion, they are capable of responding to motions in all three dimensions (Figure 2-7). In the upright position, the saccule and utricle are oriented vertically and horizontally, respectively. Therefore, the saccule can sense linear acceleration in the vertical plane, which includes acceleration in up-down and in sideways directions. The utricle senses acceleration in horizontal plane that includes acceleration in forward-backward directions [22].

Note that the saccular and utricular maculae on one side of the head are mirror images of those on the other side. Thus, a tilt of the head to one side has opposite effects on the corresponding utricle or saccule hair cells of the other side [23]. In other word, there is a redundancy in the otolith organs, like the SCCs, with similar sensors on both sides of the head.

There is also a redundancy related to the geometry of each of the otolithic membranes. Within each macula there is a curving zone, called the striola, which separates the direction of hair-cell polarization on each side. Consequently, head tilt increases afferent discharge from one part of a macula, while reducing the afferent discharge from another portion of the same macula. This extra level of redundancy in comparison with the function of SCCs makes the otolith organs probably less vulnerable to unilateral vestibular lesions.

The Vestibular nerve: The auditory and vestibular end organs both share the vestibulo-cochlear nerve (cranial nerve VIII) pathway to the brainstem, cerebellum and higher integrative centers in the brain. The hair cells of the vestibular apparatus stimulate the dendrites of the sensory bipolar neurons, the cell bodies of which reside within the vestibular ganglion. Vestibular nerve fibers are the afferent projections from the neurons of the vestibular ganglion. The vestibular ganglion is located in the Internal Acoustic Meatus (IAM), which is part of the Internal Acoustic canal (IAC). The vestibular nerve transmits afferent signals through the IAC. In addition to the vestibular nerve, the IAC contains the cochlear nerve, the facial nerve (the VII cranial nerve), and the labyrinthine artery. The vestibular nerve travels through the IAC in the petrous portion of the temporal bone, and reaches the vestibular nuclei that are located approximately at the junction of the medulla and the pons, and also reaches directly to the cerebellum [23].

In all studied species, the vestibular fibers exhibit a high and steady spontaneous firing rate at rest, when no stimulus is applied. As a result, they can transmit information by either increasing or decreasing their firing rate [24].

2.3.2 **Central Vestibular System**

Afferents from the vestibular hair cells have two main targets as vestibular input: the vestibular nuclear complex and the cerebellum (Figure 2-2). The afferents that first reach the cerebellum, called primary afferent fibers, are axons of cell bodies located in the vestibular ganglion. The secondary afferents reach the cerebellum after passing through the vestibular nuclear complex (vestibular nuclei) [25]. The vestibular nuclei (VN) are the primary processor of vestibular input, and implements direct and fast connections between incoming afferent information and motor output neurons. The cerebellum works as the adaptive processor; it monitors vestibular performance, and readjusts central vestibular processing if necessary [8]. At both locations, vestibular somatosensory and visual sensory inputs are also processed along with the vestibular input.

The vestibular nuclei (VN): The VN, located within the pons and also extended into the medulla, perform much of the processing that is needed to analyze head position and motion in order to maintain balance and posture. The VN consist of four "major" nuclei (superior, medial, lateral, and descending) and at least seven "minor" nuclei [17] . The primary afferent neurons are distributed to different parts of the ipsilateral VN. The VN between the two sides of the brainstem are connected together via a system of commissures that are mutually inhibitory.

The information to be shared between the two sides of the brainstem, such as the function of pairing plane of the SCCs or the sub-sections of the otolith organs, is transferred

by system of commissures [26]. Other than the hair cells response, the VN receive inputs from cerebellum, spinal cord, and contralateral VN.

In the VN, vestibular sensory input is processed simultaneously with other sensory information such as proprioceptive, visual, tactile, and auditory. There are extensive connections between the VN, cerebellum, ocular motor nuclei and brainstem reticular activating systems in order to provide appropriate (efferent) signals for the extra ocular and skeletal muscles that are the effector organs of VOR and VSR.

The VN (or secondary vestibular neurons) outputs have projections to the motor nuclei of extraocular muscles as well as to cerebellum, vestibular organ (efferent vestibular system), contralateral VN neurons, spinal cord, reticular formation, and the thalamocortical pathways [6].

The superior vestibular nucleus (SVN) receives inputs from vestibular primary afferent of the SCCs while other inputs include otolith organs fibers that only project to the periphery of the nucleus, afferents from the cerebellum, and inputs from contralateral medial and descending VN. Due to SCCs connections, the superior vestibular nucleus is the major relay for VORs.

The lateral vestibular nucleus (LVN) receives inputs mainly from vestibular primary afferents and fibers form the nuclei of the cerebellum. There are fewer inputs from spinal and commissural sources. The lateral nucleus sends efferent fibers to spinal cord that makes it the principal nucleus for the VSRs.

The medial vestibular nucleus (MVN) is the largest of the VN in humans and receives afferents form SCC, OTO and cerebellum. There are also large projections from contralateral medial vestibular nucleus and a small projection from reticular formation. The

medial vestibular nucleus acts as a relay for VOR, while it is also involved in VSRs and coordinates head and eye movements that occur together. Most of the commissural connections from contralateral medial VN are probably involved in compensatory vestibular mechanisms (e.g., after peripheral vestibular lesions).

The descending or inferior vestibular nucleus (DVN) is connected to all of the other nuclei and the cerebellum but has no exclusive outflow for a special reflex. A huge number of commissural fibers originate from the descending nucleus and innervate the contralateral VN. The descending vestibular nucleus acts as an integrative center for the vestibular signals from the two sides, the cerebellum, and the reticular formation.

The Cerebellum: The cerebellum is a major recipient of the VN signals, and is also a major source of input to the VN. The cerebellum function is not required for vestibular reflexes, but if it is removed, vestibular reflexes become uncalibrated and ineffective. The parts of the cerebellum responsible for handling the dynamic equilibrium signals from the SCCs are the flocculonodular lobes. The uvular lobe of the cerebellum plays a similar role in static equilibrium (for outputs of otolith organs). In fact, the cerebellar projections to the VN have an inhibitory influence on the VN.

The vestibular efferents coming from the VN and/or cerebellum, are joined by cochlear efferents, and enter the vestibular nerve. At the vestibular end organs, these few fibers branch off fully to innervate the entire sensory epithelium. Recent work suggests that the ipsilaterally projecting efferents supply the central regions of the crista, whereas the contralaterally projecting efferents supply the peripheral zone [9]. The efferent fibers terminate by making synaptic contacts with hair cells and afferent fibers [9].

2.3.3 **Vestibular System Disorders**

Peripheral vestibular dysfunction can produce a variety of signs and symptoms that overlap with some of those of Meniere's disease. A thorough evaluation by a physician is needed to identify the specific pathology behind the patient's complaints of vertigo or disequilibrium. This section describes the clinical presentation of the more common peripheral vestibular disorders.

Benign Paroxysmal Positional Vertigo: Benign paroxysmal positional vertigo (BPPV) is the most common disorder of the inner ear's vestibular system [8, 27]. It accounts for at least 20% of diagnoses made by specialists, and is the cause of approximately 50% of dizziness in older adults [28]. BPPV produces a sensation of spinning, called vertigo, which suddenly occurs with a change in head posture. In addition to vertigo, symptoms of BPPV include dizziness (lightheadedness), imbalance, difficulty concentrating, nystagmus (the rhythmic and cyclic movement of the eyes with a slow phase of vestibular origin and a fast phase of reticular origin) and nausea. Activities that bring on symptoms can vary in each person, but symptoms usually appear by changing the head's position with respect to gravity. With the frequent involvement of the posterior semicircular canal in BPPV, common problematic head movements include looking up and/or rolling over and getting out of bed.

The vertigo lasts only 30 seconds to 2 minutes, and disappears even if the precipitating position is maintained. Hearing loss, aural fullness, and tinnitus are not seen in this condition. About 70% of the cases in BPPV occur unilaterally [8]. Spontaneous recoveries are common, but recurrences can occur, and the condition may trouble the patient frequently for years.

The occurrence of BPPV is due to the displacement of loose otoconia. The otoconia may either adhere to the cupula of one SCC (usually to the posterior SCC as it has the lowest point with respect to gravity) or float freely in the long arm of the canal. The common cause of BPPV in people under age 50 is head injury, which may happen as a result of concussive force that displaces the otoconia. In people over 50, BPPV is mostly idiopathic but is generally associated with natural age-related degeneration of the otolithic membrane. BPPV is also associated with migraine [29]. Viruses affecting the ear, such as those causing vestibular neuritis and Meniere's disease are significant but unusual causes.

Diagnosis includes a medical history, physical examinations, the results of vestibular and auditory (hearing) tests, and possibly lab work to rule out other diagnoses. The key diagnostic maneuver is the Dix-Hallpike positioning test [30] while the examiner observes the patient's eyes for nystagmus with position changes. A typical response is induced by rapid position changes from the sitting to the head-hanging right or left position. Vertigo and nystagmus begin with a latency of about 1 second after the head is tilted toward the affected ear, and increase in severity within about 10 seconds; they diminish gradually after 10-40 seconds, even if the head position is maintained. The direction of nystagmus, which is usually vertical, corresponds very closely to the plane of the offending SCC; hence, the problematic semicircular canal can be identified by this method [28]. Repeating this procedure several times decreases the symptoms (adaptation of the response).

If symptoms persist longer than expected, further investigation, such as MRI, is usually made to assess for unusual causes of positional vertigo. BPPV usually resolves spontaneously within 6 to 12 months. Simple vestibular exercises or maneuvers aimed at dispersing the otoconia from the cupula can speed recovery.

For more severe symptoms unresponsive to exercises, there are surgical options including nerve section and partitioning of the labyrinth using a laser technique.

Vestibular Neuritis: Acute unilateral dizziness, known as vestibular neuritis, is the second most common cause of vertigo [8]. About 5% of all dizziness and perhaps 15% of all vertigo is due to vestibular neuritis. The condition mainly affects those aged between 30 and 60 years, with a peak for women in the fourth decade and for men in the sixth decade.

Although in most cases a definite cause is never uncovered, evidences of a viral etiology, which results in histopathologic changes of branches of the vestibular nerve (or sensory neurons or even the brainstem vestibular nucleus), are found. A clear distinction about the location of the lesion can only be made at autopsy.

When one of the two vestibular nerves is infected and hence inflamed, there will be an imbalance between the two sides communicating with the cortex, brainstem and cerebellum resulting in the symptoms. The main symptom is prolonged and severe rotational vertigo that is worsened by movement of the head associated with spontaneous horizontal rotary nystagmus beating toward the good ear, postural imbalance, and nausea. Hearing loss is not present.

It is common to have BPPV syndrome follow vestibular neuritis disease. This happens because the utricle is damaged (supplied by the superior vestibular nerve), and deposits loose otoconia into the preserved posterior canal. Therefore, evidences suggest the possibility of observation of an acute unilateral vestibulopathy and BPPV simultaneously in the same ear of an affected patient with Vestibular Neuritis [31, 32].

The diagnosis initially includes other causes of vertigo, careful history and physical examination; an audiogram is required. In severe situations, other tests such as ENG (to document the reduced responses to motion of one ear), MRI (to be sure that there is no tumor or inflammation of cochlea) and blood tests may be advised. The symptoms usually stop after a period of 48 to 72 hours, and gradual return to normal balance occurs over approximately 6 weeks.

Meniere's disease: Meniere's disease is a complex idiopathic disorder of the inner ear characterized by the three symptoms of vertigo, sensorineural hearing loss and tinnitus. It is the most common vestibular disorder after the BPPV and Vestibular Neuritis [8]. The characteristics and different aspects about this disease are described in this section.

Epidemiology of Meniere's disease: Meniere's disease is a disorder of inner ear function that can cause devastating hearing and vestibular symptoms. It is almost equally distributed between the sexes, and usually has its onset in the fourth to sixth decades of life. Up to 15% of the Meniere's patients have blood relatives with the same disease, suggesting a genetic link [33]. According to [34], 85% of Meniere's patients have a peripheral disorder in the vestibular system and only 15% will have a central disorder. Meniere's disease is usually confined to one ear in the first stages of the disease, but it often extends to involve both ears over time; after 30 years, 50% of patients with Meniere's have bilateral disease [3].

Symptoms of Meniere's disease: A typical attack is experienced as a sensation of fullness of the ear, a reduction in hearing and tinnitus followed by rotational vertigo, postural imbalance, nystagmus, nausea and vomiting. The vertigo persists approximately from 30 minutes to 24 hours. Gradually, the severe symptoms diminish, and the patient is

capable of walking within 72 hours; however, the weakness and postural unsteadiness persist for days or weeks.

During the recovery time, hearing gradually returns. It may return to the pre-attack baseline, or there may be residual permanent sensorineural hearing loss, starting at lower frequencies.

Some patients may suddenly fall without warning; this event, which may occur in later stages of the disease, is called "otolithic crisis of Tumarkin" [35]. This is associated with sudden mechanical deformation of the otolith organs, causing an activation of vestibular reflexes. Patients unexpectedly feel that they are tilted or falling (although they may be straight), and make much of the rapid repositioning themselves. As this symptom occurs without warning, it can result in severe injuries.

The symptom of vertigo usually happens due to the mismatch (conflict) between the converging sensory inputs and the expected sensory patterns existing in the CNS [36]. Due to the previous experiences and during years, the CNS has learned to assume the symmetry (same frequency and intensity) in the electric impulses generated in both labyrinths as normal. This symmetry is expressed clinically as a feeling of balance [37, 38].

During an attack, the affected labyrinth diminishes its activity which makes it incapable of maintaining even its basal firings [39]. The contralateral labyrinth, however, continues discharging normally in the CNS. In this manner, the impulses reach the CNS in an asymmetric form, even though the head is maintained in the neutral position and is still. The CNS will interpret this asymmetry as a rotating sensation of movement.

On the other hand, information of this asymmetry will also be sent to the ocular nuclei. Consequently, the gaze sways in the direction of the affected labyrinth. In response to

change, excitatory reticular neurons are activated and direct the nuclei of the ocular muscle to bring the eyeballs rapidly back to their initial position (nystagmus). Then the reticular neurons undergo an absolute refractory period, and hence a new cycle of sway of gaze is restarting (nystagmus) [37, 38]. A series of neuro-vegetative signals and symptoms add to the vertigo and the nystagmus to create the final clinical picture (nausea, vomiting, cold sweating, etc). The attack doesn't last endlessly as the nervous system sets up a series of mechanisms aiming to shut down the electrical activity of the contralateral healthy side and minimize the severity of the symptoms [37, 38].

Etiology of Meniere's disease: A phenomenon fundamental to the development of Meniere's disease is endolymphatic hydrops. However, it is still unclear whether endolymphatic hydrops itself is the cause of Meniere's disease or is a pathologic change seen in the disease. Most researchers think that Meniere's syndrome has several causes (etiologies). Reasonable possibilities are obstruction of endolymphatic outflow at the endolymphatic duct level, increased production of endolymph, or reduced absorption of endolymph caused by a dysfunctional endolymphatic sac [16].

Recently, attention has been focused on the immunologic function of the endolymphatic sac as immune disease may contribute to a substantial percentage of Meniere's disease [40]. Moreover, there is also reasonable case for Migraine being the cause of some cases of Meniere's disease. Migraine is at least an order of magnitude more common than Meniere's disease, and one can allow for the possibility that migraine may cause symptoms and complications similar in frequency to those due to Meniere's disease. About 50% of the time Meniere's patients have migraine [41].

Thus, the bottom line is that the main cause of Meniere's disease is unknown [8, 41]. It is most often attributed to viral infections of the inner ear, head injury, a hereditary predisposition, and allergy. Migraine possibly produces some symptoms that overlap with Meniere's disease [41].

Diagnosis of Meniere's disease: As defined by the American Academy of Otolaryngology-Head and Neck Surgery (AAO-HNS), there are 4 groups of certain, definite, probable, and possible Meniere's patients.

'Certain' Meniere's can only be diagnosed by autopsy and includes the above criteria plus histopathologic confirmation of endolymphatic hydrops. 'Definite' Meniere's disease is diagnosed when two or more definitive spontaneous episodes of vertigo 20 minutes or longer occurs with audiometrically documented hearing loss on at least one occasion and tinnitus or aural fullness in the treated ear while other cases are excluded. 'Probable' Meniere's are considered when one attack of vertigo has occurred with documented hearing loss on at least one occasion and tinnitus or aural fullness in the affected ear while other cases are excluded. 'Possible' Meniere's is considered if Meniere's-type episodic vertigo occurs without documented hearing loss or fluctuating sensorineural hearing loss with disequilibrium, while other cases are excluded [42].

Useful diagnostic tests for Meniere's disease include an audiogram and Electronystagmography (ENG) test. Typically, the audiogram displays an ipsilateral sensorineural hearing loss involving the lower frequencies. ENG may demonstrate a unilateral vestibular weakness on caloric testing, again involving the ear symptomatic for pressure, hearing loss, and tinnitus. Electrocochleography is useful in cases that are

unclear. The finding of enlarged summating potentials (SP) in the suspected ear is diagnostic of endolymphatic hydrops.

A brainstem-evoked acoustic response (BEAR) procedure can also be performed to screen for cochlear nerve or brainstem pathology. If the BEAR is found to be positive, MRI should be obtained to assess for central nervous system or VIIIth nerve pathology.

2.4 Vestibular Testing Methods

As mentioned before, there are other disorders that can produce the same symptoms as Meniere's disease and, thus, have to be ruled out or excluded by using different types of tests in order to develop an accurate diagnosis. An overview of general current methods as well as the EVestG, used in this study, is presented in the following sections.

2.4.1 Initial Examination and Hearing Test

The history of inner ear problems, such as information about infectious diseases or allergies, medication used in past ear problems, and the history of disease in patient's family are important parts of evaluation. Moreover, initial evaluation based on physical examination of the ears (to rule out obvious infections), head and neck, and the part of the nervous system related to balance is helpful to be performed.

Hearing test is a common assessment, which displays how well sounds are detected at different pitches and volumes and how well similar-sounding words are distinguished. According to AAO-HNS diagnostic criteria, hearing loss of Meniere's patients is described as the followings [42]:

- In unilateral cases the average of thresholds at 0.5, 1, 2 and 3 kHz is 20dB or poorer in the affected ear than on the opposite side.

- In bilateral cases the average of threshold values at 0.5, 1, 2 and 3 kHz is > 25 dB in each ear.

2.4.2 **Electronystagmography (ENG)**

ENG includes series of tests that record eye movements in order to examine vestibular function and visual-vestibular interactions using electro-oculography (EOG) [43]. ENG enables the quantitative measurement of the eye movement properties in terms of slow component velocity, frequency, and amplitude of the nystagmus. It can also measure how these variables change in absence of eye fixation (e.g., with eyes open in a dark room). ENG shows abnormality in Meniere's patients with unilateral decreased vestibular response in the affected ear.

Electro-oculography (EOG) is the simplest and most available system for recording eye movement. The basis of this method is the potential difference between cornea and retina, which is aligned parallel to the longitudinal axis of the eye. The EOG enables non-invasive recording of eye movements with accuracy of about 1º in horizontal and vertical ranges of ≤40º and ≤20º, respectively. Main disadvantages of this method include eye blink artefacts, muscle activity interference, poor signal to noise ratio (SNR), and unstable baseline cornea-retinal potential. Furthermore, torsional eye movement cannot be recorded; also, recordings of vertical eye movements are not accurate and depend on lighting condition of test room [1, 49].

Video-oculography is a relatively newer method for recording eye movements. This method includes an infra-red video camera which is connected to a computer running digital image processing routines to extract eye position form the images. The advantages of this method include better resolution (0.1-1º), fast set up time and absence of electrical

noise from sources inside or outside body. This method is also better tolerated by patients and can detect torsional eye movements. However, this method is only possible with eyes wide open, and shows poor contrast between pupil and iris in some patients [1, 49].

Magnetic coil is another technique for the recording of horizontal, vertical and torsional eye movement with a very high resolution with minimal fluctuations. In this method special contact lenses with embedded coils of fine wire are placed on top of cornea. Then, subject sits inside a cage that induces magnetic field. Eye movement causes a small current in the coil which is amplified and recorded. With this method the eye movements can be measured in all three dimensions and eye movement trajectories can be extracted, which are very useful for detecting SCC abnormality in vestibular diseases such as vestibular neuritis, benign paroxysmal positioning vertigo (BPPV) and isolated lesions of a particular canal. The clinical use of this method is not popular due to the difficulty of wearing this kind of contact lens which requires anaesthetic drops, making this method semi-invasive [44].

2.4.3 **Caloric Irrigation Test**

Caloric testing analyzes eye reflexes. Caloric irrigation is frequently employed for examination of the VOR because each labyrinth can be studied separately, while stimulus can be applied with simple equipment. Caloric irrigation is ideal for detecting the unilateral lesions at the levels of labyrinth and vestibular nerve.

In caloric test the external ear canal is subjected to air or water flow at a temperature of 7ºC above or below body temperature (37ºC). The temperature difference is conducted from the external ear canal to the inner ear and causes a gradual temperature change from one side of the SCC towards the other side. Hence, the endolymph fluid will circulate (via

a convection current) within the canal, and causes deflection of cupula and eye movements away and towards the ear respectively [45].

Among the SCCs, the horizontal canal is the closest to the external ear that is source of temperature change, therefore; most of the horizontal nystagmus responses are related to the horizontal canal excitation [1]. It is also possible to tilt the patient head in a way to stimulate the two other SCCs as well [46].

The functionality of the vestibular system periphery is determined via assessment of the induced VOR. The maximum velocity of the slow component eye movements is measured. As a general rule, speeds less than 5º per second are considered abnormal. In Meniere's patients caloric response diminishes with increased disease duration, and a canal dysfunction of 35% to 50% is commonly observed in the affected ear.

The main drawback associated with caloric irrigation is the efficacy of heat transfer between external canal and inner ear that varies with regional blood flow, size of ear canal, length of heat transmission path and heat conductivity of the temporal bone [47]. In addition, because of slow speed in heat transfer, the caloric irrigation is similar to a single and slow rotational vestibular stimulus around 0.003 Hz [45].

2.4.4 **Rotational Testing**

In order to assess VOR, vestibular system can also be evoked by rotations of the head or the whole body. Rotational testing has two major advantages over caloric irrigation. First, the rotational testing is not related to physical properties of external ear and temporal bone, while in caloric stimulation these physical features affect the results [48]. Second, examination of VOR at different frequencies is possible with rotational testing, whereas caloric testing is equivalent to examination at only one frequency. Rotational testing is the

only reliable test for detecting bilateral vestibular dysfunction. However, since rotation stimulates both labyrinths simultaneously, it is not very useful for detecting unilateral vestibular abnormalities such as unilateral Meniere's cases [49].

To quantify the vestibular function during rotational testing, magnitude (gain) and timing (phase shift) of the eye movements are determined. The gain of the VOR is defined by ratio of slow component eye velocity to head rotation velocity, and the phase shift is time delay between eye and head motion. In other words, a gain of 1 and phase difference of 180 degree resembles an eye movement with the same velocity of head but in an opposite direction, which is a perfect VOR [1]. The VOR is at its optimum level within frequency range of natural head oscillations (during walking and running), which is between 0.6-8 Hz [50].

The rotational chair is currently a standard method used for rotational testing. In this method a patient sits on the chair, and the velocity and frequency of the chair rotation are adjusted by the computer that enables recording VOR responses at different frequencies and velocities in terms of VOR gain and phase difference. Laboratories have provided normal range of VOR responses in age-matched groups, which can be used for evaluating recorded responses [45].

2.4.5 **Electrocochleography (ECOG)**

ECOG is another method in assessment and monitoring of vestibular function, which has been claimed to be useful for Meniere's diagnosis. ECOG records electrical activity generated in the cochlea and auditory nerve due to auditory stimulus. ECOG responses are recorded via two methodologies: trans-tympanic and extra-tympanic. Trans-tympanic recording (invasive) involves a needle electrode passed through the tympanic membrane,

while non-invasive extra-tympanic ECOG involves an electrode consisting of a wick being placed on extra-tympanic sites such as the ear canal or the lateral surface of the tympanic membrane. The ECOG responses are much smaller in amplitude when recorded at extra-tympanic sites (smaller signal to noise ratio). On the other hand, extra-tympanic recording are non-invasive and generally painless. The reference and ground electrodes are positioned on the earlobe and forehead respectively [51].

The stimulus in ECOG usually consists of alternating polarity acoustic clicks in order to eliminate the appearance of stimulus artefacts [52]. The response that is measured in ECOG usually occurs within 10 millisecond of the stimulus onset [51]; however, recording should continue for at least 300-1000 stimuli in order to increase signal to noise ratio by averaging over many time intervals. The final response includes the following components: the cochlear microphonic (CM), cochlear summating potential (SP), and the auditory nerve action potential (AP) [52].

Figure 2-8 shows an example of ECOG waveform recorded from a healthy subject. Different methods have been suggested for measurement of the SP and AP values. The amplitudes can either be measured with respect to a baseline [53] or measured with using the peak to peak amplitudes [51]. Peak to peak absolute amplitudes are preferred in extra-tympanic recordings due to considerable amount of variation in the baseline values [51].

Cochlear microphonic (CM): CM is an alternating current (AC) response generated by the instantaneous displacement pattern of the basilar membrane evoked by acoustic stimuli. CM is often difficult to be distinguished from the stimulus artefact in non-invasive recordings and is cancelled when using alternating polarity clicks [54].

Cochlear summating potential (SP): The SP is a direct current (DC) response generated within the cochlea and represents the rectified smoothed basilar membrane displacement [51]. SP duration is closely associated with the duration of the acoustic stimulus. It has been reported the normal duration of the SP to be between 0.3 and 0.45 milliseconds [52].

It is believed that an increased endolymph volume and pressure alter the hydro mechanical properties of the cochlea which results in distorting the normal vibratory asymmetry of basilar membrane. Consequently, this distortion increases the magnitude of SP which is a property used in diagnosis of Meniere's disease.

Auditory nerve action potential (AP): The averaged activity of the potentials (as opposed to the resting potentials) caused by the synchronous firing of thousands of auditory nerve fibers is known as the compound action potential or action potential (AP). The AP represents the number of nerve fibers firing; thus a high degree of synchrony of neural firing is necessary for producing a well- defined AP. AP can also reflect the hair cell output [55].

The duration of AP from its onset to P1 (see Figure 2-8) is usually between 0.8 and 1.25 milliseconds. The latency of AP in ECOG recording is the time between the onset of stimulus and the N1 peak. The magnitude of AP is known to reflect the number of fibers which are firing simultaneously [52].

The latency of AP, duration, and magnitude of the AP are usually used to interpret the ECOG waveform recordings. It is well documented that in Meniere's patients, the amplitude of SP is greater than normal and also particularly with respect to AP. SP and AP amplitudes are subject to variation within normal population which can be due to electrode

placement. SP amplitude varies between 0.1 to 1 and AP changes between 0.6 and 3 μv [52]. Amplitude of ratio seems to be a more consistent measure of the ECOG response which varies from 0.1 to 0.4 in normal subjects (mean value of 0.25).

The SP/AP ratio derived from ECOG greater than 0.4-0.5 is considered abnormal and may represent the hydrops which helps to rule out Meniere's disease [51]. However, [56] states that "Of those with definite Meniere's, (only) 66.7% had abnormally elevated SP/AP ratios". It is mentioned that the sensitivity of the SP/AP ratio to diagnose Meniere's is 60-71%.

It should be noted that subjects must be able to hear or nothing will be recorded while performing an ECOG test. Practically, it is unrealistic to get an ECOG on someone with more than a 40-50 dB sensorineural hearing loss [51]. Hence, in order to have the best candidate for diagnosis of Meniere's patients via ECOG the patient is permitted to have a mild sensorineural hearing loss. This limitation reduces the feasible population of patients to those who are in early stage of Meniere's disease and are not old enough (> 60 years) to lose their hearing due to age. Unfortunately, ECOG results are rarely reported as a function of hearing, making it difficult to interpret in most studies [57].

As about 6% of the population has hydrops on autopsy [16], this indicates 6% of a normal population would have a positive ECOG. Considering that only 0.2% people have Meniere's disease, one would expect a high number of false-positives and low number of false negatives in ECOG testing.

Recently, a variant ECOG ratio (SP/AP area ratio) is suggested as an improved method of detecting Meniere's disease. In this method, the SP area is determined from the onset of response (compared to baseline), to the first point after the AP where the response returns

to baseline. In other words, it actually includes not only the SP but the entire AP. The AP area is determined from the onset of the AP through its negative peak, and to the first opposite polarity peak (only contains the AP notch). A study based on this method has reported a high testing sensitivity (92%) and specificity (84%) diagnostic results in which the ECOG ratio results of 178 suspected Meniere's patients, collected within 5 years, were compared to the received diagnoses of these individuals from their physicians; however, it also mentions that the method is only applicable to individuals without much hearing loss and thus not suitable for the majority of Meniere's subjects [51].

In summary, ECOG is a vestibular test that is proposed to be used as an additional assessment, when other tests have failed to produce a clear answer. Also, it has been suggested to be a useful test when one is planning an invasive treatment such as gentamicin injection. Nevertheless, ECOG has not been accepted as a screening test due to its low specificity (high false positives).

2.5 Electrovestibulography (EVestG)

The limitations of vestibular measurement techniques provide motivation to search for new, alternative diagnostic methods, specific to different vestibular disorders. EVestG [11, 58] is a relatively new diagnostic technique that has been developed to detect specific vestibular field potentials; one of its applications is claimed to be in in diagnosis of vestibular disorders, particularly Meniere's disease. EVestG is a technique similar to ECOG, wherein the acoustic stimulus is replaced by a passive whole body tilt. EVestG is a non-invasive technique to record neural activity from the vestibular apparatus and VN; it measures a vestibular driven response stimulated by passively whole body tilting the subject, who is seated in a hydraulic chair located in an electromagnetically and

acoustically shielded chamber. The EVestG signal is recorded during dynamic and static phases via an electrode in each ear resting proximal to the tympanic membrane [11, 58]. The electrodes are painlessly positioned and rested close to subject's left and right ear drums.

The vestibular response signal, extracted by EVestG technology, is called a field potential (FP). The FPs are generated by the synchronous firings of groups of vestibular hair cells both randomly and at the onset of the stimulus, and their shape, in general, is similar to the SP/AP plot observed in ECOG. However, in contrast to ECOG, FPs extracted from EVestG signals are not time-locked to the stimulus. Instead, a wavelet-based data mining technique, called Neural Event Extraction Routine (NEER), is used to detect average FP from the floor noise in the recorded signal [11, 58]. Compared to ECOG, EVestG technique has the advantage of recording a "direct" dynamic vestibular response to both excitatory and inhibitory inputs (an applied tilt). Moreover, unlike ECOG, EVestG measurements can be performed even in individuals with hearing impaired. Therefore, EVestG may act as a more specific technique for detection of vestibular dysfunctions. The detailed explanation of EVestG technology is presented in the next chapter.

As discussed before, vestibular system makes extensive interactions with neural centers within the CNS in sending and receiving information. Thus, hypothetically, direct measurement of the vestibular system responses using EVestG can indirectly reflect activity in brain regions and neural pathways. EVestG has shown the potential to have other diagnostic applications, particularly in the area of Parkinson's disease and depression [59, 60].

Regarding Meniere's disease diagnosis, EVestG signals were analyzed in a preliminary early study in a small sample size, and showed significant differences in terms of increased Sp/Ap ratio as well as decreased dynamic range of response for Meniere's subjects compared to control ones [61]. However, no specific classification was performed based on the introduced differences. Nevertheless, this suggests EVestG signal analysis may act as a useful adjunct to assist in diagnosis of Meniere's disease.

2.6 Classification Schemes

The major contribution of this thesis is characteristic feature extraction sensitive to Meniere's disease from EVestG signals and the design of a robust diagnostic classification scheme. Thus, this section briefly reviews different classification methods for biological data.

Machine learning techniques and classification algorithms have found many applications in analysis of biological and clinical data [62]. In general, machine learning techniques are divided into three categories: supervised learning, unsupervised learning, and reinforcement learning [63], amongst which supervised learning has been frequently used in biological signal processing.

Depending on the nature of the input data, an appropriate algorithm can be selected leading to optimal classification achievements such as high accuracy and/or low processing time [64]. A major common challenge is the stochastic and heterogeneous nature of the biological data [65] that requires a large population in order to design a robust classification scheme; however, in investigational studies such as this thesis, recruitment of a large population of patients is almost impossible; thus the classification method should be designed considering these issues.

Another non-ideal factor is the missing values, which can originate from different stages of the experiment (e.g., the noise or artefact in the data collection system, withdrawal of the subject from part of the test or questionnaire, etc). In order to handle missing data several strategies can be considered, which are summarized in [66]. The basic approaches in handing the missing values are: discarding instances associated with missing values, acquiring missing values, imputation or employing reduced feature models. The first two methods are usually not feasible in real clinical applications with a small number of subjects. Imputation uses an estimation of the missing feature or of its distribution to generate predictions from a given classifier model. A simple example is to substitute the missing values in the training dataset by the mean value of the available training instances (samples) belonging to the same class, and in the test dataset by the mean value of the entire training feature vector independent of the class membership of the test sample. However, imputed data is not an actual data, and variance estimations need to reflect this uncertainty.

The reduced-feature model technique represents an alternative approach, which is generating a new model that employs only the "available" features. Assuming there are measurements (features) from different modalities and a designed classifier for every modality, if a missing feature is encountered, no classifier is trained for that feature in that modality. Then, the decisions of all the available classifiers can be combined, in several different ways [67], in order to make a final decision. This is called "Fusion of classifiers" which has shown competitive results compared to imputation methods. This method is computationally less expensive compared to imputations; hence, might be preferred in practical applications [67]. This technique for handling missing data benefits from the idea

of using ensemble classifiers. According to the ensemble classifier systems [68], it is clear that no single approach is optimal and that multiple methods and approaches have to be used. The idea behind it is to consult "several experts". It can be compared to the natural behavior of humans to seek a second (or third) opinion before making an important decision.

In this project, in order to handle aforementioned non-idealities which reduce classifier's performance, an ad-hoc classification scheme similar to classifier fusion scheme is proposed to address these challenges; that is described in the next chapter, in detail.

For the described classification scheme, a suitable underlying classifier is needed. Since obtaining enough (training and testing) dataset is always with difficulty in real applications and "small" dataset is usually available, a simple classifier with few parameters to be estimated such as Linear, and Quadratic Discriminant Analysis (LDA and QDA) are beneficial.

2.7 Summary

This chapter reviewed the anatomy of vestibular system and periphery, common vestibular disorders including Meniere's disease, and current vestibular testing methods such as hearing, ENG, caloric, and rotational tests as well as ECOG test. We also introduced the new EVestG technology and briefly explained the classification theme useful for EVestG data. In the forthcoming chapter, we will discuss about the methodology of using EVestG data for diagnosis of Meniere's in detail.

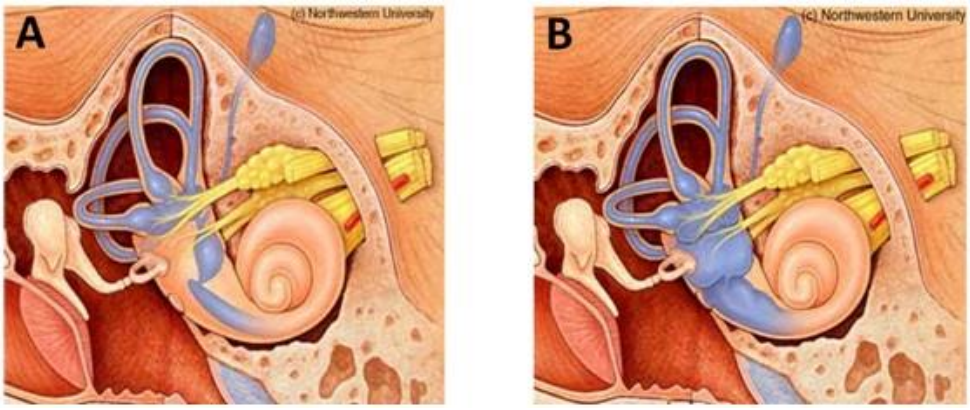

Figure 2-1. The Normal membranous labyrinth (A), and Dilated membranous labyrinth in Meniere's disease (B). Illustration is adapted with permission from [15].

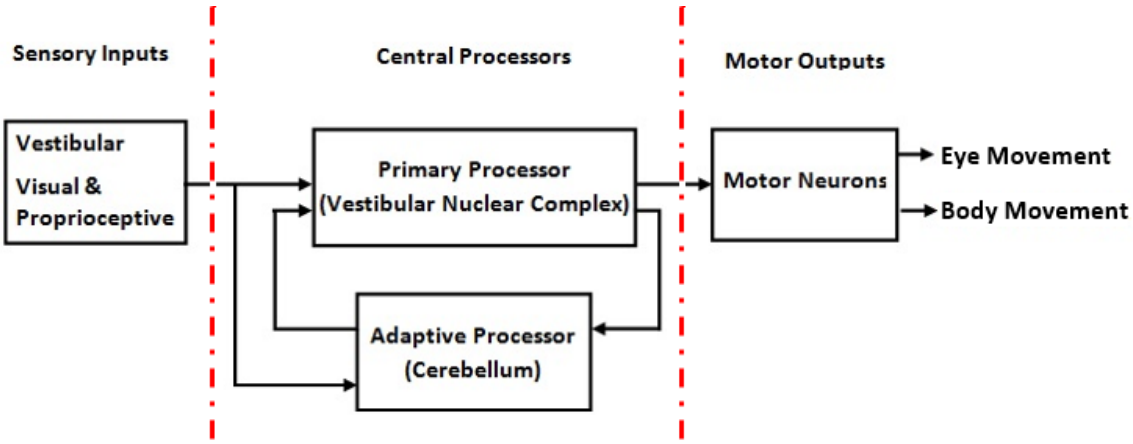

Figure 2-2. Block diagram illustrating the main components of the vestibular system. Illustration is adapted with permission from [69].

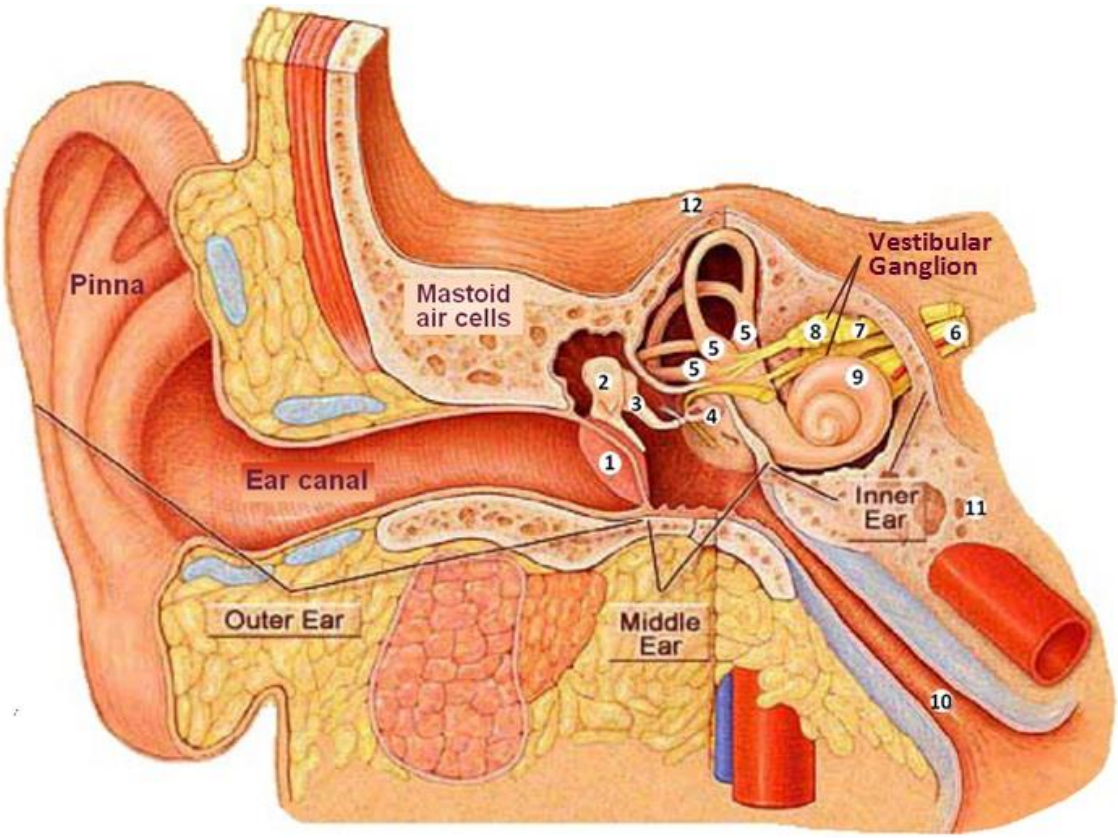

Figure 2-3. Anatomy of the peripheral vestibular system in relation to the ear. Marked locations are as follows: 1. Eardrum, 2. Malleus, 3.Incus, 4. Stapes, 5. Semicircular canals, 6. Auditory nerve, 7. Facial nerve, 8. Vestibular nerve, 9. Cochlea, 10. Eustachean tube, 11. Temporal bone, 12. Labyrinth. Illustration is adapted with permission from [41].

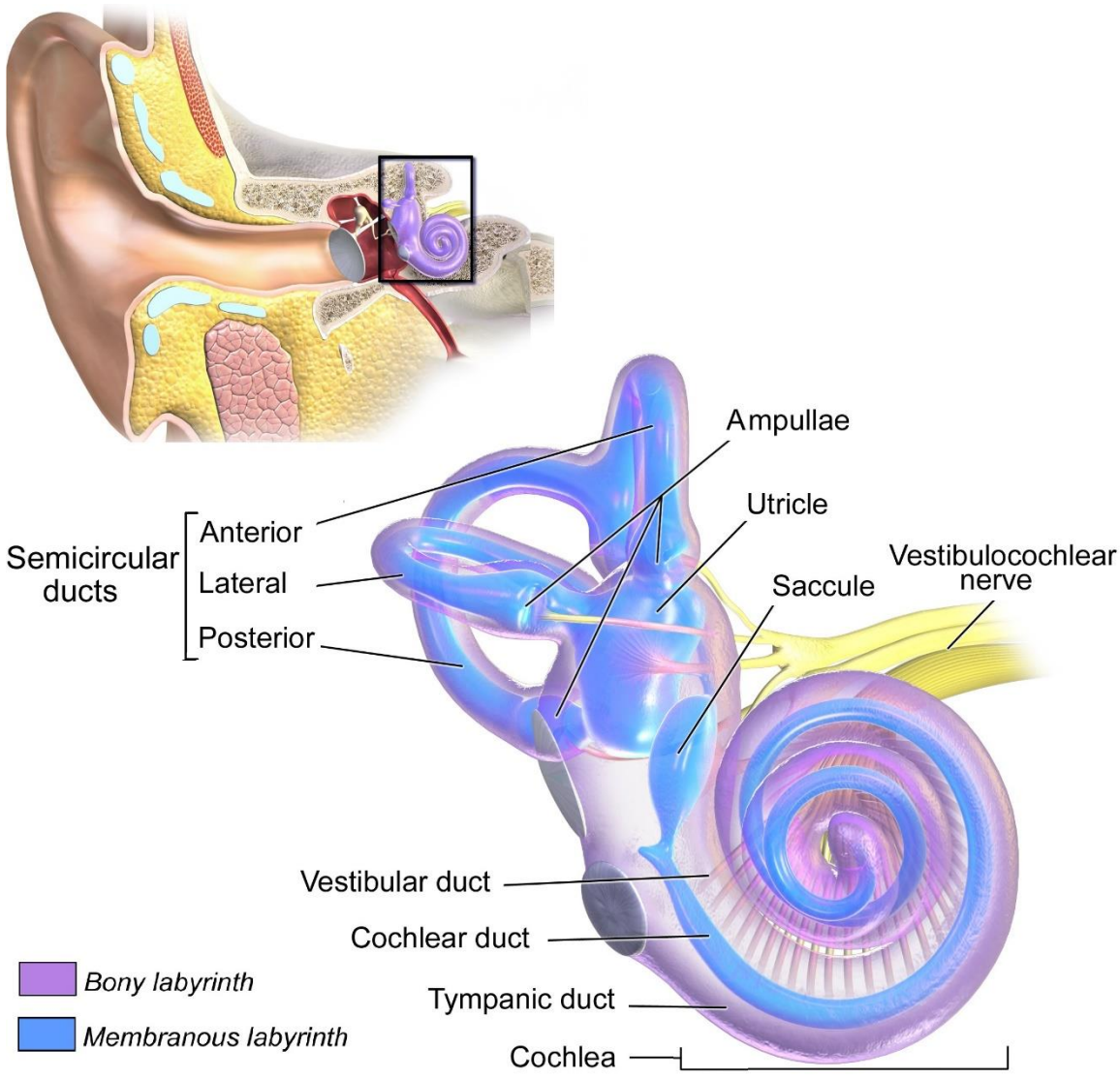

Figure 2-4. The bony labyrinth and membranous labyrinth [70].

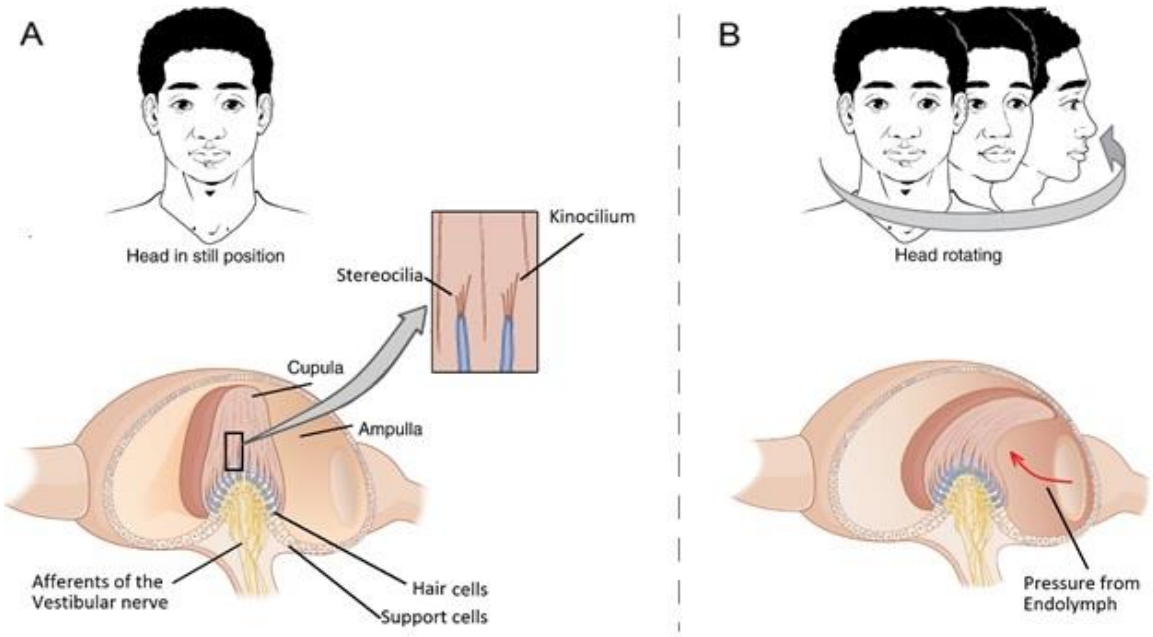

Figure 2-5. The ampulla in horizontal semicircular canal: A) before, and B) at the head rotation [70].

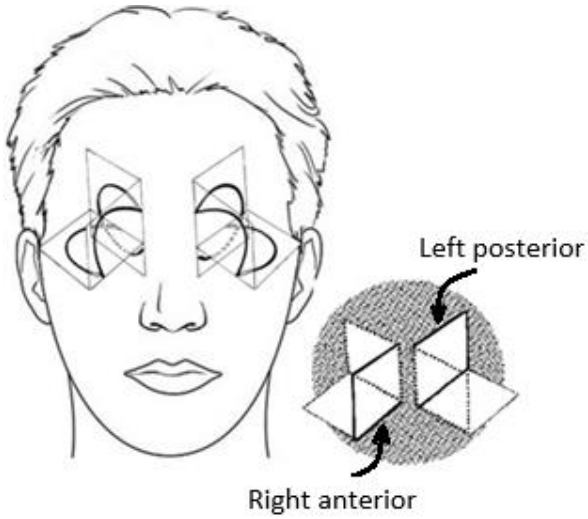

Figure 2-6. Orientation of the semicircular canals: The canals on each side are mutually perpendicular and are paired with conjugate canals on the opposite side of the head (e.g., the paired planes for left posterior and right anterior canals are marked).

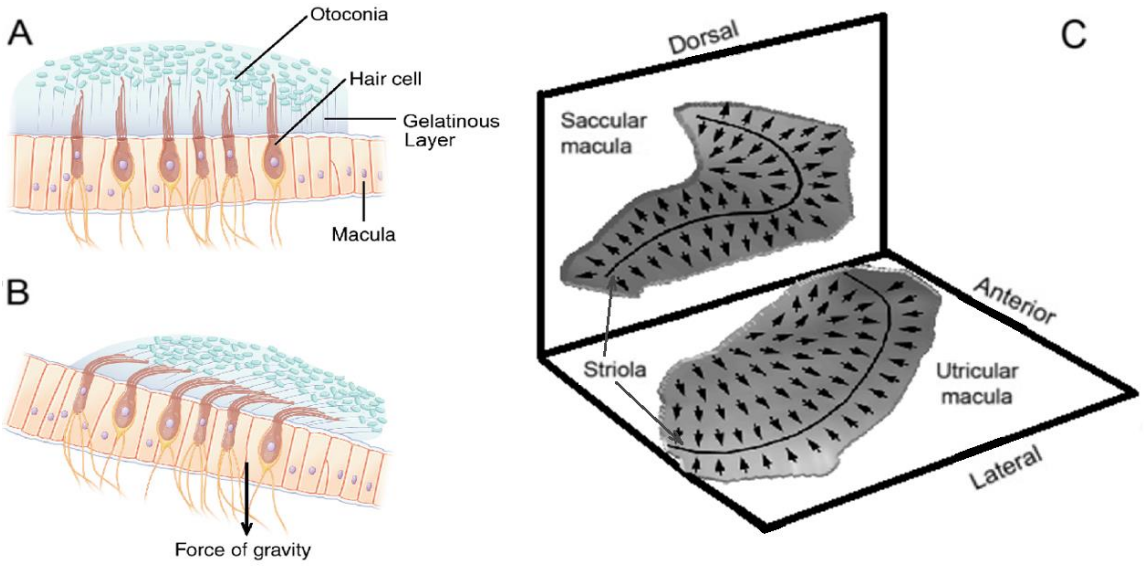

Figure 2-7. Macula of the utricle and saccule. (A) Structure of the macula. The kinocilia of the hair bundles are shown with thick lines. On each side of the striola, the hair cells have opposite orientation. (B) Otolith displacement and deflection of the hair cells. (C) Orientation of saccular and utricular maculae. Arrows show the direction in which the hair cells are maximally depolarised [71].

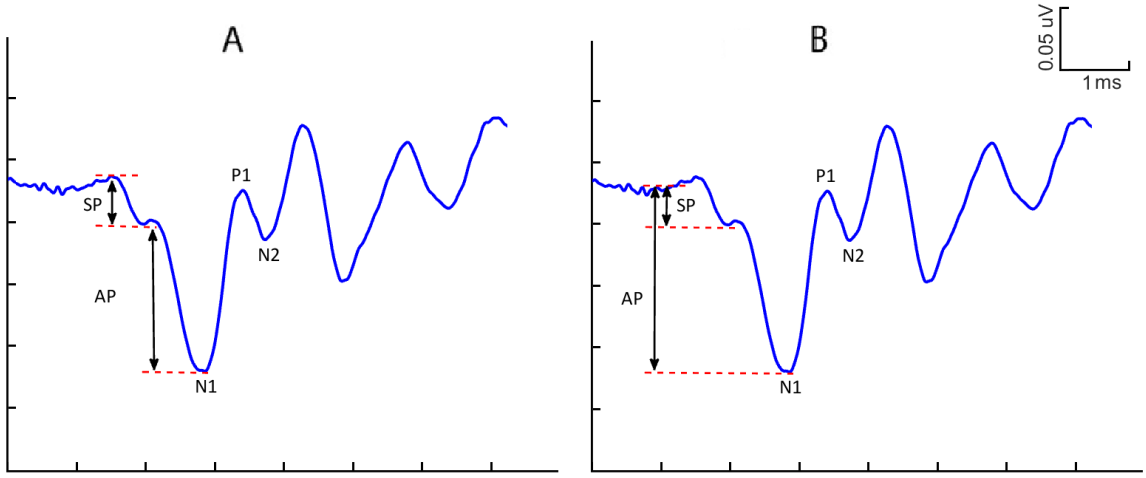

Figure 2-8. Normal electrocochleogram recorded from tympanic membrane in response to clicks with alternating polarity. Summating potential (SP) and action potential (AP) amplitudes can be measured from peak to peak (A) or with reference to a baseline value (B). Amplitude/time scale is 0.05μv/1 ms. Illustration is adapted with permission from [72].

CHAPTER 3 Methodology

3.1 Overview

The purpose of this chapter is to provide introductory information on the EVestG recording system setup and recording protocol as well as the procedure of preparing study participants before recording. We will then explain the participants' demographic information, EVestG signal analysis, feature extraction, feature selection, and the designed classification method.

3.2 Recording Apparatus

A schematic of the EVestG recording system is depicted in Figure 3-1. The EVestG recording technique is similar to that of electrocochleography (ECOG). Like ECOG waveforms EVestG signals are low in amplitude (microvolts or smaller); hence, electrodes must be placed as close as possible to the vestibular end organs. EVestG signals of this study were acquired using a specialty electrode called TM-ECOGtrode produced by Bio-logic, France. The electrode consists of a fine silver wire protected with a soft plastic shield.

The tip of TM electrode has a soft, conductive hydro-gel (depicted in Figure 3-2A), which is moistened using conductive gel before it is inserted into the ear canal (Figure 3-2B). Conductive gel is applied to lower the overall electrode impedance as well as the electrical artefacts associated with relative electrode motion on the skin. Similarly, the thermal noise produced by the electrode‘s impedance would also be reduced [73].

The active electrode was placed in both ear canals proximal to the ear drum. Reference electrodes (Biopac EL254S for earlobe and EL258S for forehead) were placed on the ipsilateral earlobes, and a common ground electrode was placed on the forehead. The left and right ears’ signals were collected using Spike2 software using a CED-1902 signal amplifier (50Hz/60Hz notch filter, 10k-100k gain, and 1Hz high pass filter), and digitized by an analog to digital converter (CED1401) at a sampling rate of 41.666 kHz. Such high sampling rate was needed in order to detect any SP notch in the recorded signals and characterise the overall AP shape and surrounding regions well. The gain of the amplifier was adjusted in the mentioned range to prevent output saturation; typically it was set to 20k.

To stimulate the vestibular system, passive whole body tilts are delivered via a computer that controls hydraulic chair (Figure 3-3). The hydraulic chair can passively move the body and consequently the head in a way to resemble the head‘s pitch, yaw, or roll motions as well as a linear up and down translations. Hydraulic systems are beneficial in applications that require control of large forces to generate smooth motions. Other advantage of using hydraulic systems over electrical motors is their relatively lesser electrical noise. The bell-shaped velocity profile and the resulted displacement profile of the chair movement used in this study are depicted in Figure 3-4. For every tilting stimulus, the chair movement (to

or from the tilting position) has acceleration and deceleration phases, which each take 1.5 seconds and are called OnAA and OnBB segments, respectively.

3.3 Participant's Preparation

Prior to commencement of the EVestG recordings, all participants signed a consent form, approved by the Biomedical Ethics Board of University of Manitoba, Canada or Alfred Hospital, Australia after they were provided with detailed information about the procedures involved in the experiment. The referred patients were already asked not to take any vestibular impacting medications 24 hours prior to the experiment.

3.3.1 **Primary Tests and Questionnaire**

Otoscopy was initially performed to dismiss the subjects with too much wax in their ear canal, or any signs of visible abnormality or damages to the eardrum (changes in colour of the ear drum can be an indication of middle ear disease). All participants went through three preliminary tests of otoscopy, audiometry, and balance test prior to EVestG recording.

Participants' balance was assessed by instructing them to stand on one leg with their eyes open, and then close their eyes for 5 seconds. While this test was run for all participants, however, its purpose was only for recruiting healthy control subjects and to ensure they had a normal level of balance skills.

Moreover, for every subject two questionnaires, Montreal Cognitive Assessment (MoCA) scale [74] and Montgomery Asberg Depression Rating Scale (MADRS) [75] were completed. These were applied for cognitive decline and depression evaluation respectively. Again, the purpose of these tests was only to reduce the variability among

study participants such that they were all free of depression and had a normal cognitive score.

The Vestibular Disorders Activities of Daily Living Scale (VADL) was also applied to patients in order to assess the level of vestibular impairments in their routine daily life tasks. The aim was to score patients' functional limitations due to their inner ear disease and investigate the correlation of the scores with EVestG test results.

Although we did the VADL test, the scores were not reliable. The reason was that, the individuals were expected to answer the questions according to their current vestibular conditions. However, many patients related their responses to their last attack period (either partially or totally) instead. Thus a correlation analysis between VADL and EVestG features would not be meaningful.

A description about these questionnaires can be found in Appendix A.

3.3.2 **Electrodes Attachments**

To prepare participants for EVestG recordings, forehead and earlobe skin sites were cleaned using an alcohol wipe to reduce the impedance between the electrode and skin. Conductive gel was added to the electrodes contact surface before they were placed on the skin. Electrodes were fixated on the skin using medical adhesive tapes. The ground electrode was placed at the center of forehead and the reference electrodes were placed on the ipsilateral earlobes using double-sided adhesive ring tapes.

After examination of the ear canal and eardrum, the hydro-gel end of TM electrode was moistened using conductive gel, and carefully inserted into the ear canal under the feedback of participant. Once the electrodes were inserted into the ear canal and secured to the ear with a piece of tape, a small foam ear plug was compressed and inserted into the ear canal

beneath the TM electrode to avoid its movement and to further attenuate unwanted auditory stimuli.

Once the electrodes were connected subjects were asked to seat in the hydraulic chair, electrodes were connected to signal conditioning device and the raw EVestG signals were observed on the computer monitor outside the recording anechoic chamber. The raw signals were checked to have an acceptable SNR. That is, the raw signals and their frequency spectrum were monitored on computer, while all electrodes were attached to the subject.

To avoid extra-vestibular influences, such as neck muscle artefacts, participants were instructed to relax and their head was secured using two head rests attached to the chair. To reduce ocular artefacts, the participants were asked to keep their eyes closed during the recording.

3.4 Recording Protocol

A complete EVestG recording [11, 58] includes seven different tilting stimuli: 15 cm upward movement of the chair, while the subject is either in upright sitting position (up/down tilt) or in supine position (supine up/down), 40 degree rotation of the chair to the right side, either in upright sitting position (rotation tilt) or in supine position (supine rotation), 40 degree tilting of the upright sitting chair to the right side (ipsilateral right and contralateral left tilts), 40 degree tilting of the upright sitting chair to the left side (ipsilateral left and contralateral right tilts) and 40 degree tilting of the upright sitting chair backward (back/forward tilt). The Contralateral (CT) and ipsilateral (IT) tilts together are called as side tilt. These movements are the motion settings of the EVestG system and the same for each trial. Each tilt goes back to center before starting another tilt. Each of these movements

can selectively and predominantly stimulate a vestibular sensory organ which is sensitive to motion in that direction.

EVestG recording for every stimulus (chair tilt) takes 60 seconds including: 1) 20 seconds, called Background recording (BG), while the chair is still in the center position; 2) 3 seconds chair movement to one of the predefined motion profiles as selected by operator; 3) 17 seconds resting in the tilted position; 4) 3 seconds turning to the center; 5) 17 seconds resting in center position.

During the experiment the position waveform of the chair is also recorded together with the raw EVestG signals from left and right ears (Figure 3-5). It is used for synchronization of the segments of interest for analysis which will be explained later in this chapter.
After seven tilts' recordings are completed, the active ear electrodes are removed from the ears and left free in order to record the system response (for 60 seconds). Then, the ears recorded signals along with the system response are fed to the NEER algorithm to extract the FP signals.

3.5 Participants

As mentioned earlier, there was a study of Meniere's disease via EVestG signals (11 patients with Meniere's and 18 age-matched controls) in [61], for which the signals were recorded at the EVestG Lab at the Alfred Hospital, Melbourne, Australia. In this study, we used the same dataset of the above study [61] and a few more unpublished data from the same Lab (Alfred Hospital) as training dataset to extract characteristic features and design a robust algorithm for classification of patients with Meniere's disease while started to recruit patients in Canada for test dataset. Thus, our training dataset included EVestG signals of 14 Meniere's patients (54.2±9.7 years, 4 males) and 16 healthy individuals

(56.1±5.5 years, 7 males). The test dataset included EVestG recorded signals of 21 individuals (55.7±10.5 years, 12 males) with unknown "dizziness" diagnosis at the time of testing and analysis, recruited in Riverview Health Center (RHC) Lab, Winnipeg, Canada. Initially, we were informed to have 256 potential dizzy patients; however, only 91 agreed to be contacted for EVestG recording appointment. Although we planned to compensate the patients time, spent for EVestG experiment, with a ($15) gift card and mentioned this when contacting every individual, but only 21 subjects participated in our study. Once, the diagnoses of the referred patients were known, we also selected EVestG signals of 10 age-matched healthy control volunteers (57.4±4.9 years, 4 males) that were already recorded and available at RHC Lab.

All the referred individuals recorded in Canada had undergone clinical assessments including hearing, ENG, caloric, and rotational chair test at the Health Science Center of Winnipeg, Canada, prior to EVestG recording; we were blind to those results, and were given the clinical diagnosis only at the stage of determining the accuracy of the algorithm on the test dataset.

The control (train and test) subjects had all normal hearing and balance, with no history of vestibular or neurological conditions; their MoCA and MADRS scores were also in the normal category. On the other hand, one RHC referred patient had a MADRS score of 7/60 indicating the patient has a mild depression. All Meniere's training subjects achieved normal scores in MoCA and MADRS tests.

In this study, we had both training and test data of only five tilts (CT, IT, back/forward, up/down sitting position, and rotation in upright sitting position tilts); the supine up/down

and supine rotation Alfred (training) data were not collected due to recording room size constraints. In RHC (testing) data we recorded all the seven tilts stimuli.

3.6 Signal Analysis

In preprocessing stage, the recorded EVestG signals were analyzed offline via a patented signal processing technique, called the NEER [11], which detects and localizes individual vestibular FPs in the EVestG recordings.

Through NEER algorithm, each recording was divided into different time segments according to the position waveform of the chair in a same pattern for every tilt. Figure 3-6 shows the segmentation of the signal for side tilt stimulus. The six periods of interest in every tilt are 1.5 seconds before the movement which is labeled as background (BGi) segment, the 3 seconds tilting stimuli (acceleration and deceleration phases labeled as OnAA and OnBB segments), the 1.5 seconds before returning the chair to background position (labeled as return to center BGi or RTC BGi segment), and the 3 seconds stimuli following that (labeled as RTC OnAA and RTC OnBB segments). The acceleration/deceleration segments were selected as they give the largest differences compared to the background.

The output of the NEER algorithm for the above 6 segments and in every tilt are two main signals: FP signal and its firing pattern (the registered locations of FPs occurrences in terms of sample/time). Figure 3-7 shows a typical output of the NEER's FP signal including a potential SP notch, and AP notch. The firing pattern of the FP signal is presented by two signals: 1) the time intervals between each two successive FP loci or AP notch points (Figure 3-8), and 2) the probability distribution of the time intervals estimated by the normalized histogram of the time interval data (as shown in Figure 3-9). The

histogram was generated based on the calculated time intervals during each segment. The histogram consisted of 25 time bins logarithmically ranged from 0.5 to 25 millisecond. Each histogram was then normalized by dividing each bin number by the total number of time intervals. Therefore, from each of the aforementioned 6 segments three signals (FP signal and its two firing pattern representations) were analyzed (18 signals for each ear) for each subject. All signals were normalized by their maximum (absolute maximum) value prior to analysis.

Figure 3-10 shows a typical normalized EVestG FP signal of a control subject. The FP waveform's minimum point (AP notch) is called AP point, and the time duration approximately 3-6 millisecond before and after the AP are considered as the pre- and post-potential intervals. We observed a distinct difference between the pre- and post-potential parts of the FP curve between the Meniere's and control groups of the training dataset. Thus, several linear and non-linear features were extracted from these two time regions for further analysis. Moreover, we investigated the changes in the difference between segments of each tilt's signal to examine the effects of dynamic changes from resting to acceleration or deceleration, and also the differences between the two phases (acceleration/deceleration) of movement. In addition, the differences (L-R) between the left and right ears' signals were investigated to test for vestibular asymmetry. We also used the sum of the left and right signals (L+R) in order to extract features resulted from any bilateral ear reaction.

It should be noted that since the NEER algorithm [11] removes segments of the original signal that are corrupted by large artefact (due to hydraulic chair, muscle artefact, movements, poor electrode contact, etc.), not all the segments were of 1.5 seconds duration; we excluded the segments shorter than 1.36 seconds. Therefore, not every subject had all

the extracted features (missing data). In order to handle missing data in our small dataset, we designed an ad-hoc diagnostic classification system that is described in more details in the following sections.

3.7 Feature Extraction

Feature selection was made using the training data. We calculated several statistical and fractal features from the FP signal and its two firing pattern representations. Since these signals are considered as stochastic signals, hence we used their statistical properties in order to describe them. On the other hand, based on literature [76, 77] and our previous studies [59, 60], we found fractal measurements a powerful tool to differentiate between a healthy and a non- healthy signal. Thus, we chose two well-known fractal dimension measurements, Higuchi fractal dimension (HFD) [78], and entropy-based dimensions such as the Information dimension (ID) [79] and the Correlation dimension (CD) [79], which are suitable for calculating complexity of biomedical signals.

Therefore, the mean, rectified mean, standard deviation, skewness, kurtosis, HFD, ID, and CD of the pre- and post-potential intervals of every FP signal. For a brief description of fractal dimension calculation, please see Appendix B. We also calculated the total energy and the average power of the aforementioned intervals for the range of 100-11000 Hz. The 100 Hz low cutoff frequency was chosen to remove muscle's interference. On the other hand, since the width of a dip in the vestibular response is in the range of 0.1 millisecond, EVestG signals are extended up to 10000 Hz. The 11000 Hz is the frequency, at which the amplifier begins to roll off. Hence, we used the range of 100-11000 Hz.

For the firing pattern signals we calculated the mean, standard deviation (SD), skewness, kurtosis, mode, median, the ID, CD, HFD of the time interval signals as well as

the number of firings of the firing signals (Nof). We also selected the time intervals smaller than one standard deviation from average; these represent the time intervals of high frequency firing rate. We calculated the average of these time intervals as a feature and called as average of minimums or "Ave – min".

We calculated the correlation of probability distribution function (PDF) of the time interval signals with the FP signals in order to investigate any relationship between the pattern of firing and the FP signal's shape.

3.8 Feature Selection

There are two general approaches to feature selection: filters and wrappers [80, 81]. Filter type methods are essentially data pre-processing or data filtering methods. Features are selected based on the intrinsic characteristics, which determine their relevance or discriminant powers with regard to the targeted classes. Simple methods based on mutual information [82] or statistical tests (t-test, F-test) have been shown to be effective [83-85]. They also have the virtue of being easily and very efficiently computed. In filters, the characteristics in the feature selection are uncorrelated to that of the learning methods; therefore, they have better generalization property.

In wrapper type methods, feature selection is "wrapped" around a learning method: the usefulness of a feature is directly judged by the estimated accuracy of the learning method. One can often obtain a set with a very small number of non-redundant features [80, 86], which gives high accuracy, because the characteristics of the features match well with the characteristics of the learning method. Wrapper methods typically require extensive computation to search the best features.

In order benefit from both above approaches and to reduce the number of features, we used minimal-redundancy-maximal-relevance (mRMR) feature selection method [87] in order to rank the features based on mutual information of the features with respect to the target class and to each other; we only used features that passed statistical significant test. Thus, at first stage of the study we applied normality Lilliefors [88] test on every feature values to make sure if we can reject the null hypothesis that data come from a normally distributed population at 5% significance level. Since we could not reject the null hypothesis, we confined statistical test to parametric statistical analysis; we applied Analysis of Variance (ANOVA) [89] on randomly selected 70% subsets of the training dataset for every feature to select features with most significant difference between the groups of Meniere's and controls. In all statistical tests a *p*-value less than 0.05 was considered significant. Then, we applied mRMR on the selected features.

The mRMR method has been shown to rank features based on the least redundancy among themselves and the highest relevance to the target class; this is done through selecting (adding) one feature at a time called "first-order" incremental search [87].

Given the input data of N samples and M extracted features ($X = \{x_i, i = 1, \dots, M\}$) and the target classification variable c, the mRMR method finds from the M-dimentional observation space (R^M) a subset (S) of m features ($S = \{x_i, i = 1, \dots, m\}$) that optimally characterizes c. By "Optimal characterization" condition we mean identifying the set of m features by jointly selecting the features which obtain minimal classification error or maximal accuracy (maximal-relevance) and are almost uncorrelated features which can maximally represent the original space covered by the entire dataset (minimal-redundancy).

The maximum relevance and the minimum redundancy criteria are both measured based on mutual information calculation [90].

In case of two random variables *x* and *y*, *I* is defined in terms of their probabilistic density functions $p(x)$, $p(y)$, and $p(x,y)$as follows:

$$I(x;y) = \int\int p(x,y) log \frac{p(x,y)}{p(x)p(y)} dxdy \quad (4.1)$$

Maximum relevance ($max\ D(S,c)$) criterion is defined by the mean value of all mutual information values between individual feature x_i and class *c* as follows:

$$D = \frac{1}{|S|}\sum_{x_i \in S} I(x_i, c) \quad (4.2)$$

It is likely that features selected according to Max-Relevance could have rich redundancy, i.e., the dependency among these features could be large. Therefore, the following minimal redundancy ($min\ R(S)$) criterion can be added to select mutually exclusive features [91].

$$R = \frac{1}{|S|^2}\sum_{x_i, x_j \in S} I(x_i, x_j) \quad (4.3)$$

In this approach, the first feature is selected due to the Max-Relevance criterion. Then, an iterative search method adds one feature at a time such that by having a set of *m-1* feature space, S_{m-1}, the m^{th} feature is chosen to achieve the maximum of equation 4.2 and minimum of equation 4.3. The criterion combining the above two constraints is called Min-Redundancy-Max-Relevancy (mRMR) [87], and simultaneously optimizes D and R spaces as below:

$$max\ \Phi(\mathrm{D}, \mathrm{R});\ \ \Phi = \mathrm{D} - \mathrm{R} \quad (4.4)$$

The respective incremental algorithm optimizes the following condition:

$$\max_{x_j \epsilon X - S_{m-1}} \left[I(x_j; c) - \frac{1}{m-1}\sum_{x_i \epsilon S_{m-1}} I(x_j; x_i) \right] \quad (4.5)$$

Using mRMR method, we selected the top 5 features ranked by mRMR algorithm for each tilt's signals as the characteristic features for classification.

3.9 Classification

After selecting the top 5 features using mRMR algorithm, we designed an ad-hoc classification method, which is very similar to ensemble-base classification algorithms. Since Meniere's disease occurs due to different vestibular and neural patho-physiologies, different measurements (features) can be considered as different symptoms/signs, which together characterize the medical condition exhibited by a Meniere's patient. Considering the fact that some of these features may not be present (missing) at the time of diagnosis, we can use a simpler version of the reduced-feature models technique. Our ad-hoc diagnostic algorithm was developed using the training dataset, and then evaluated on the test dataset (unbiased testing).

Once classification of training and test data of 5 tilts (in upright position) were fulfilled, we compared their results in order to identify the optimal stimulus/tilt for Meniere's disease diagnosis. We then compared our classification method on the optimal tilt data with the most common versions of ensemble-based classification algorithms, which are structurally similar to our purposed classifier.

3.9.1 **Average Voting Classifier**

For each tilt we designed an ad-hoc voting classification system made of 5 single-feature classifiers using linear discriminant classification algorithm (LDA) [63]. Average voting classifier is an ad-hoc classification scheme that we suggest for 2-group classification data of heterogeneous populations (i.e. biological data), in which each feature is considered in a

similar manner of a symptom to vote as Meniere's or non-Meniere's for each subject using a classifier (LDA in this study). This design handles the missing data well without the need to remove the subject's data or to replace it by mean value.

To train the single-feature classifiers (and hence the average voting classifier), since our training dataset was small, we used leave-one-out routine to avoid over-fitting problem. Leave-one-out is a routine, in which in every fold one subject's data is left-out for testing and the rest used for training the classifiers; this routine was repeated till every subjects' data was used as test once. As we have had 2-group classification, for simplicity, we assigned a vote of 0 for non-Meniere's or 1 for Meniere's. Then, the votes of all single-feature classifiers for every subject were averaged. If the average vote was > 0.5 (or < 0.5), then the subject was considered as Meniere's patient (or non-Meniere's). The average vote on the boundary line (=0.5) is considered as misclassification when calculating accuracy. We also replaced LDA method with Quadratic discriminant classification algorithm (QDA) [63] in order to investigate if the data are separable in quadratic way and compare the results with LDA classification results.

The trained classifier using the features selected from the training dataset was then applied to the test dataset. Thus, the training and test results were completely independent. This routine was applied for all the 5 stimuli (tilt) data recorded for patients in the upright position. The same feature selection and leave-one-out classifier training was also done for the EVestG signals of the two movements with patients in supine positions; however, as only the RHC dataset included these movements' data (due to having a newer version of the EVestG chair), those results are presented and discussed separately.

3.9.2 **Ensemble Classifier**

The ad-hoc classification method's performance was compared with that of three most common ensemble algorithms: Bootstrap Aggregation (Bagging) [92, 93], Adaptive Boosting (AdaBoost) [94-97] and Subspace [98] methods. All of these selected ensemble methods are capable of handling missing values and need minimal set of parameters which liken them to our non-parametrical approach. We expected AdaBoost algorithm to produce the closest results to our method as it is known to be one of the top 10 algorithms in data mining [99]. Our intent was to compare the performance of our ad-hoc classifier with its reasonable ensemble counterparts to investigate the best possible performance on our dataset.

An ensemble learner is a meta-algorithm that tries to solve the classification problem by employing many identical classifiers, called weak learners, and combining their votes. We selected decision stumps (single threshold on a feature) as the weak learners of ensemble methods with the same type of classifier used in our ad-hoc method (LDA, QDA) so that the methods would be comparable. We also gave only mRMR selected features to the ensemble classifiers in order to make a fair comparison independent from feature selection techniques.

In Bagging classification [92] many replicas of the dataset would be generated by random selection with replacement, and decision trees would be built on these replicas. In testing, the Bagging ensemble takes simple voting among the built decision trees to predict the label of the test sample. The Subspace algorithm [98] first chooses random equal-size subsets of the available features without replacement and trains a weak learner on each of the non-overlapping sub-sets. The test sample would be assigned to the class that has

highest average score among the weak learners. In this study, we selected Discriminant Analysis classifier (instead of K Nearest Neighbor classifier) as the base learner for Subspace method to provide maximum similarity with the ad-hoc method.

AdaBoost algorithm [94-97] performs its task by sequentially taking a weak leaner and invoking it several times on different subsets of training set. These consecutive subsets are constructed by pseudo-random selection of the training samples based on the latest probability distribution over them. In each AdaBoost round, the probability of selecting incorrectly labeled samples, in the next round, would be increased while the probability of correctly labeled examples would be decreased. The procedure starts with initiating a uniform probability distribution over samples and changing it in each round according to the outcome of last week learner. The next weak learner would be constructed by minimizing the summation of the weighted errors based on the selected training set and the weight of each sample in the modified distribution. After completing a pre-defined number of rounds, AdaBoost gives weight to each of the produced weak learner proportional to its classification performance on the training set. According to the number of available features (=10), for all boosting classifiers, a number of weak learners was set to 50 to avoid over-fitting problem.

3.10 Summary

In this chapter, we described our recording experiment, the data of the study, signal analysis and the designed classification method. We also addressed application of similar classifiers in order to compare their results with our classifier's performance. The results and the discussion about them will be presented in the next chapter.

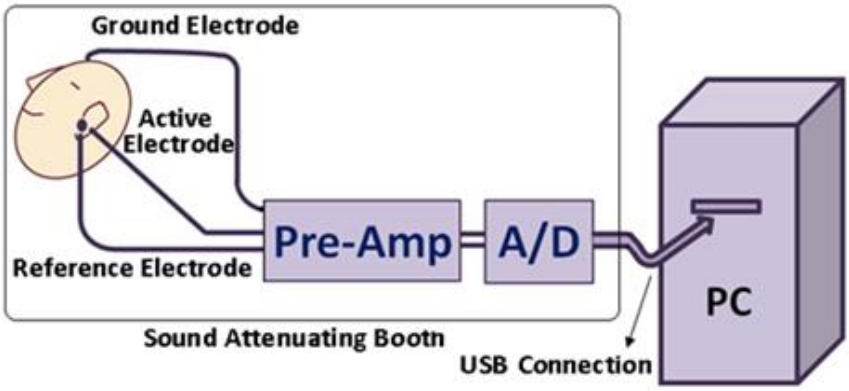

Figure 3-1. Summary diagram of recording setup.

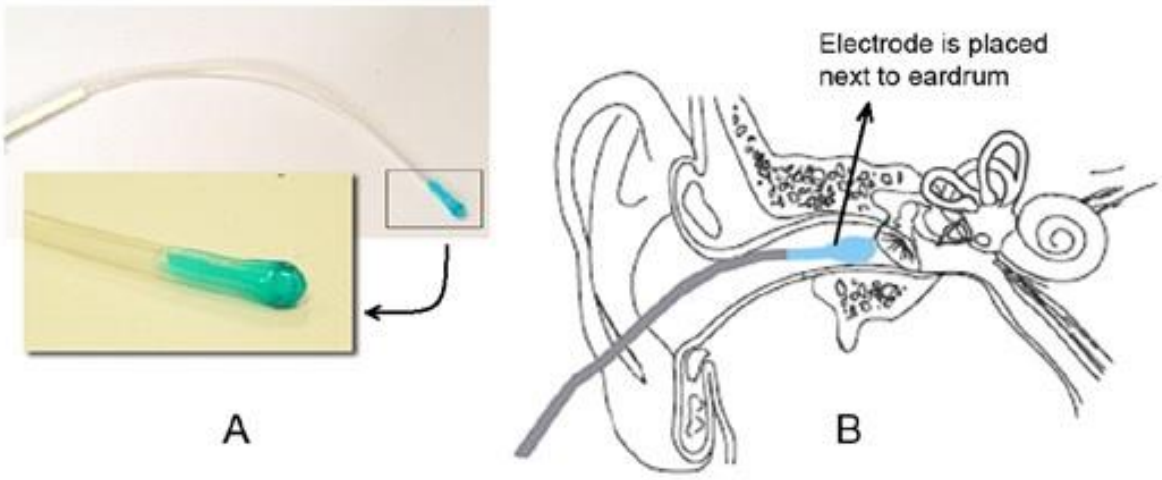

Figure 3-2 Bio-Logic electrode and its placement for recording. Illustration is adapted with permission from [11].

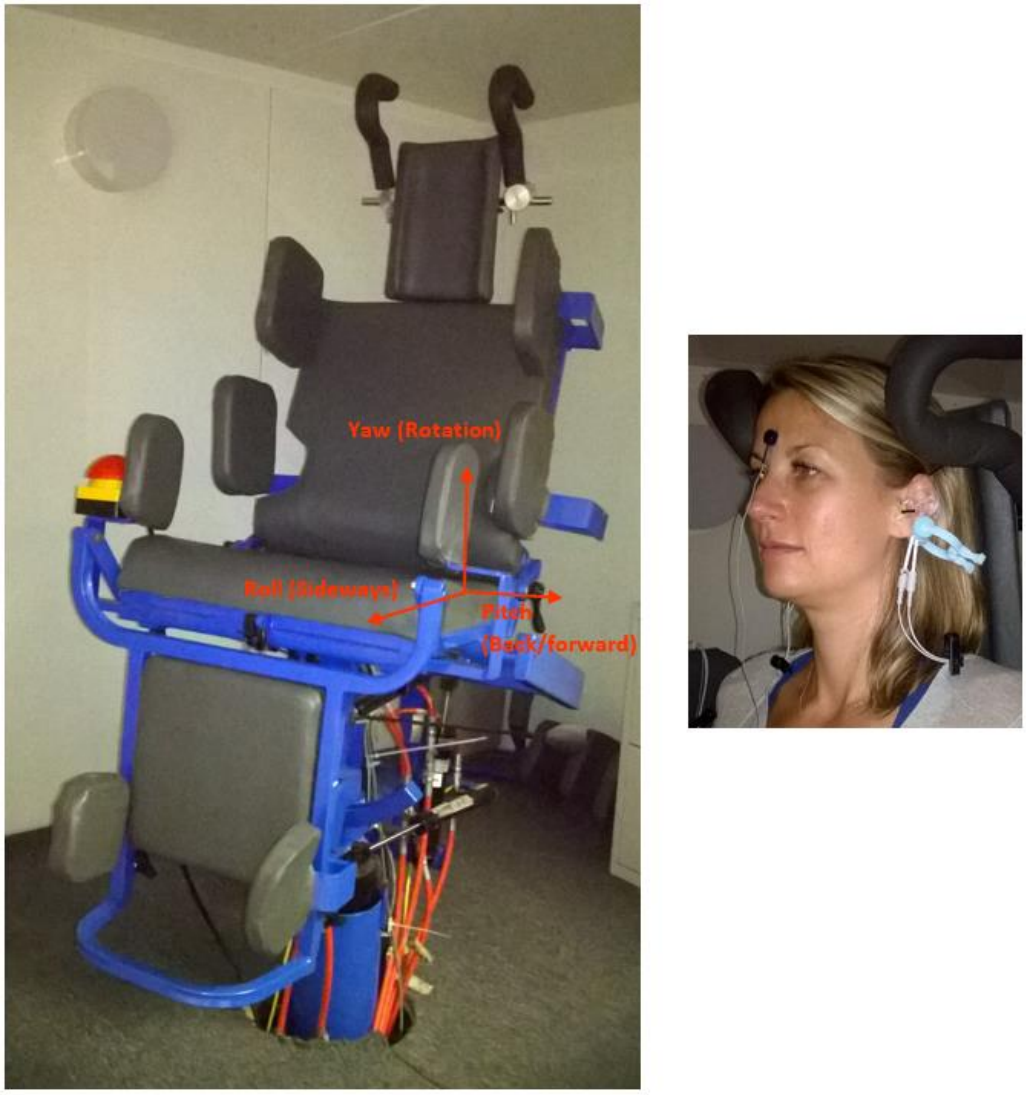

Figure 3-3. The Hydraulic chair, and electrode placements in a volunteer.

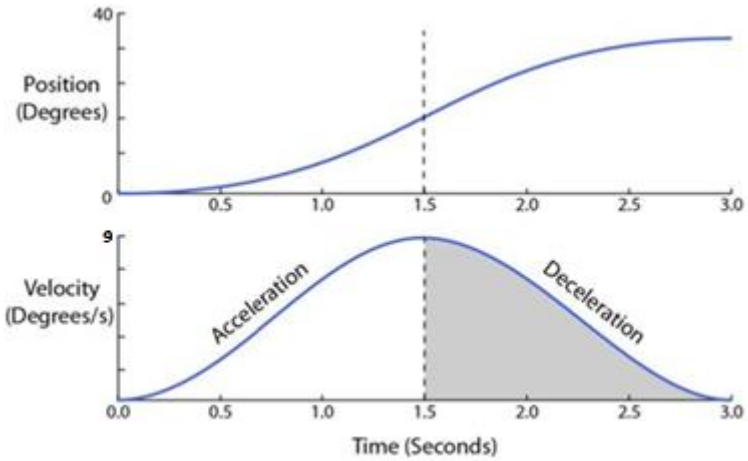

Figure 3-4 Position and velocity profiles of the vestibular stimulus. Acceleration and deceleration of the chair movement (1st and 2nd 1.5 seconds) are separated by the dashed vertical line. Illustration is adapted with permission from [11].

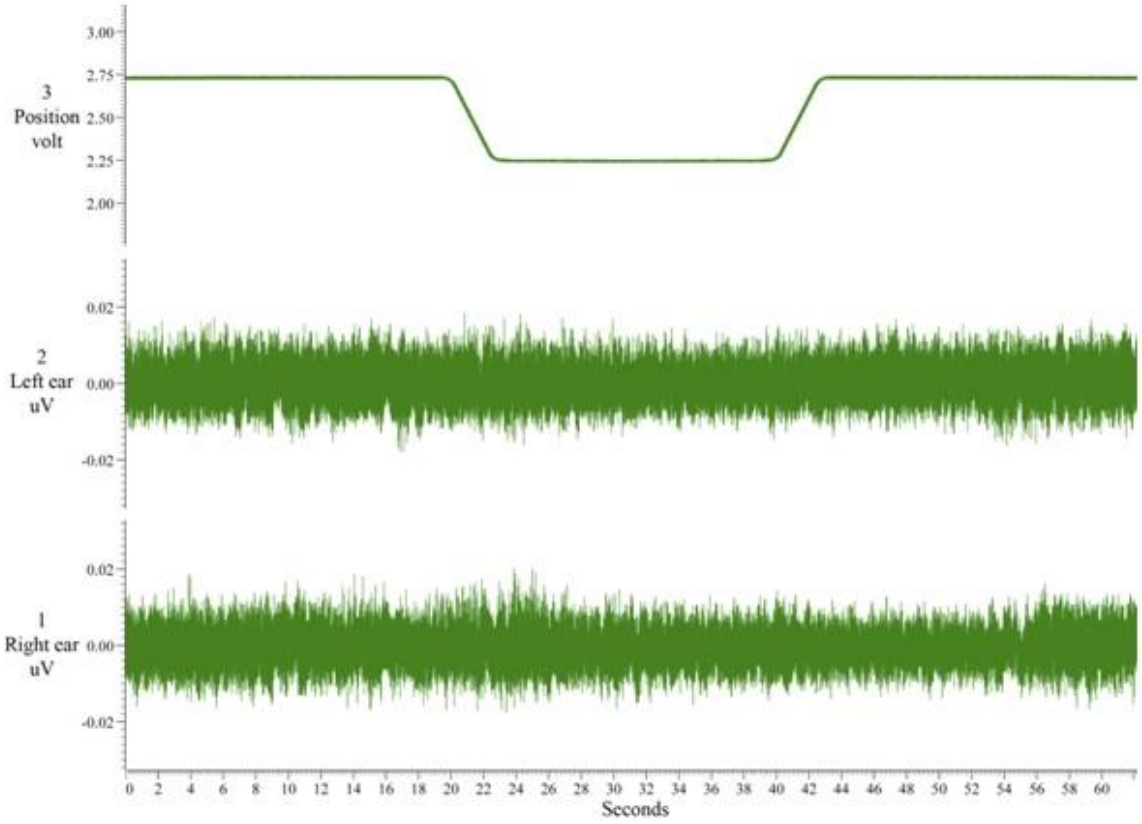

Figure 3-5 Screen capture of the recorded signals as displayed in Spike7 environment. Position waveform is displayed on top together with raw EVestG recordings from left and right ears (middle and bottom plots).

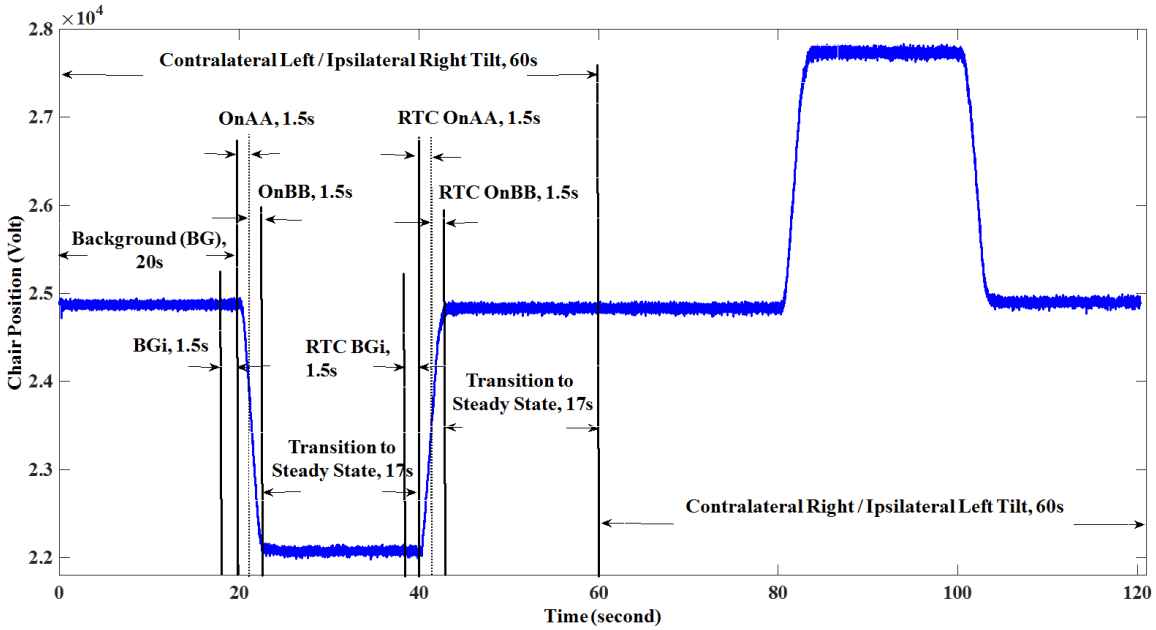

Figure 3-6 Segmentation of EVestG recordings according to motion profiles in side tilt.

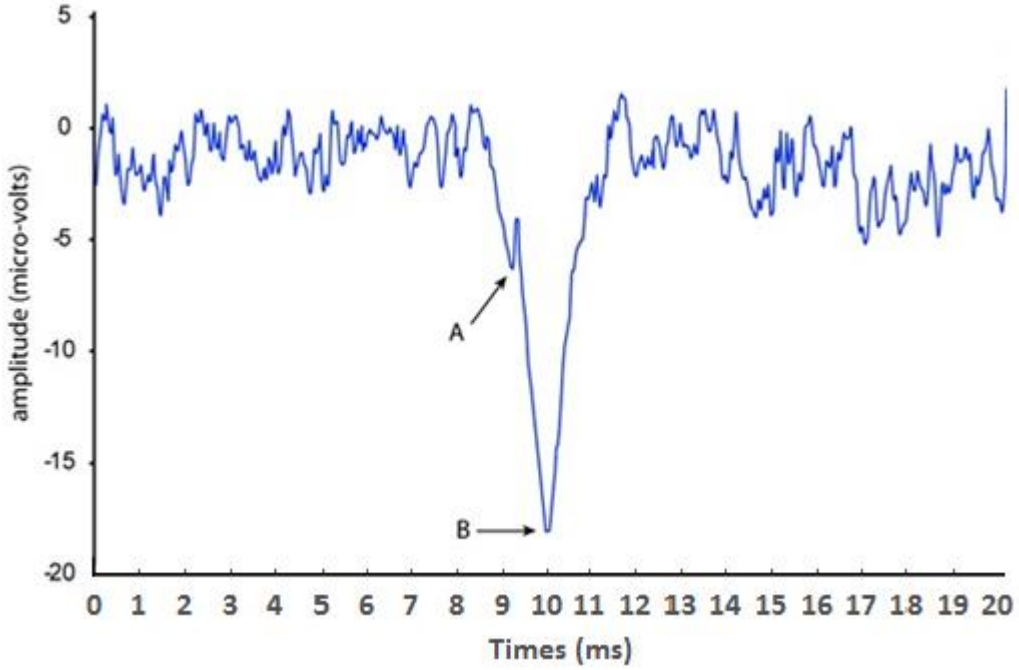

Figure 3-7 A typical output of the NEER algorithm; FP signal: (A) potential SP notch and (B) AP notch.

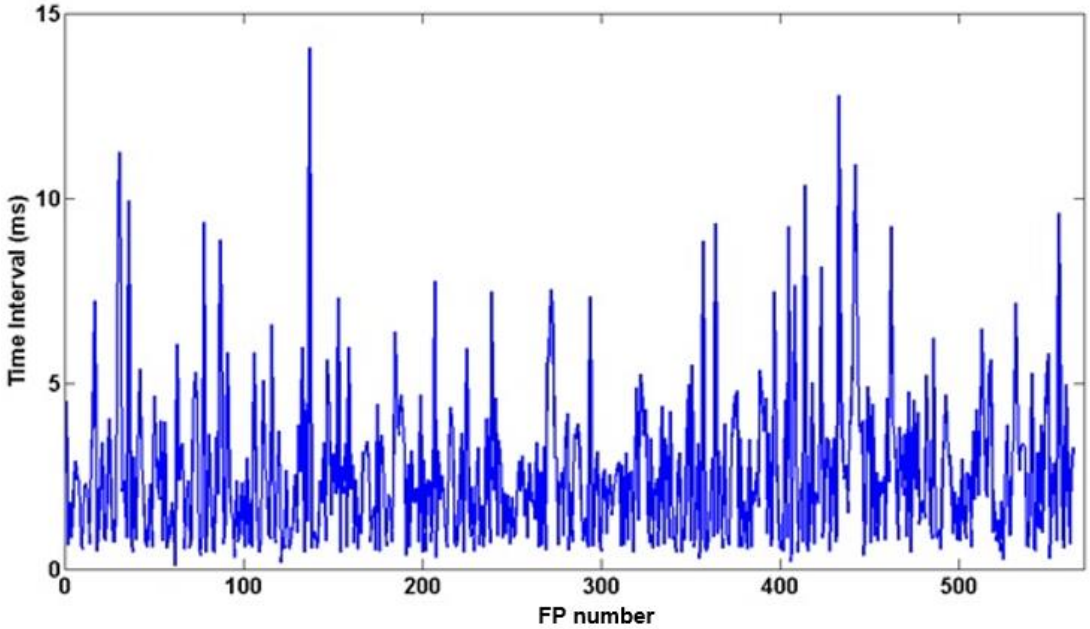

Figure 3-8 A typical time interval signal of the FP occurrences of the OnBB segment for a CT tilt, left ear of a control subject.

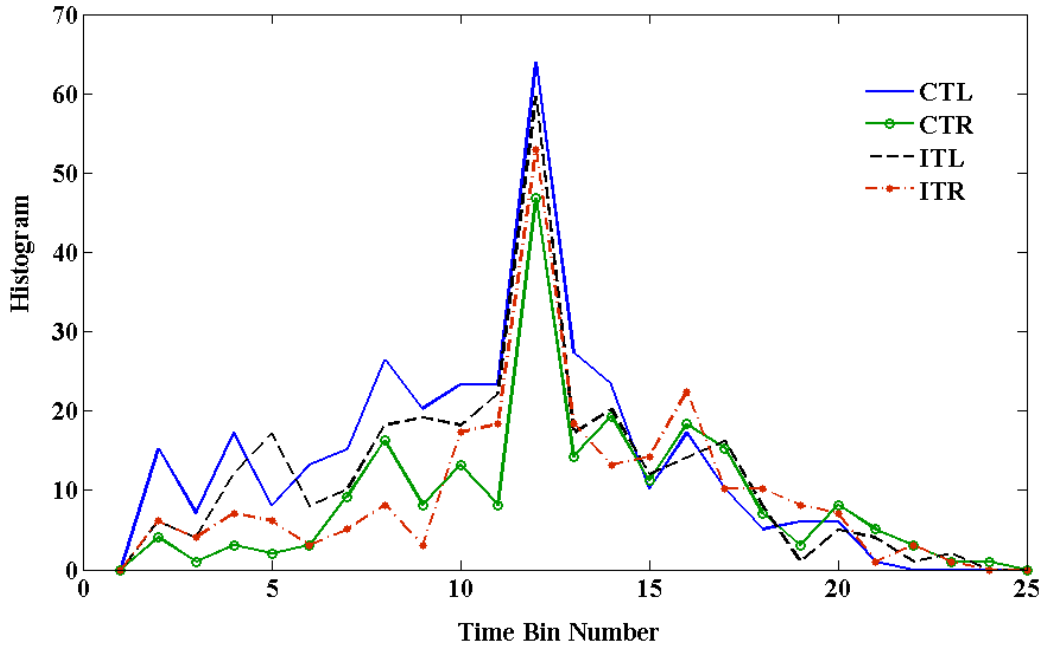

Figure 3-9 The histogram of the time interval signal for IT tilt left and right ear (ITR, ITL) and for CT tilt left and right ear (CTR, CTL) for the same control subject in Fig 3-8. Horizontal axis corresponds to different time bins which are logarithmically spreaded and in millisecond. Vertical axis denotes the number of events in each bin.

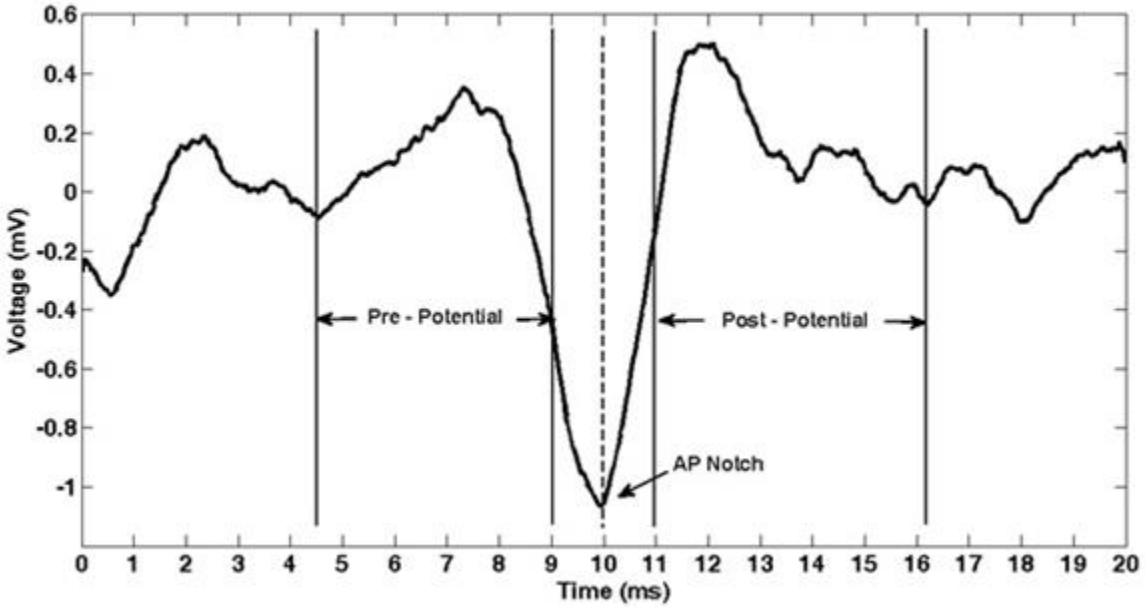

Figure 3-10. The normalized EVestG field potential of a typical control subject. The time durations of 4.5 ms (4.5 – 9.0 ms) and 5.2 ms (11.0 – 16.2 ms) before and after the AP are considered the pre- and post- potential intervals, respectively.

CHAPTER 4 **Results and Discussion**

4.1 Overview

In this chapter, the results of our classification method for seperating Meniere's from control subjects are presented followed by a discussion on selecting an optimum tilt, which results in the highest performance in terms of sensitivity and specificity. The results of the optimum tilt are then discussed in more details. Moreover, the results of similar classifiers in comparison to the designed ad-hoc classifier in this thesis are presented and discussed.

4.2 Meniere's/ Control Classification

Out of many features extracted from the contralateral (CT), ipsilateral (IT), back/forward, rotation, and up/down tilts' signals, 20, 50, 30, 15 and 17 features, respectively, were found significantly different among Meniere's patients and controls of the training dataset. Out of these features we used the 5 top features ranked by the mRMR algorithm as the best features for classification (Tables 4-1 to 4-4). In these tables, other

than the name of the selected feature, the original signal from which the feature was calculated and the significance level of the feature is shown.

The features are grouped in three categories based on their derivation: 1) the features calculated from the FP signals, 2) those calculated from one of the firing pattern representations, and 3) those calculated from the correlation calculation between the PDF of the time interval signals with the FP signals. The names of the features are summarized for the sake of space; also, the suffix of FP and frn_ptrn has been used to refer to the first (field potential signals) and second (firing pattern representation of FPs) categories of features, respectively. For example, the names of "Kurtosis_Pre_FP", "Energy_Pre_FP" or "Mean_abs_Pre_FP" show that the features are found by calculation of the kurtosis, total energy (from the entire frequency range), or mean of absolute value of the pre potential interval of the field potential signal (pre and post potential intervals are shown in Figure 3-10). The third category of features was simply named as correlation without any suffix.

As described in previous chapter, the designed ad-hoc voting classifier uses single-feature classifiers at its first level before getting the average vote. We examined both QDA and LDA as the first level classifiers. QDA classifiers' results showed a small (1% or 2%) improvement in accuracy compared to those of LDA classifiers for every tilt. However, the improvements were not large enough to reduce the possibility of the overfitting problem; thus, we decided to use (and demonstrate) only LDA results as they show more robustness in terms of classification performances.

The results of our ad-hoc voting system using LDA classifications in a leave-one-out routine of the training dataset (Alfred Hospital's data) are shown through Figures 4-1 to 4-4. Table 4-5 shows the summarized performance of classifications for the five upright

position tilts for the training dataset. The unclassified cases are those with a tie in vote as the assignment to either group. As can be seen in Table 4-5, using the training dataset, the side and up/down tilt classifiers achieved the highest accuracies (87% and 80%), respectively. Rotation and back/forward tilts showed a lower accuracy (70%).

The results of classifications of the test dataset (independent of training set – RHC's data) are shown in Figures 4-5 to 4-8. Among the 21 referred patients suspected of Meniere's in the test dataset, 9 of them (S1, S3, S7, S10, S12, S15, S18, S20, and S21) were clinically diagnosed with Meniere's disease, 3 subjects (S5, S8, and S13) were diagnosed with Benign paroxysmal positional vertigo (BPPV), 3 subjects (S2, S4, and S9) with Vestibular Neuritis, 1 Subject (S16) with Recurrent vestibulopathy, 1 Subject (S14) with VBI (Vertebra-basilar insufficiency), 1 subject (S19) with Barotrauma, and 3 subjects (S6, S11, and S17) were considered as non-Meniere's with non-specified dizziness. To simplify reading the results in Figures 4-5 to 4-8, the names of the diseases that the subjects were diagnosed with, are aligned with the subjects' numbers.

Table 4-6 shows the summarized performance of classifications for the five upright position tilts for test datasets. As can be seen in Table 4-6, using the test dataset, the side tilt showed the highest accuracy (84%), while the back/forward, rotation, and up/down tilts showed much lower accuracies (63%, 50%, and 31% , respectively). It should be mentioned that the classification results of non-Meniere's individuals with other types of dizziness were excluded from calculations of classifiers' performances (sensitivity, specificity, and accuracy) within the test dataset.

Note that for training dataset, we had only two groups of Meniere's and Healthy, while in the test dataset we also had non-Meniere's who were not considered healthy, but they

were not Meniere's patients either. However, as we were kept blind to the exact diagnosis of the individuals in the test dataset till the end of study, we only trained our classifier routine for two groups classification of Meniere's and Healthy (non-Meniere's); after all, the goal has been to provide an aid for Meniere's diagnosis. In addition, the number of non-Meniere's individuals with other types of dizziness, was not enough to run a post-hoc study on 3 or 4 groups classification to identify each of those conditions separately.

It is worth to note that side and back/forward tilts stimulate almost all the vestibular whilst the sitting up/down motion predominantly stimulates the saccule. The rotation predominantly stimulates the horizontal SCC suggestive the horizontal SCC has less impact on classification accuracy. Overall, the evidence suggests tilt selection may have an effect on classification accuracy.

A contributing factor in the up/down tilt's poor classification results, was probably due to the fact that this tilt's signals of the controls in the test dataset were noisier than the others. This was found by comparing the average ± standard deviation of the all tilts' signals in the two training and test dataset. We found that the up/down tilt signals of the test dataset were much noisier than the up/down tilt signals of the training dataset and also noisier than the other tilts' signals of the test dataset.

4.3 Supine Tilts Classification

As mentioned earlier, supine up/down tilt mainly stimulates the utricle while supine rotation tilt stimulates utricle, saccule and SCC components. Since our training dataset (Alfred's data) did not have the supine tilts' signal, we could not investigate the classification results using supine tilts' signals in the same manner as the other tilts. However, we did investigate the supine tilts' signals for classification in the test dataset

(RHC dataset), but we acknowledge that even with using leave-one-out routine the results are considered as training results because there were no independent groups for training and testing for supine tilts' signals; thus, the feature selection would be biased.

We extracted 20 and 37 features for supine rotation and supine up/down tilts, respectively. The results presented in Tables 4-7 and 4-8 show the 5 top features selected by the mRMR algorithm as the best features of these tilts. The classification results (Table 4-9) showed 89% and 83% accuracy for supine rotation and supine up/down, respectively. Data of one of the 10 RHC control individuals (S3) could not be analyzed due to noise corruption in rotation, supine up/down, and supine rotation tilts.

4.4 Discussion

So far, the classification results of the training and test datasets for the side, back/forward, rotation, and up/down tilts as well as classification of (training) results of supine tilts have been presented. In the following sections we discuss the candidate tilt for best classification of Meniere's versus control individuals.

4.4.1 Tilts' Results Comparison

In this study we aimed to investigate the seven orthogonal EVestG tilts for their use in Meniere's classification from health controls, and possibly come up with an optimum tilt for such purpose and simplify the recording protocol. Overall, the results of the side and back tilts showed the highest classification accuracies for Meniere's diagnosis compared to those of rotation and up/down tilts. The fact that side tilt stimulates almost the entire inner ear (including semicircular canals (SCCs) and otolithic organs) can be a strong justification for its best classification performance. Similarly, back/forward tilt stimulates

mostly anterior/posterior SCC, utricle and partially the saccule both in displacement and with respect to gravity. On the other hand, the upright rotation tilt stimulates predominantly the horizontal SCC, and the upright up/down tilt stimulates predominantly the saccule. Indeed, the rotation (in upright position) classification result was poor in both training and test datasets; this implies that horizontal SCC may have a lesser impact compared to the other vestibular organs. Extending this finding to the vertical SCCs (based on the supine recording data), we reason that the otolithic organs and more specifically the utricle (based on our sitting upright vertical (saccular) translation findings) might be the major contributors in Meniere's disease.

Generally, the endolymphatic fluid pressure (hydrops) is considered as the main cause of Meniere's disease that can occur inside the SCCs as well as otolithic organ [41]. Studies suggest that hydrops may force the utriculo-saccular duct (which separates the utricle and SCCs from the saccule and cochlea) to open and let endolymphatic fluid flow into utricle resulting in a change of utricular function due to an increase in its volume [100, 101]. On the other hand, there is evidence confirming that the vestibular response to brief head tilt stimuli is mostly the response of neurons innervating the utricle [101, 102].

A previous study has shown that in a simple neural model including SCCs and utricle, the change in firing rate of the utricle in response to a head (side or back/forward) tilt is much larger (a minimum order of 2-3 orders of magnitude) than the changes in firing rates of the SCCs [101, 102]. This model did not consider the effect of saccule, and assumed it would be negligible as the electrical potential of the utricle has a greater dynamic range than that of the saccule [103]. This is congruent with our EVestG recording results implying that EVestG recordings might be dominated by utricle response in side and

back/forward tilts. Taking into account that utricular maculae is closer to stapes, and thus to the EVestG recording electrode than the saccule and SCC sensory structures, it is more likely that the EVestG response is mostly driven from utricle [11]. Therefore, the tilts which stimulate mainly the utricle, such as side and back tilts, appear to be most diagnostic to Meniere's diagnosis through EVestG analysis. For this reason the supine rotation and supine up/down tilts are also expected to produce good results as they are designed to stimulate predominantly the labyrinth and utricle respectively.

The supine up/down tilt mainly stimulates utricle, while the supine rotation tilt stimulates the labyrinth. The high classification performances for the supine tilts (on the RHC data) confirm the utricle is likely the major responder at the EVestG electrode. In addition, in supine tilts, compared particularly to side tilt there is much lower level of noise in terms of motion artefacts as the subject is not supporting their head. Thus, in future studies, when the supine tilt data are expanded, it may show superiority to back/forward or side tilts in terms of classification accuracy.

4.4.2 **Side Tilt's Results in Detail**

Since the side tilt produced the best test classification accuracy, its results are discussed more in detail. For illustration purpose only, Figure 4-9 shows the mean and standard error region of two features (Feature #3 and #10 from Table 4-1); the classifiers of these two features showed the highest test accuracy among the 10 selected side tilt (both CT and IT stimuli) features. As can be seen, there is a clear separation of the mean values between the control and Meniere's subjects. However, the actual data did have some overlap; note that the circles around the mean show only the standard error.

Since the population of patients in this study was not large, a thorough interpretation of the features and their relation to the pathological physiology of the disease or their physiological significance cannot be fully elucidated; however, a review about the performance of the selected best features (shown in Table 4-1) are as follow:

Four out of the ten selected features (f1, f5, f9, and f10) resulted from fractal calculations. These features represent the complexity (either information dimension or Higuchi dimension) of the time interval signal as well as pre and post potential intervals of acceleration and deceleration segments from side tilt. Among these features, three of them (f1, f5, and f9) showed higher values for control group in comparison to those of Meniere' while feature (f10) showed the opposite result. According to f1 and f9, which are calculated based on only one segment (OnBB), they indicate that control signals in the deceleration (and possibly acceleration) period could be more complex or contain more information compared to their comparative Meniere's signals; however, this fact may not be true for the subtraction of two segments of the FP signal. Overall, the result is congruent with the general observation of higher complexity in healthy biological signals observed in other studies [76, 77].

- One feature (f2) resulted from the mean of the post-potential interval for the acceleration phase of the IT tilt. It showed that control subjects had larger mean value in the post-potential interval compared to those of Meniere's. This might be suggestive of an altered repolarization (K+) mechanism in patients.
- Two of the selected features (f3 and f8) resulted from kurtosis calculations. Control subjects showed lower kurtosis values and closer to the zero line compared to those

of the Meniere's subjects. This implies the probability distribution of controls' signals is closer to a normal distribution than that of the Meniere's signals.

- Feature (f4) predominantly represents high frequency components of the firing rate. This feature was found to be higher in control group, congruent with complexity measure mentioned above.
- One feature (f6) resulted from skewness calculation of the pre-potential interval for the difference between RTC OnAA and RTC OnBB (right) segments for the IT tilt. Skewness is a measure of asymmetry; for a normal curve it is equal to zero. This feature showed positive values for control group and negative values for Meniere's group. This implies that there is an asymmetry in the vestibular response during acceleration and deceleration phases, but this asymmetry (skewness) in control and Meniere's groups were in opposite directions. As OnAA and OnBB segments of IT tilt are reflective of excitatory and inhibitory stimulations, this may be indicative of a skew in excitatory and inhibitory signaling.
- Feature (f7) was the mean of absolute value of post-potential interval of acceleration phase between left and right signals. It showed higher asymmetry between left and right ears signals for Meniere's subjects compared to those of control subjects. Considering the fact that the majority of Meniere's subjects were unilaterally affected by Meniere's disease, this feature is likely reflective of the dysfunction in the more affected side.

The voting classification results showed 78.5% and 94% sensitivity and specificity for the training dataset (Alfred Hospital's data) and 78% and 90% sensitivity and specificity

for test dataset (RHC data).The results of our proposed classifications method in comparison with the clinical diagnoses are summarized as the followings:

- Seven out of the nine (S1, S3, S7, S10, S12, S15, S18, S20, and S21) clinically diagnosed Meniere's subjects were classified correctly (78% sensitivity).
- One (S1) of the two miss-classified Meniere's subjects (S1 and S15) had received 5 Gentamicin injections (this treatment severely impairs/destroys the vestibular function) to the right side twice, each 12 months apart prior to our assessment. Thus, Subject S1 could be excluded.
- Out of the nine subjects with BPPV, Vestibular Neuritis, VBI, Barotrauma, and Recurrent Vestibulopathy (S2, S4, S5, S8, S9, S13, S14, S16, S19), four of them (S9, S14, S16 and S19) were basically unclassified as they had a final vote of 0.5 on the boundary line. It is possible to use the strength of the vote (the post-probability of the voting LDA classifiers) to break the tie in the final vote; however, it should be noted that our classifier was not trained for these disorders; it was only trained to identify Meniere's from controls. Thus, the fact that these individuals were not found as either healthy or Meniere's, can be considered a positive outcome for the proposed classifier.
- The three referred subjects with non-specified dizziness (S6, S11, and S17) were classified correctly as non-Meniere.
- Out of the 10 age-matched control test subjects, 9 were classified correctly (90% specificity).

These results indicate the proposed ad-hoc classification method using EVestG data is robust since the training and testing accuracies were close to each other despite the fact

that data were recorded at two different sites with two different hydraulic tilting chair (but with the same protocol). Although the method was designed for classification of control subjects from Meniere's patients (using the training dataset), it showed adequate robustness for detecting other non-Meniere's vestibular disorders.

4.4.3 **Classifiers Comparison**

Adopting the same selected features used for the proposed ad-hoc classifier, we applied three structurally similar ensemble methods (Adaboost, Subspace and Begging) only on side tilt data, which already showed the best performance compared to other tilts. The results of training classifiers showed 100% accuracy for Adaboost method and 97% accuracy for Subspace and Bagging methods. However, much poorer testing results were achieved for test dataset. Tables 4-10, 4-11, and 4-12 show the test accuracies for Adaboost, Subspace, and Bagging methods, respectively.

Based on these results, while the accuracy of the three ensemble classifiers were much higher for training dataset they performed poorly in the test dataset; this is a classic example of overfitting problem and lack of robustness. On the other hand, our ad-hoc average voting classifier achieved a high accuracy for both training (87%) and test (84%) dataset. Thus, our ad-hoc classifier outperformed ensemble algorithms. The fact that the accuracy of designed classifier in training and test datasets were close, demonstrate its robustness. It is important to point out that due to randomness of feature selection in Bagging and Subspace methods, all of the algorithms were applied 50 times to the dataset and then, the average results on sensitivity, specificity and accuracy were reported.

Among the ensemble classifiers applied to the test dataset, Subspace obtained highest accuracy compared to the other ensemble methods; however, it should be noted that

Subspace showed the lowest sensitivity to the class of Meniere's patients compared to AdaBoost and Bagging. As expected, AdaBoost showed higher sensitivity in comparison with Bagging method, but it could not reach the sensitivity level of our ad-hoc classifier. As the training dataset was not noisy, the inferior performance of AdaBoost cannot be attributed to its well-known susceptibility to the outliers [104, 105], rather than lack of having fitness with the proposed classification problem. One explanation can arise from comparing the complexity of the employed algorithm. While the number of classifiers used by our ad-hoc method was equal to the number of the features (=10 classifiers), the proposed ensemble algorithms were developed based on a more complex combination of weak learners (=50 weak learners). This higher complexity could lead to over-fitting on the training dataset, which is congruent with the training accuracies. However, based on our empirical results using less number of weak learners for the ensemble method did not lead to better performances. Nevertheless, the number of weak learners for the ensemble algorithms cannot be tuned according to the test accuracies as it contradicts with the basic assumption that test data should be unseen.

In general, the average voting classification showed more reliable results. This method seems logically reasonable as well; one advantageous of this method is its simplicity, which is also very similar to the way a physician diagnoses a condition or disease. Typically, a physician goes through the results of several tests each confirming the existence of a symptom; then, decides on a diagnosis based on the existence of the majority of the symptoms; our proposed ad-hoc method acts in the same manner. It would be advantageous to test its reliability in larger population as well as other datasets.

4.5 Summary

In this chapter, we presented the results of our study regarding Meniere's diagnosis. We first presented our designed classifier results over different EVestG tilts' data, then introduced and reasoned the side tilt as the optimum tilt to be used in Meniere's/control classification. We also investigated and discussed the supine tilts classification; though it could be only discussed as training results because we had supine tilts' data only in RHC dataset. Finally, we compared and discussed our ad-hoc voting classification results for side tilt's data with the results of three ensemble classification methods.

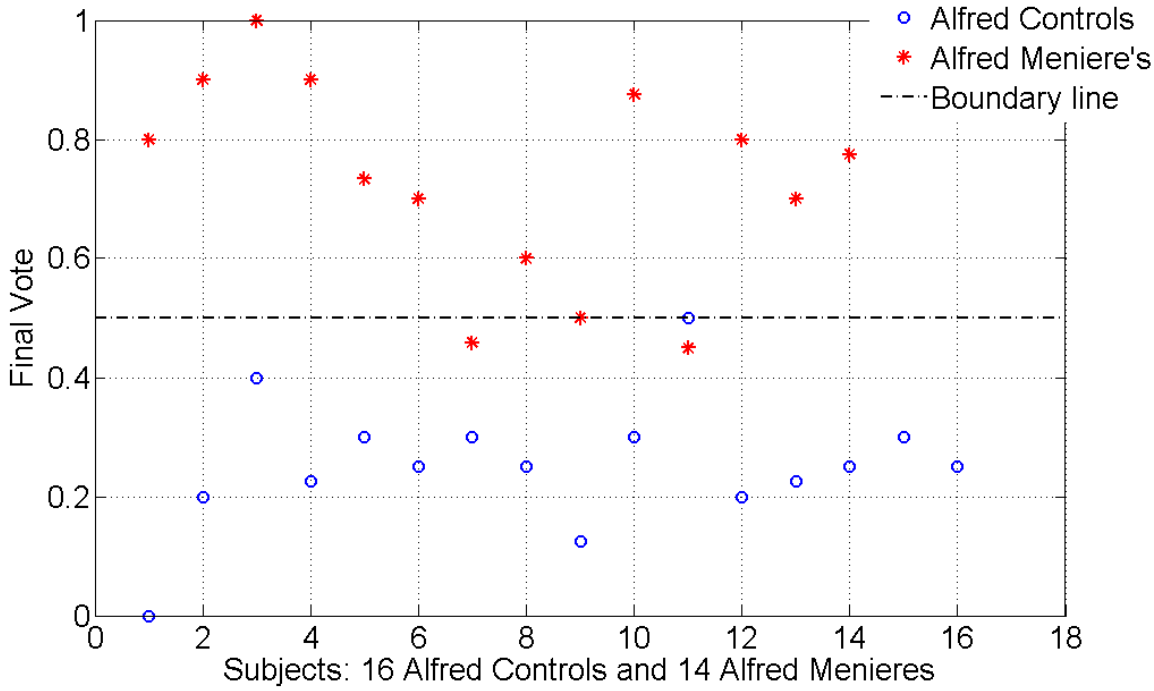

Figure 4-1. Classification results of the training subjects for side (CT&IT) tilt.

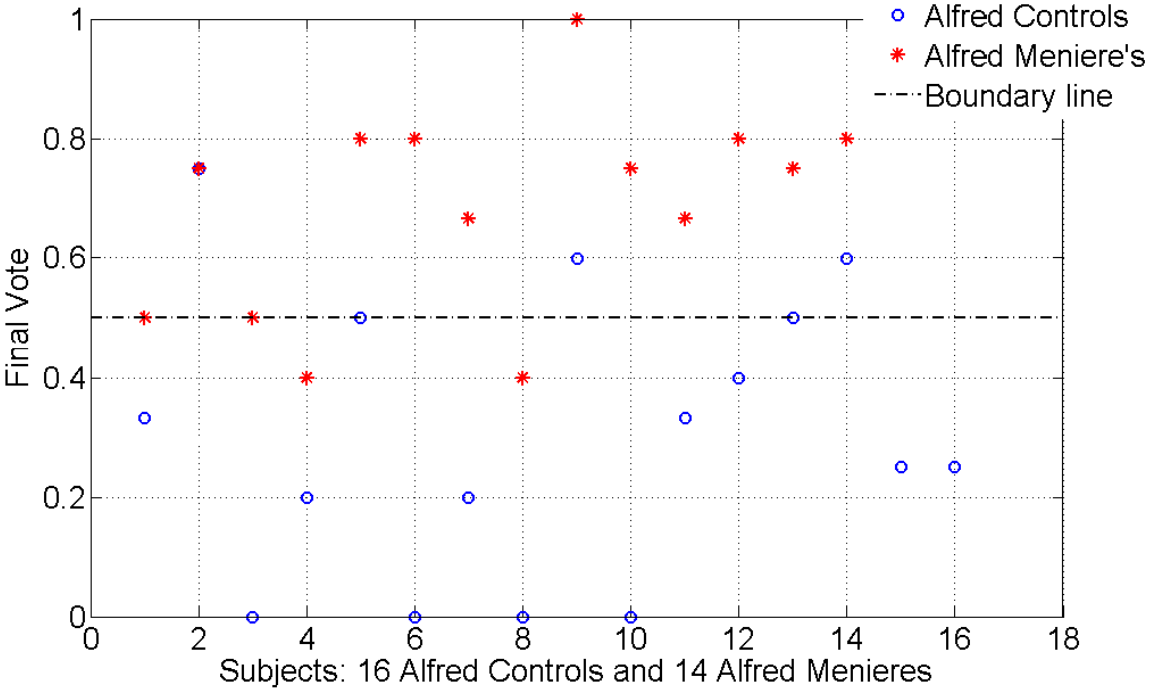

Figure 4-2. Classification results of the training subjects for back tilt.

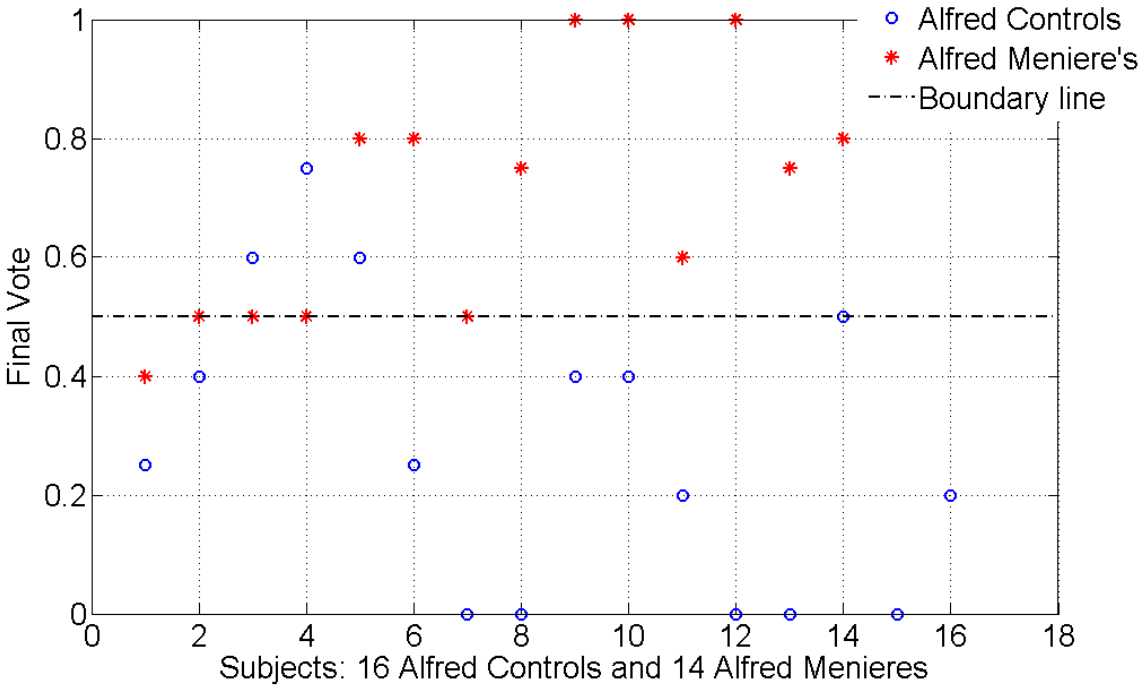

Figure 4-3. Classification results of the training subjects for rotation tilt.

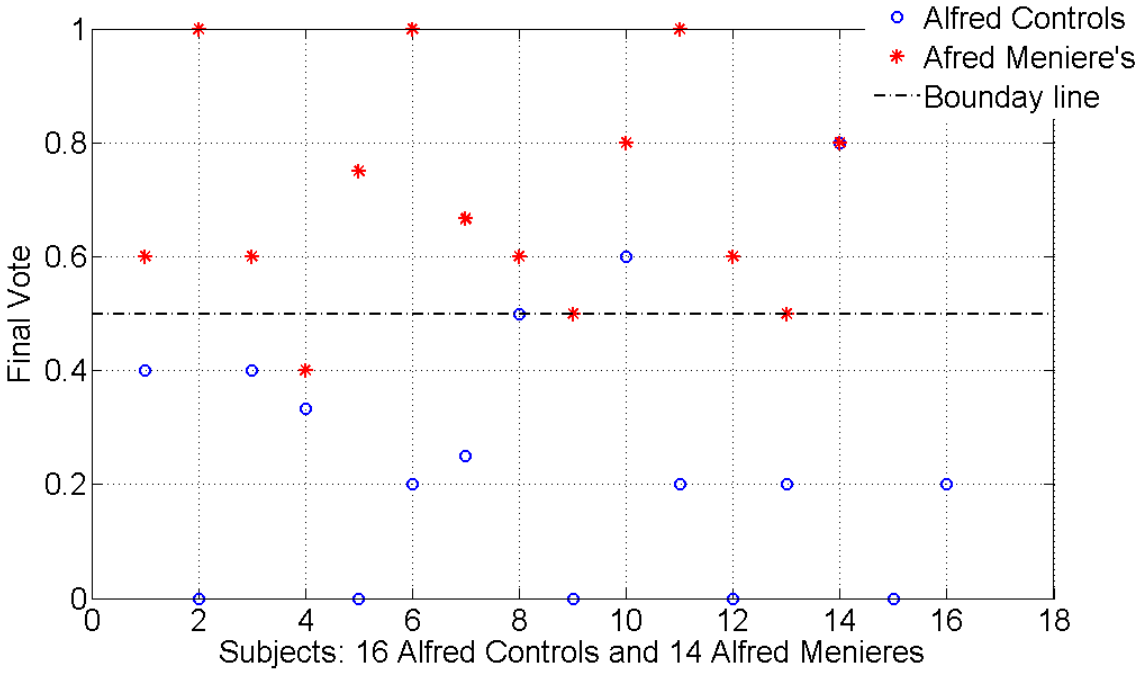

Figure 4-4. Classification results of the training subjects for up/down tilt.

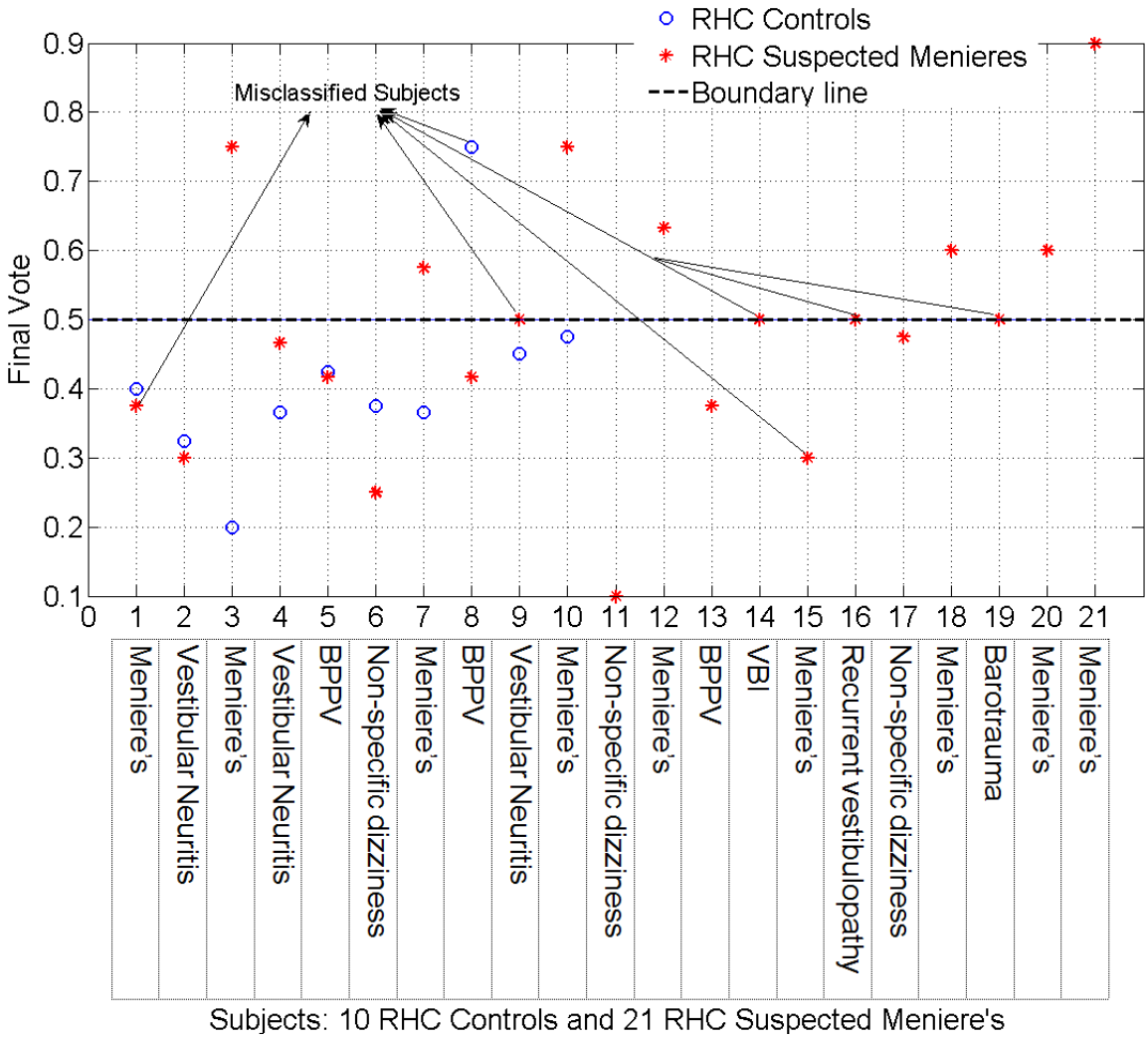

Figure 4-5. Classification results of the testing subjects for side (CT&IT) tilt.

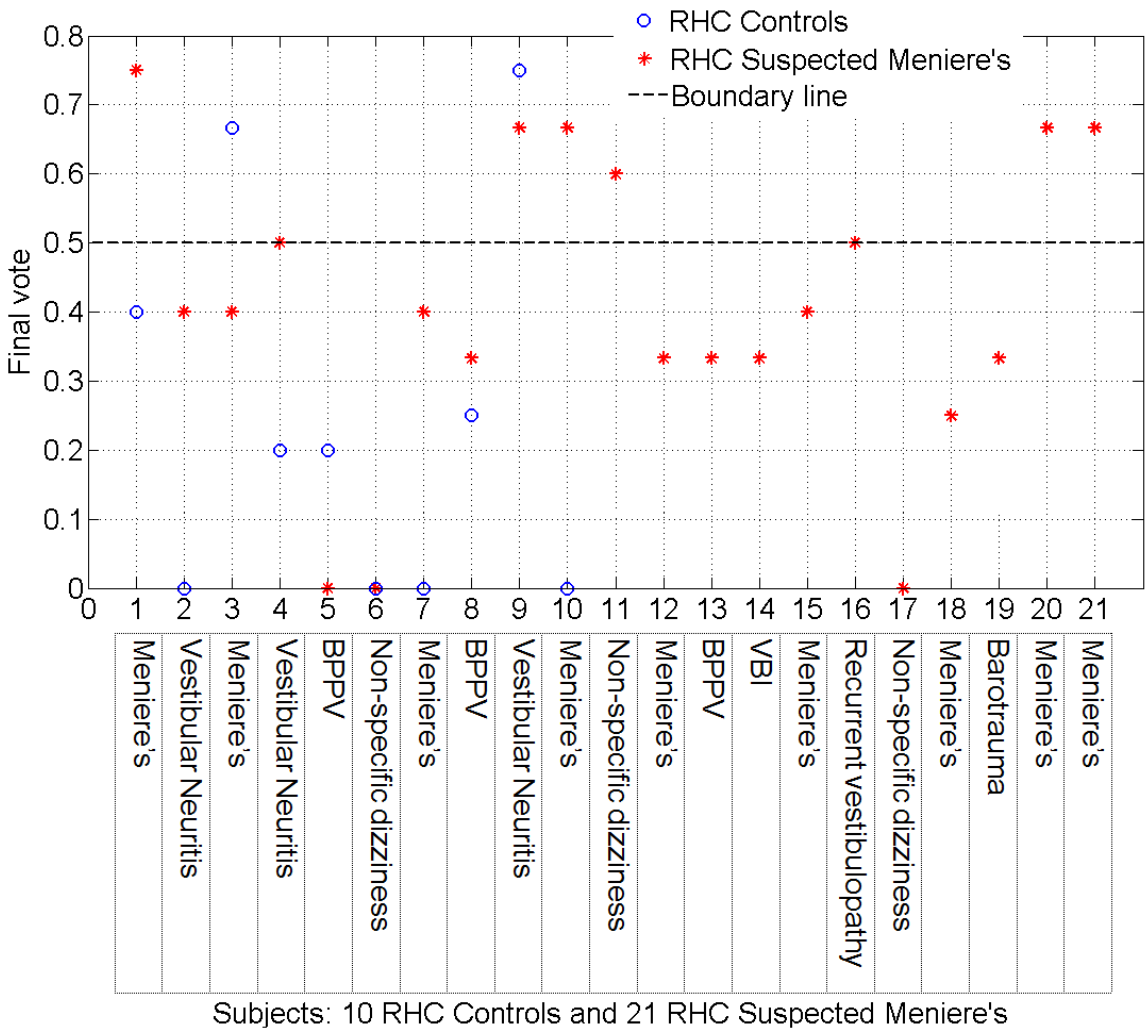

Figure 4-6. Classification results of the testing subjects for back tilt.

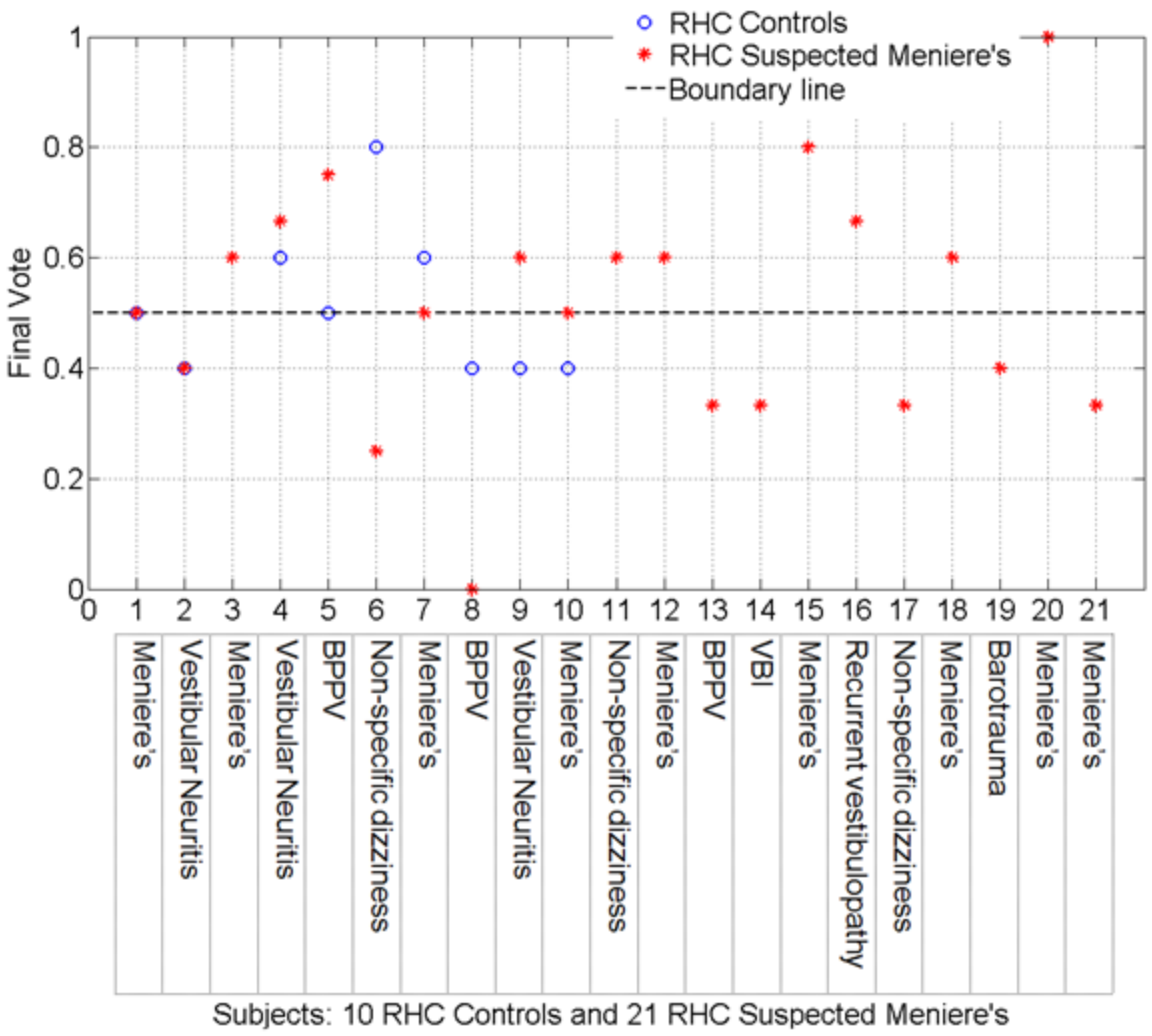

Figure 4-7. Classification results of the testing subjects for rotation tilt.

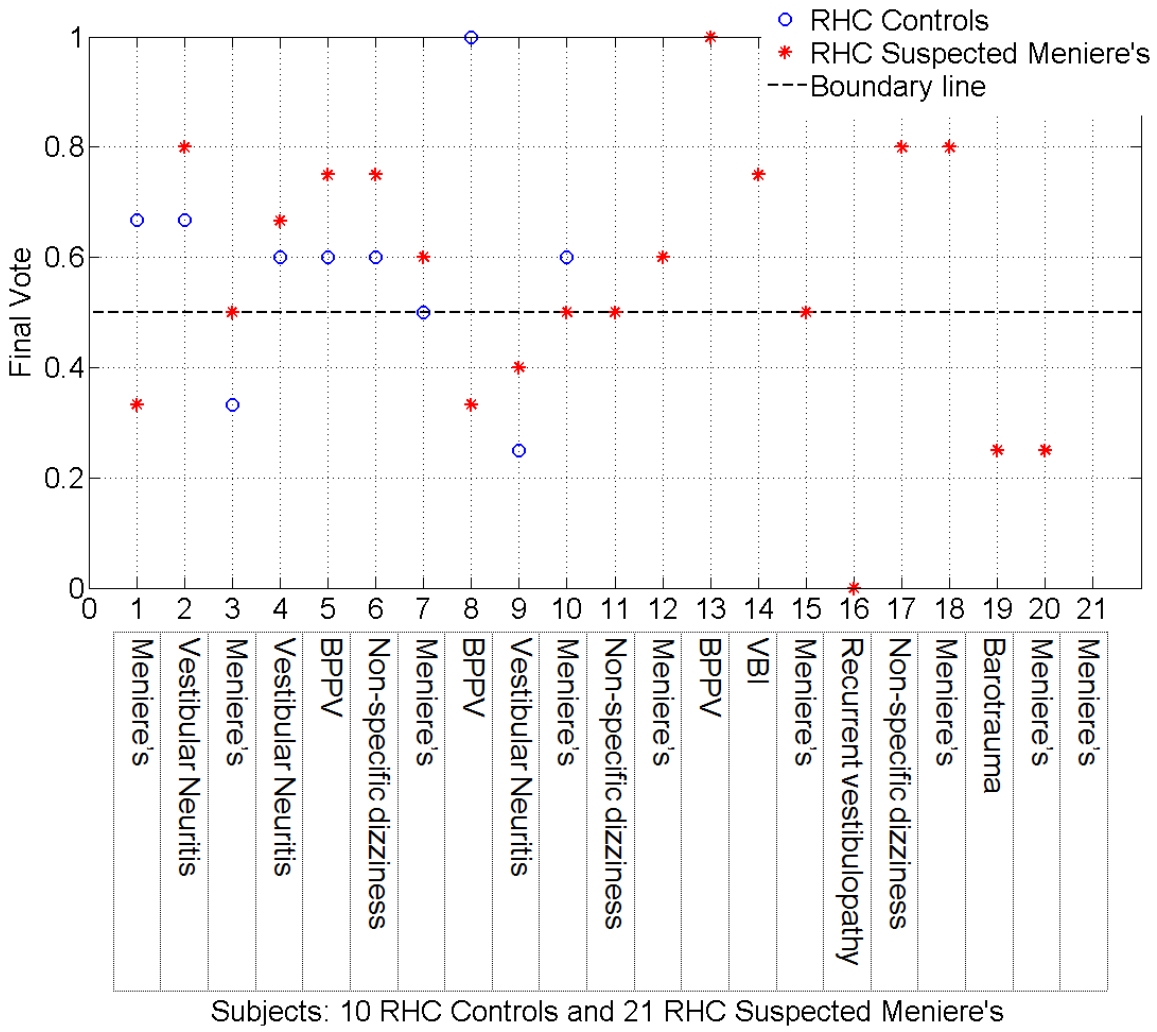

Figure 4-8. Classification results of the testing subjects for up/down tilt.

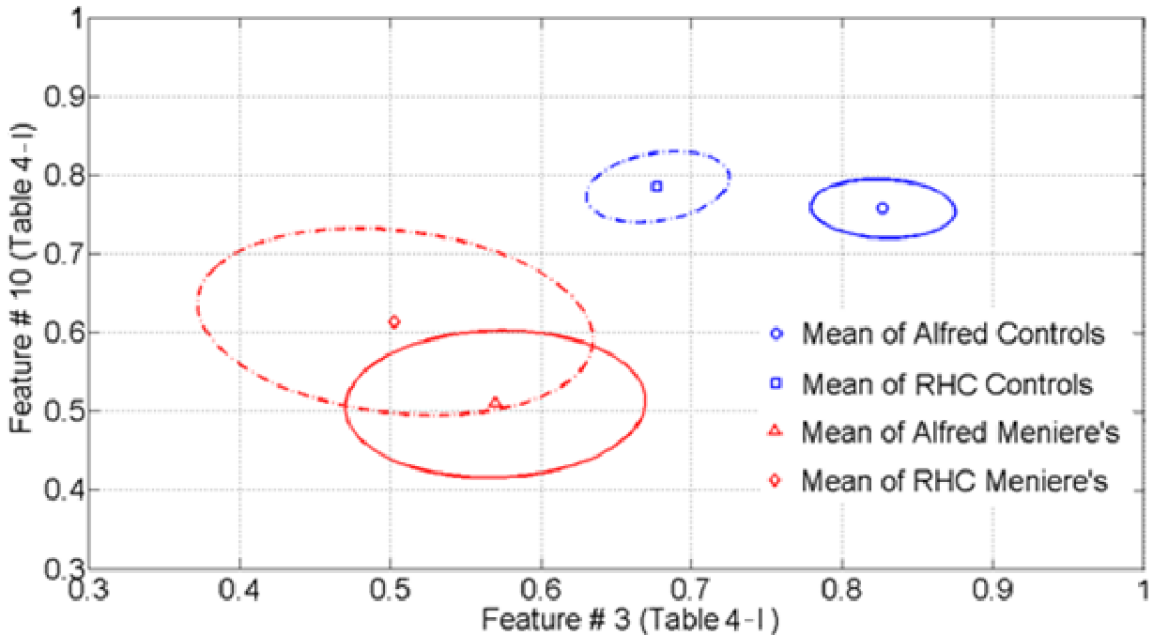

Figure 4-9. Scatter plot of the mean and standard error regions of two best features of side tilt derived from Meniere's (red) and healthy (blue) data of training (solid curve) and testing (dashed curves) dataset.

Table 4-1. Five best features for CT (feature 1-5), IT (feature 6-10) tilts.

Feature Number	Feature Name	Original Signal	controls (mean±std)	Meniere's (mean±std)
1	ID_ frn_ptrn *	OnBB – (L+R)	0.75±0.18	0.58±0.18
2	Mean_Post_FP*	RTC OnAA – (L)	0.15±0.22	-0.02±0.11
3	Kurtosis_Post_FP*	OnAA – (R)	2.3±0.65	3.5±1.50
4	Ave_min_ frn_ptrn *	OnAA – OnBB – (L+R)	0.05±0.017	0.03±0.018
5	Higuchi_Pre_FP*	BGi – OnBB – (R)	1.38±0.11	1.26±0.08
6	Skewness_Pre_FP**	RTC OnAA– RTC OnBB – (R)	0.57±0.26	0.02±0.38
7	Mean_abs_Post_FP**	RTC OnAA – (L–R)	0.15±0.06	0.39±0.19
8	Kurtosis_ frn_ptrn *	RTC OnAA – (R)	6.15±1.24	8.85±4.60
9	Higuchi_Post_FP*	OnBB – (R)	1.27±0.085	1.19±0.06
10	Higuchi_Post_FP*	RTC BGi – RTC OnAA (L)	1.29±0.056	1.42±0.17

* MEANS $P<0.05$ AND ** MEANS $P<0.01$.

Table 4-2. Five best features for Back/forward tilt.

Feature Number	Feature Name	Original Signal
1	CD_Post_FP*	OnBB – (L)
2	mode_ frn_ptrn **	BGi – OnBB – (L+R)
3	PreEnergy_FP**	RTC OnBB – (L–R)
4	Correlation*	BGi – OnAA – (L)
5	ID_Pre_FP*	BGi – OnAA – (R)

* MEANS $P<0.05$ AND ** MEANS $P<0.01$.

Table 4-3. Five best features for Rotation tilt.

Feature Number	Feature Name	Original Signal
1	Std_Pre_FP**	BGi – OnBB – (L)
2	Skewness_Post_FP*	OnBB – (L–R)
3	Kurtosis_Pre_FP*	RTC BGi – RTC OnAA – (R)
4	Mean_abs_Pre_FP*	OnAA – (R)
5	Mode_ frn_ptrn *	RTC BGi – RTC OnAA – (L–R)

* MEANS $P<0.05$ AND ** MEANS $P<0.01$.

Table 4-4. Five best features for Up/down tilt.

Feature Number	Feature Name	Original Signal
1	Higuchi_Pre_FP**	RTC OnAA – (R)
2	Mode_ frn_ptrn **	RTC OnAA – RTC OnBB – (L+R)
3	Mean_abs_Pre_FP*	RTC OnBB – (R)
4	Skewness_Pre_FP**	RTC BGi – (L–R)
5	Higuchi_Post_FP*	BGi – (R)

* MEANS $P<0.05$ AND ** MEANS $P<0.01$.

Table 4-5. True and EVestG-assigned classes of the training dataset

	True/Assigned Classes	**Meniere's**	**Non-Meniere's**	**Unclassified**
Side Tilt	Meniere's (n=14)	11	2	1
	Healthy controls (n=16)	0	15	1
	Sensitivity of detecting Meniere's (%): 11/14= 78.5 **Specificity of detecting controls (%): 15/16= 94** **Accuracy (%): 87**			
Back/ forward Tilt	Meniere's (n=14)	10	2	2
	Healthy controls (n=16)	3	11	2
	Sensitivity of detecting Meniere's (%): 10/14=71 **Specificity of detecting controls (%): 11/16= 69** **Accuracy (%): 70**			
Rotation Tilt	Meniere's (n=14)	9	1	4
	Healthy controls (n=16)	3	12	1
	Sensitivity of detecting Meniere's (%): 9/14=64 **Specificity of detecting controls (%): 12/16= 75** **Accuracy (%): 70**			
Up/ down Tilt	Meniere's (n=14)	11	1	2
	Healthy controls (n=16)	2	13	1
	Sensitivity of detecting Meniere's (%): 11/14= 78.5 **Specificity of detecting controls (%): 13/16= 81** **Accuracy (%): 80**			

Table 4-6. True and EVestG-assigned classes of the test dataset (RHC)

	True/Assigned Classes	**Meniere's**	**Non-Meniere's**	**Unclassified**
Side Tilt	Meniere's (n=9)	7	2	0
	BPPV or VN (n=6)	0	5	1
	RV, VBI or Barotrauma (n=3)	0	0	3
	Non-specific dizziness (n=3)	0	3	0
	Healthy controls (n=10)	1	9	0
	Sensitivity of detecting Meniere's (%): 7/9 =78 **Specificity of detecting controls (%): 9/10=90** **Accuracy (%): 84**			
Back/ forward Tilt	Meniere's (n=9)	4	5	0
	BPPV or VN (n=6)	1	4	1
	RV, VBI or Barotrauma (n=3)	0	2	1
	Non-specific dizziness (n=3)	1	2	0
	Healthy controls (n=10)	2	8	0
	Sensitivity of detecting Meniere's (%):4/9=44 **Specificity of detecting controls (%): 8/10= 80** **Accuracy (%): 63**			
Rotation Tilt	Meniere's (n=9)	5	1	3
	BPPV or VN (n=6)	3	3	0
	RV, VBI or Barotrauma (n=3)	1	2	0
	Non-specific dizziness (n=3)	1	2	0
	Healthy controls (n=10)	3	4	2
	Sensitivity of detecting Meniere's (%): 5/9= 56 **Specificity of detecting controls (%): 4/9=44** **Accuracy (%): 50** **Note:** one control data (S3) is out of analysis due to noise.			
Up/ down Tilt	Meniere's (n=9)	4	2	3
	BPPV or VN (n=6)	4	2	0
	RV, VBI or Barotrauma (n=3)	1	2	0
	Non-specific dizziness (n=3)	2	0	1
	Healthy controls (n=10)	7	2	1
	Sensitivity of detecting Meniere's (%): 4/9= 44 **Specificity of detecting controls (%): 2/10=20** **Accuracy (%): 31.5**			

Table 4-7. Five best features for Supine up/down tilt

Feature Number	Feature Name	Original Signal
1	SD_ frn_ptrn **	OnAA – OnBB – (L–R)
2	Mode_ frn_ptrn *	BGi – OnAA – (R)
3	median_ frn_ptrn **	RTC BGi – RTC OnBB – (L–R)
4	Higuchi_Pre_FP**	BGi – OnBB – (L)
5	Kurtosis_Post_FP**	RTC BGi – RTC OnAA – (L)

* MEANS $P<0.05$ AND ** MEANS $P<0.01$.

Table 4-8. Five best features for Supine rotation tilt

Feature Number	Feature Name	Original Signal
1	Higuchi_Pre_FP**	BGi – OnAA – (L)
2	ID_Post_FP*	OnAA – OnBB – (R)
3	Mean_Post_FP**	RTC OnBB – (R)
4	NoF_ frn_ptrn *	RTC BGi – (L)
5	Higuchi_Post_FP**	BGi – OnAA – (L)

* MEANS $P<0.05$ AND ** MEANS $P<0.01$.

Table 4-9. True and EVestG-assigned classes of the RHC dataset

	True/Assigned Classes	**Meniere's**	**Non-Meniere's**	**Unclassified**
Supine rotation Tilt	Meniere's (n=9)	8	1	0
	Healthy controls (n=10)	1	8	0
	Sensitivity of detecting Meniere's (%): 8/9= 89 **Specificity of detecting controls (%): 8/9=89** **Accuracy (%): 89** **Note:** one control data (S3) is out of analysis due to noise.			
Supine up/ down Tilt	Meniere's (n=9)	6	1	2
	Healthy controls (n=10)	0	9	0
	Sensitivity of detecting Meniere's (%): 6/9= 67 **Specificity of detecting controls (%): 9/9= 100** **Accuracy (%): 83** **Note:** one control data (S3) is out of analysis due to noise.			

Table 4-10. True and EVestG-assigned classes of side tilt test dataset using AdaBoos method

	True/Assigned Classes	**Meniere's**	**Non-Meniere's**
Side Tilt	Meniere's (n=9)	5	4
	BPPV or VN (n=6)	1	5
	RV, VBI or Barotrauma (n=3)	2	1
	Non-specific dizziness (n=3)	0	3
	Healthy controls (n=10)	4	6
	Sensitivity, Specificity, Accuracy (%): 56 , 60 , 58		

Table 4-11. True and EVestG-assigned classes of side tilt test dataset using Subspace method

	True/Assigned Classes	**Meniere's**	**Non-Meniere's**
Side Tilt	Meniere's (n=9)	3	6
	BPPV or VN (n=6)	1	5
	RV, VBI or Barotrauma (n=3)	2	1
	Non-specific dizziness (n=3)	0	3
	Healthy controls (n=10)	0	10
	Sensitivity, Specificity, Accuracy (%): 33 , 100, 68.4		

Table 4-12. True and EVestG-assigned classes of side tilt test dataset using Bagging method

	True/Assigned Classes	**Meniere's**	**Non-Meniere's**
Side Tilt	Meniere's (n=9)	4	5
	BPPV or VN (n=6)	1	5
	RV, VBI or Barotrauma (n=3)	3	0
	Non-specific dizziness (n=3)	0	3
	Healthy controls (n=10)	3	7
	Sensitivity, Specificity, Accuracy (%):44, 70, 58		

CHAPTER 5 **Conclusion and Future Work**

5.1 Conclusion

The result of this study has been encouraging on the use of EVestG signals to extract characteristic features sensitive to Meniere's disease. Specifically, the side tilt's signals showed characteristic features with more sensitivity and specificity compared to other tilts' signals. Additionally, supine tilts have shown the potential for Meniere's/control classification; as inherently the noise level in supine tilts' data is lesser than in other tilts, it should be tested in future with a larger dataset.

One reason for the noisy data in our experiment were due to the use of different types of (active and reference) electrodes with different impedances. Hence, background signals such as power line interferences, which typically appear as peaks of 50/60 Hz harmonics in frequency domain and occur from a common mode voltage, will be converted to differential mode by mismatched differential electrode impedances and will seriously affect SNR. This causes NEER to detect a noisy FP or firing pattern signal. Recently, in our team EVestG signals with two similar active and reference electrodes were recorded

and shown to yield a significant (p<0.05) higher SNR [72]. The results confirmed the use of mentioned electrodes instead of different electrodes in the traditional ECOG method.

Overall, the results of this study show the potential of EVestG signals towards generating an adequate set of bio-features as a diagnostic and monitoring aid for dizziness related diseases, especially Meniere's disease. The importance of this method is that it may prove to be also an assistive tool for differentiating different confounding pathologies. The results may lead to a more accurate objective and non-invasive clinical assessment assist of Meniere's disease diagnosis. It can be a quick screening tool as the experiment in an optimized system will take about half an hour and the analysis, once written as a user-friendly software, will take only a few minutes.

5.2 Future Work Recommendations

While we are encouraged by the results, we must point out that the size of the dataset is still small. In fact, 256 potential participants (dizzy patients) were identified by the collaborating physician, out of which 91 agreed to be contacted about EVestG recording. However, only 21 individuals actually participated and completed the EVestG test. The rest of patients who agreed to be contacted, either did not show up at the EVestG recording appointment or rejected to be a participant in the study when contacted. This illustrates the difficulty in recruiting patients for the study. Although EVestG testing is safe, quick and free of adverse effects, Meniere's patients, particularly those who do not feel well, are reluctant to participate.

On the other hand, as mentioned before, EVestG signals have shown potential in diagnosis of other diseases such Parkinson's and depression diseases in other studies [59, 60]. Additionally, most of Meniere's patients are also suffering from a mild/moderate

depression and anxiety disorders as they become debilitated in their daily living lifestyle due to this disease. Although we had only one patient with mild depression in our dataset, still there is a chance of having more depressed patients in a larger dataset. Hence, it is necessary to investigate if the selected features in this study are exclusive for diagnose of Meniere's disease rather than representative of other diseases or other abnormal neurological conditions. This requires using separate datasets of patients with relevant diseases and improving our two-class classifier to a multi-class classifier algorithm.

Moreover, classification results may be improved by using Support Vector Machine (SVM) classifier instead of LDA classifier in our ad-hoc classification method. This is due to the fact that SVM computes the optimal hyper plane with respect to margin maximization, which usually ends up in better performances in classification results compared to LDA [106].

Considering the above points, the following improvements and works are suggested as future studies:

- Apply the same selected features on the available datasets from patients with Parkinson's, concussion and depression.
- Evaluation of the proposed algorithms on a larger dataset using all the tilts including supine tilts and perhaps modifying the experiment by utilizing similar recording electrodes.
- Development of classifiers for patients with only depression or one vestibular illnesses, such as BPPV and Vestibular Neuritis and avoid correlated features. Then, prepare a similar average voting system for the results of classification so that each test subject would have a final vote of diagnosis for every disease. Thus,

building a smart classifier which identifies every patient with the disease that is associated with the highest achieved vote.

- Substitution of LDA classifiers with SVM ones in our ad-hoc method.

This is an ongoing study and we hope to extend this research until it will be a beneficial practical method in clinical diagnostic area.

Appendix A. Questionnaires

A.1 Montreal Cognitive Assessment (MoCA)

MoCA is designed as a rapid screening instrument for mild cognitive dysfunction [74]. It assesses different cognitive domains such as the followings:

- Attention
- Concentration
- Executive functions
- Memory
- Language
- Visuoconstructional skills
- Conceptual thinking
- Calculations
- Orientation

Administering the MoCA for cognitively healthy people takes about 10 minutes. The total possible score is 30 points; it is calculated by the sum all sub-scores with adding one

point for an individual who has 12 years or fewer of formal education. A final total score of 24 and above is considered normal.

A.2 Montgomery Asberg Depression Rating Scale (MADRS)

MADRS is a rating scale comprised of ten items and used for assessment of depression levels. Each item is rated between 0 and 6 (a 7-point scale) where 0 indicates absence of the symptom and 6 indicates extreme presence of the symptom [75]. The time frame of the scale covers 1 month prior to the test.

The items rated are:

- Apparent and reported sadness
- Inner tension
- Reduced sleep and appetite
- Concentration difficulties
- Lassitude
- Inability to feel
- Pessimistic and suicidal thoughts

A score of 0-6 indicates normal or recovered from depression, 7-19 mild depressive symptoms, 20-34 moderate depression and 35-60 exhibits severe depression.

A.3 Vestibular Disorders Activities of Daily Living Scale (VADL)

VADL is an assessment tool designed to evaluate self-perceived disablement in individuals with vestibular impairment [107]. It includes 28 items each evaluating the effects of vertigo and balance disorders in everyday activities of daily living. The tool is initially designed to be useful for evaluating functional limitation and perceived disability before and after therapeutic intervention.

The items are broken down into 3 subscales: functional, ambulatory, and instrumental. The functional subscale evaluates the individual's perception of basic self-maintenance tasks (such as sitting up from lying down or dressing up the body); the ambulatory subscale evaluates perception of mobility related skills (such as walking on surfaces or going on steps) and the instrumental subscale looks at self-perception in higher-level more socially complex tasks (such as driving a car or playing a sport).

The questionnaire requires individuals to rate their self-perceived disablement level on a scale that ranges from 1 (independent) to 10 (too difficult, no longer performed); the maximum score would be 280. Subject are also supposed to rate every item based on their current performance compared to their performance before developing an inner ear problem.

Appendix B. Fractal Dimension Calculations

B.1 Introduction

Fractal objects arise from a variety of sources and have been observed frequently in nature as well as in theoretical models [108]. These objects can be a geometrical figure, a process or a set of data like a time series, etc. FD is usually interpreted as the measure of the degree of space-filling (meandering, roughness, brokenness, or irregularity) of an object.

One of the exceptional mathematical characteristics of a fractal object is that it can be described by a non-integer or a fractional value called "Fractal dimension (FD)" that exceeds its topological dimension [109, 110]. This non-integer value results when measuring an intrinsic property (associated with fractal's geometry, entropy, variance, etc.) of the fractal called self-similarity or self-affinity. In fact, the self-similarity of the object is confirmed if a portion of the object is exactly or approximately a scaled down version of itself; however, this is only true for theoretical fractals. In contrast, for natural fractals the scales are different in different directions (several scaling factor); hence, they are called self-affine fractals.

Appendix B.

Assuming frequent measurements of a length of a simple object like a curve with a measurement scale of size r, the length of the curve, $L(r)$, will be the number, $N(r)$, of such scale required to cover the curve length from one end to the other. If the scale size approaches zero, the length of the curve will approach a finite value (in Euclidean space) as below:

$L(r) = \lim_{r\to 0} N(r)$ r = constant $\qquad L(r) = \lim_{r\to 0} N(r)\, r^{D\varepsilon}$ = constant $<\infty$ (B.1)

This is contrary in a fractal object; meaning that if the scale size decreases toward zero, the length of the fractal increases to an unlimited value ($L(r)\to\infty$). In fact, $L(r)$ can only be constant in a specific condition when assuming an exponent, D, for the scale size, r, in a power-law relationship such as below:

$$L(r) = N(r)r^{D} \tag{B.2}$$

Thus, the new exponent, which was $D = 1$ in equation (B.1), may suppress the rate of diverging $L(r)$ to a point that it may become constant (at some critical value D_L) according to the following criteria:

$$\begin{cases} if\ D < D_L & L(r)\to\infty \\ if\ D = D_L & L(r) = constant \\ if\ D > D_L & L(r)\to 0 \end{cases} \tag{B.3}$$

This critical exponent value D_L is no longer an integer value and is called length fractal dimension. It can be shown that D_L is related to the slope of the log-log plot of successive measurements of $L(r)$ [111].

In the same way as the above simple example, if a power-law relation for a self-similar fractal object satisfies as below;

$$N_r \sim (\tfrac{1}{r})^{D} \quad for\ r\to 0 \tag{B.4}$$

Where N_r is the number of self-similar objects used to cover the original object, and r is the ratio used to subdivide the original object into N_r self-similar objects [79, 112]; then, FD is defined as:

$$D = \frac{\log(N_r)}{\log(1/r)} \tag{B.5}$$

For real (natural) objects, which are not self-similar, we cannot apply the formula in (B.5) directly to obtain the FD. Instead, the estimated FD based on empirical approach must be used. Many methods have been proposed, and developed in the literature [79, 112]. These methods differ in the ways they approximate the quantity N_r in the above equation, but similarly they use some version of the power-law relationship between the measured quantities of an object and step sizes to derive the estimates of the critical exponent.

The quantity of an object is expressed in terms of, for example, length, area, or number of boxes (cells) needed to cover the object. The step size refers to the scale or resolution of measuring units used. The common procedure for most of methods consists of three following steps:

- Measure the quantities of the object under consideration using various step sizes.
- Plot log of measured quantities versus log of step sizes and fit a least squares regression line through the data points.
- Use the slope of the regression line to derive the critical exponent of the object called as FD.

Fractal objects can be analyzed in three different aspects: 1) measuring the geometry or the shape of the projection of a fractal object while relied on the uniform distribution assumption of the shape properties called as morphological fractal dimension, 2) measuring the information (uniform or non-uniform) distribution of a fractal object called as entropy

fractal dimension, 3) measuring fractal properties of a changed version of the original fractal using a transformation function called as transform fractal dimension.

FD analysis is widely used as an analytical tool in a variety of research areas particularly signal processing (of biological signals) [111, 112]. It measures the irregularity or the complexity of the signal; complexity is defined as patterns and their organization into hierarchies, which often change by time and can be grouped into several classes such as structural, dynamic, functional, synergetic, and design complexity [113]. As the dimension of a line or segment is equal to one and the dimension of a plane is equal to two, then FD of a signal is a continuous real value between one and two depending on the degree of irregularity of it. The more complex the signal, the higher the FD value will be.

We will explain Higuchi fractal dimension and Entropy based fractal dimension, which are two effective methods for calculation of FD, used in this work.

B.2 Higuchi Fractal Dimension

Among the various morphological fractal dimension methods, the Higuchi fractal method is well suited for studying signal fluctuation in one dimension. In 1988 Higuchi proposed an efficient algorithm for measuring the FD of discrete time sequences [78]. Higuchi's algorithm calculates the FD directly from time series. It has already been used to analyze the complexity of biological signals [114].

Given a one dimensional time series $X = x[1], x[2], \ldots, x[N]$, the algorithm to compute the HFD can be described as follows:

Form k new difference time series X_k^m with different lags which is defined by

$$X_k^m = \left\{x[m], x[m+k], x[m+2k], \ldots, x\left[m + int\left(\frac{N-m}{k}\right) \times k\right]\right\} \quad \text{(B.6)}$$

where k and m are integers, $int\left(\frac{N-m}{k}\right)$ means the integer part of the number, k indicates the discrete time interval between points, whereas $m = 1, 2, \ldots, k$ represents the initial time value. The length of each new time series can be defined as follows:

$$L(m,k) = \frac{1}{k}\left(\sum_{i=1}^{int(\frac{N-m}{k})} | x[m+ik] - x[m+(i-1)\times k] |\right) \times \left[\frac{N-1}{\left(int\left(\frac{N-m}{k}\right)\times k\right)}\right], \quad \text{(B.7)}$$

Where N is length of the original time series X, and $[\frac{N-1}{(int\left(\frac{N-m}{k}\right)\times k)}]$ is a normalization factor as the number of terms in a k-series varies and normalization must be used.

Then, the length of the curve for the time interval k is defined as the average of the k values $L(m,k)$, for $m = 1, 2, \ldots, k$:

$$L(k) = \frac{1}{k}\left(\sum_{m=1}^{k} L(m,k)\right) \quad \text{(B.8)}$$

Finally, when $L(k)$ is plotted against $1/k$ on a double logarithmic scale, with $k = 1, 2, \ldots, kmax$, the data should fall on a straight line, with a slope equal to the FD of X. Thus, HFD is defined as the slope of the line that fits the pairs $\{ln[L(k)], ln(1/k)\}$ in a least-squares sense. In order to choose an appropriate value of the parameter $kmax$, HFD values were plotted against a range of $kmax$. The point at which the FD plateaus is considered a saturation point; that should be selected as the $kmax$ value. A value of $kmax$ = 8 was chosen for our study (the minimum value of k starts from 2).

B.3 Entropy-Based Fractal Dimensions

Entropy can be defined as the amount of information needed to specify the state of a system to a resolution of r. Entropy is known as the measure of disorder in physical systems, or the amount of information that may be gained by observations of disordered systems [115]. Entropy-based fractal dimensions differ significantly from the

morphological dimensions since they can deal with non-uniform distributions in the fractals. This is understandable because the morphological dimensions are purely metric and not following probabilistic concepts. The information dimension (ID) and correlation dimension (CD) are special cases related to generalized entropy concept as introduced by Alfred Renyi in 1955 [116]. Both dimensions are improvements of the geometric definition of covering a fractal object by N_k volume elements (vels) with a diameter or radius r_k (which k shows the order of covering).

B.3.1 Information Dimension (ID)

The simplest entropy-based fractal dimension is related to the first-order Shannon entropy [117]. Let's consider an arbitrary fractal that is covered by N_k vels, each with a diameter r_k at the k^{th} covering. The estimation of the information dimension, considers the density of the fractal, as determined from the relative frequency of occurrence of the fractal in each intersecting vel. If n_{jk} is the frequency with which the fractal enters (intersects) the j^{th} vel of size r_k in the k^{th} covering, then its ratio to the total number of intersects, N_{Tk} , of the fractal with all the vels is an estimate of the probability of the fractal, p_{jk} , within the j^{th} vel, and is given by:

$$p_{jk} = \lim_{k\to\infty} \frac{n_{jk}}{N_{Tk}}, \tag{B.9}$$

where

$$N_{Tk} = \sum_{j=1}^{N_k} n_{jk} \tag{B.10}$$

With this probability distribution at the *k*th covering (counted through the box-counting method [111], the average (expected) self-information (i.e., $I_{jk} = log\ (1 / p_{jk})$) of the fractal contained in the N_{1k} vels can be expressed by the Shannon entropy H_{1k} given as:

$$H_{1k} = \sum_{j=1}^{N_k} p_{jk} I_{jk} = -\sum_{j=1}^{N_k} p_{jk}\, log(p_{jk}) \quad \text{(B.11)}$$

Notice that the subscript H_{1k} denotes that the Shannon entropy is of the first order which assumes independence between all the vels. If the following power-law relationship holds:

$$C^{H_{1k}} \sim (\frac{1}{r_k})^{D_1}, \quad \text{(B.12)}$$

where C is a constant, then the information fractal dimension is

$$D_I = \lim_{k\to\infty} \frac{H_{1k}}{\log(1/r_k)}, \quad \text{(B.13a)}$$

or

$$D_I = \lim_{r\to 0} \frac{H_{1r}}{\log(1/r)} \quad \text{(B.13b)}$$

D_I can be obtained from the slope of a log-log plot of Shannon's entropy H_{1k} versus precision $(1/r_k)$.

B.3.2 Correlation Dimension (CD)

The information dimension reveals the expected spread in the non-uniform probability distribution of the fractal, but not its correlation. The correlation fractal dimension was introduced to address this problem. Let's consider a setting identical to that required to define the information dimension, *ID*. If the following power-law relationship holds:

$$(\sum_{j=1}^{N_k} p_{jk}^2)^{-1} \sim (\frac{1}{r_k})^{D_c}, \quad \text{(B.14)}$$

then the correlation dimension is

$$D_C = \lim_{k\to\infty} \frac{-\log \sum_{j=1}^{N_k} p_{jk}^2}{\log(1/r_k)}, \quad \text{(B.15a)}$$

or

$$D_C = \lim_{k\to\infty} \frac{\log \sum_{j=1}^{N_k} p_{jk}^2}{\log(r_k)} \quad \text{(B.15b)}$$

D_C can be obtained from the slope of a log-log plot of the second-order entropy H_2 versus precision $(1/r_k)$ and called as *CD*. It is clear that the numerator is different from the Shannon first-order entropy in the information dimension. It can be shown that it has the meaning of a correlation between pairs of neighboring points in the fractal. This correlation can be expressed in terms of a density-density correlation (or pair correlation) function. It is also known as the correlation sum, or correlation integral. This interpretation can lead to a very fast algorithm for computing the correlation dimension [76, 118]. There are numerous examples in the literature for computing the correlation dimension of natural fractal objects. Correlation dimension is, in fact, the information dimension between the pairs of points which the distance of each pair of points is less than a resolution (the diameter of a vel in a k^{th} covering). Both ID and CD represent a weighted average measure of the actual distribution of self-information over the fractal in each cover.

Appendix C. Linear and Quadratic Discriminant Analysis

Linear Discriminant analysis (LDA) is a standard classification method originally developed in 1936 by R. A. Fisher. It is simple, mathematically robust, and often produces results whose accuracy is as good as more complex methods especially when dealing with low dimensional data. LDA separates data of different classes based on the assumption that the data are from normal distribution with equal covariance matrices. Having x as the feature vector and c_j as j classes, according to Bayes rule x is assigned to a class in which it has the highest posterior probability. This criteria results as following:

$$\text{Max Pr}(c_j|x) = argmax_j\left[x^T\sum_j^{-1}\mu_j + c\right], \quad (4.6)$$

where $\text{Pr}(c_j|x)$ is the posterior probability, μ_j is the mean vector, and $\sum_j$ is the covariance matrix of vector x. c is a constant in the above formula. In a two class problem, this results in a decision boundary that maximizes the distance between the two classes' means and minimizes the variance of within classes [63].

Quadratic Discriminant analysis (QDA) is a generalization of LDA in terms of covariance matrices of classes. In QDA, the LDA assumption changes to data of classes

with normal distribution but with different covariance matrices; hence the covariance matrix needs to be estimated for every class and the decision boundary will be a quadratic function. The classifier formula is as follows,

$$\text{Max Pr}(c_j|x) = argmax_j \left[-\frac{1}{2}x^T\sum_j^{-1}x + x^T\sum_j^{-1}\mu_j + c\right] \quad (4.7)$$

In general, QDA tends to fit the data better than LDA as it allows for more flexibility for the covariance matrix. However, it has more parameters to estimate, and it may over fit the data in a small sample set.

Appendix D. Publications

List of publications by candidate:

Published Journal Papers:

1. **Dastgheib Z.**, Lithgow B, Blakley B and Moussavi Z, Application of Vestibular Spontaneous Response as a Diagnostic Aid for Meniere's Disease, Annals of Biomedical Engineering, Vol. 44(5), Sept 2015.

2. **Dastgheib Z.**, Lithgow B, Blakley B and Moussavi Z, A New Diagnostic Vestibular Evoked Response, Canadian Journal of Otolaryngology - Head & Neck Surgery, Vol. 44(1), No. 14, April 2015.

3. Blakley B, **Dastgheib Z**, Lithgow B and Moussavi Z, Preliminary Report: Neural Firing Patterns Specific for Meniere's Disease, Canadian Journal of Otolaryngology - Head & Neck Surgery, Vol. 43(1), No. 52, 2014.

4. **Dastgheib, Z. A.**, B. Lithgow, and Z. Moussavi. Diagnosis of Parkinson's disease using Electrovestibulography, *J. Medical and Biological Engineering and Computing (MBEC),* Vol. 50, No. 5, PP: 483-91. May 2012.

Published Conference Papers:

1. **Dastgheib, Z.**, Omid Ranjbar Pouya, B. Lithgow., Z. K. Moussavi. Comparison of a new ad-hoc classification method with Support Vector Machine and Ensemble classifiers for the diagnosis of Meniere's disease using EVestG signals, *29'th IEEE Canadian Conference on Electrical and Computer Engineering*, Vancouver, Canada, May 2016.

2. **Dastgheib, Z.**, B. Lithgow., Z. K. Moussavi. Vestibular Spontaneous Response as a Signature for Parkinson's Disease. *34rd Annual International IEEE EMBS Conference of the IEEE Engineering in Medicine and Biology Society*. San Diego, California, USA, 3704-07, Sep 2012.

3. **Dastgheib, Z.**, B. Lithgow., Z. K. Moussavi. Application of Fractal Dimension on Vestibular Response Signals for Diagnosis of Parkinson's Disease. *33rd Annual International IEEE EMBS Conference of the IEEE Engineering in Medicine and Biology Society*. Boston, MA, USA, Sep 2011.

References

[1] R. Baloh and V. Honrubia, *Clinical Neurophysiology of the Vestibular System.* Oxford Univ Press, 2001.

[2] I. K. Arenberg, T. J. Balkany, G. Goldman and R. C. Pillsbury, "The incidence and prevalence of Meniere's disease -- a statistical analysis of limits," *Otolaryngol. Clin. North Am.,* vol. 13, pp. 597-601, Nov, 1980.

[3] J. Stahle, U. Friberg and A. Svedberg, "Long-term progression of Meniere's disease," *Acta Otolaryngol.,* vol. 111, pp. 78-83, 1991.

[4] F. Cunha, F. A. Settanni and F. F. Gananca, "What is the effect of dizziness on the quality of life for patients with Meniere's disease?" *Rev. Laryngol. Otol. Rhinol. (Bord),* vol. 126, pp. 155-158, 2005.

[5] J. P. Anderson and J. P. Harris, "Impact of Meniere's disease on quality of life," *Otology & Neurotology,* vol. 22, pp. 888-894, 2001.

[6] A. H. Söderman, D. Bagger-Sjöbäck, J. Bergenius and A. Langius, "Factors influencing quality of life in patients with Meniere's disease, identified by a multidimensional approach," *Otology & Neurotology,* vol. 23, pp. 941-948, 2002.

[7] A. Vassiliou, P. V. Vlastarakos, P. Maragoudakis, D. Candiloros and T. P. Nikolopoulos, "Meniere's disease: Still a mystery disease with difficult differential diagnosis," *Ann. Indian. Acad. Neurol.,* vol. 14, pp. 12-18, Jan, 2011.

[8] S. J. Herdman, *Vestibular Rehabilitation.* FA Davis, 2007.

[9] P. W. Flint, *Cummings Otolaryngology Head and Neck Surgery.* London: Mosby, 2010.

[10] A. Garrett, D. Heibert and B. Lithgow, "Electrovestibulography: The" DC" potential used to separate meniere's disease and benign paroxysmal positional vertigo," in *Proc. IEEE EMBS,* 2007, pp. 2381-2384.

[11] B. Lithgow, "A methodology for detecting field potentials from the external ear canal: NEER and EVestG," *Ann. Biomed. Eng.,* vol. 40, pp. 1835-1850, 2012.

[12] C. A. Birch, "Meniere's disease. Prosper Meniere (1799-1862)," *Practitioner,* vol. 213, pp. 391-392, Sep, 1974.

[13] T. L. Thompson and R. Amedee, "Vertigo: a review of common peripheral and central vestibular disorders," *The Ochsner Journal,* vol. 9, pp. 20-26, 2009.

[14] R. H. Margolis and G. L. Saly, "Asymmetric hearing loss: definition, validation, and prevalence," *Otol. Neurotol.,* vol. 29, pp. 422-431, Jun, 2008.

[15] T. C. Hain, "*Etiology (cause) of Menieres Syndrome*," [Online]. Available: http://www.dizziness-and-balance.com/disorders/menieres/men_eti.html;.

[16] S. D. Rauch, S. N. Merchant and B. A. Thedinger, "Meniere's Syndrome and Endolymphatic Hydrops Double-Blind Temporal Bone Study," *Annals of Otology, Rhinology & Laryngology,* vol. 98, pp. 873-883, 1989.

[17] S. N. Merchant, J. C. Adams and J. B. Nadol Jr, "Pathophysiology of Meniere's syndrome: are symptoms caused by endolymphatic hydrops?" *Otology & Neurotology,* vol. 26, pp. 74-81, 2005.

[18] J. E. Hall, *Guyton and Hall Textbook of Medical Physiology*. Elsevier Health Sciences, 2010.

[19] P. Bach-y-Rita, *The Control of Eye Movements.* Elsevier, 2012.

[20] S. S. Kenneth and M. Carol, *Anatomy and Physiology: The Unity of Form and Function.* McGraw-Hill. Boston, Massachusetts, USA, 1998.

[21] V. J. Wilson and G. Melvill Jones, *Mammalian Vestibular Physiology.* Plenum Press, 1979.

[22] H. O. Barber and C. W. Stockwell, *Manual of Electronystagmography.* CV Mosby Company, 1976.

[23] D. Purves, G. J. Augustine, D. Fitzpatrick, L. C. Katz, A. Lamantia, J. O. McNamara and S. M. Williams, *Neuroscience.* Sunderland: Sinauer, 2001.

[24] J. M. Goldberg and C. Fernandez, "Physiology of peripheral neurons innervating semicircular canals of the squirrel monkey. I. Resting discharge and response to constant angular accelerations," *J. Neurophysiol.,* vol. 34, pp. 635-660, Jul, 1971.

[25] A. Brodal, *The Vestibular Nuclei and their Connections: Anatomy and Functional Correlations.* Oliver and Boyd, 1962.

[26] A. Brodal, *Neurological Anatomy in Relation to Clinical Medicine.* Oxford University Press, USA, 1981.

[27] D. Froehling, M. Silverstein, D. Mohr, C. Beatty, K. Offord and D. Ballard, "Benign positional vertigo: Incidence and prognosis in a population-based study in olmsted county, minnesota," in *Mayo Clinic Proceedings*, 1991, pp. 596-601.

[28] M. Fetter and F. Sievering, "Three-dimensional eye movement analysis in benign paroxysmal positioning vertigo and nystagmus," *Acta Otolaryngol.*, vol. 115, pp. 353-357, May, 1995.

[29] A. Ishiyama, K. M. Jacobson and R. W. Baloh, "Migraine and benign positional vertigo," *Ann. Otol. Rhinol. Laryngol.*, vol. 109, pp. 377-380, Apr, 2000.

[30] M. R. Dix and C. S. Hallpike, "The pathology symptomatology and diagnosis of certain common disorders of the vestibular system," *Proc. R. Soc. Med.*, vol. 45, pp. 341-354, Jun, 1952.

[31] M. Fetter and J. Dichgans, "Vestibular neuritis spares the inferior division of the vestibular nerve," *Brain*, vol. 119, pp. 755-764, 1996.

[32] W. Buchele and T. Brandt, "Vestibular neuritis--a horizontal semicircular canal paresis?" *Adv. Otorhinolaryngol.*, vol. 42, pp. 157-161, 1988.

[33] R. C. Dedhia, "Epidemiology of Ménière's Disease," *Meniere's Disease: Evidence and Outcomes*, pp. 7-12, 2010.

[34] T. J. Balkany, B. Sires and I. K. Arenberg, "Bilateral aspects of Meniere's disease: an underestimated clinical entity," *Otolaryngol. Clin. North Am.*, vol. 13, pp. 603-609, Nov, 1980.

[35] A. Tumarkin, "The Otolithic Catastrophe: a New Syndrome," *Br. Med. J.*, vol. 2, pp. 175-177, Jul 25, 1936.

[36] T. Brandt, *Vertigo: Its Multisensory Syndromes*. Springer Science & Business Media, 1999.

[37] B. F. Mccabe and J. H. Ryu, "Experiments on vestibular compensation." *Laryngoscope*, vol. 79, pp. 1728-1736, 1969.

[38] B. McCabe, "Vestibular physiology in understanding the dizzy patient," *J. Otolaryngol. Soc. Aust.*, vol. 3, pp. 388-392, 1972.

[39] S. S. da Costa, L. C. de Sousa and M. R. Piza, "Meniere's disease: overview, epidemiology, and natural history," *Otolaryngol. Clin. North Am.*, vol. 35, pp. 455-495, 2002.

[40] M. Brenner, D. L. Hoistad and T. C. Hain, "Prevalence of thyroid dysfunction in patients with Meniere's disease," *Archives of Otolaryngology–Head & Neck Surgery,* vol. 130, pp. 226-228, 2004.

[41] T. C. Hain, "*Meniere's Disease*," [Online]. Available: http://www.dizziness-and-balance.com/disorders/menieres/menieres.html.

[42] E. M. Monsell, T. A. Balkany, G. A. Gates, R. A. Goldenberg, W. L. Meyerhoff and J. W. House, "Committee on Hearing and Equilibrium guidelines for the diagnosis and evaluation of therapy in Meniere's disease*," *Otolaryngology-Head and Neck Surgery,* vol. 113, pp. 181-185, 1995.

[43] S. A. Bhansali and V. Honrubia, "Current status of electronystagmography testing," *Otolaryngology-Head and Neck Surgery,* vol. 120, pp. 419-426, 1999.

[44] T. Brandt and M. Strupp, "General vestibular testing," *Clinical Neurophysiology,* vol. 116, pp. 406-426, 2005.

[45] T. D. Fife, R. J. Tusa, J. M. Furman, D. S. Zee, E. Frohman, R. W. Baloh, T. Hain, J. Goebel, J. Demer and L. Eviatar, "Assessment: vestibular testing techniques in adults and children: report of the Therapeutics and Technology Assessment Subcommittee of the American Academy of Neurology," *Neurology,* vol. 55, pp. 1431-1441, 2000.

[46] S. Aoki, Y. Arai, K. Yoda and S. Nishida, "A head-tilt caloric test for evaluating the vertical semicircular canal function," *Acta Otolaryngol.,* vol. 129, pp. 1226-1231, 2009.

[47] A. Baertschi, R. Johnson and G. Hanna, "A theoretical and experimental determination of vestibular dynamics in caloric stimulation," *Biol. Cybern.,* vol. 20, pp. 175-186, 1975.

[48] R. W. Baloh, A. W. Sills and V. Honrubia, "Impulsive and sinusoidal rotatory testing: a comparison with results of caloric testing," *Laryngoscope,* vol. 89, pp. 646-654, 1979.

[49] R. Baloh, K. Hess, V. Honrubia and R. Yee, "Rotational testing in patients with bilateral peripheral vestibular disease," *Laryngoscope,* vol. 95, pp. 85-88, 1985.

[50] G. Grossman, R. Leigh, L. Abel, D. Lanska and S. Thurston, "Frequency and velocity of rotational head perturbations during locomotion," *Experimental Brain Research,* vol. 70, pp. 470-476, 1988.

[51] J. A. Ferraro, "Electrocochleography: a review of recording approaches, clinical applications, and new findings in adults and children," *J. Am. Acad. Audiol.,* vol. 21, pp. 145-152, 2010.

[52] J. Ferraro, L. G. Best and I. K. Arenberg, "The use of electrocochleography in the diagnosis, assessment, and monitoring of endolymphatic hydrops," *Otolaryngol. Clin. North Am.,* vol. 16, pp. 69-82, Feb, 1983.

[53] R. H. Margolis, S. C. Levine, E. M. Foamier, L. L. Hunter, S. L. Smith and D. J. Lilly, "Tympanic electrocochleography: normal and abnormal patterns of response," *International Journal of Audiology,* vol. 31, pp. 8-24, 1992.

[54] J. W. Hall, *Handbook of Auditory Evoked Responses.* Allyn & Bacon, 1992.

[55] J. A. Ferraro and J. D. Durrant, "Electrocochleography in the evaluation of patients with Meniere's disease/endolymphatic hydrops," *J. Am. Acad. Audiol.,* vol. 17, pp. 45-68, 2006.

[56] H. H. Kim, A. Kumar, R. A. Battista and R. J. Wiet, "Electrocochleography in patients with Meniere's disease," *Am. J. Otolaryngol.,* vol. 26, pp. 128-131, 2005.

[57] W. Chung, D. Cho, J. Choi and S. H. Hong, "Clinical usefulness of extratympanic electrocochleography in the diagnosis of Meniere's disease," *Otology & Neurotology,* vol. 25, pp. 144-149, 2004.

[58] B. J. Lithgow, "A neural response system," WO2008144840 A1, Dec 4, 2008.

[59] Z. Dastgheib, B. Lithgow and Z. Moussavi, "Diagnosis of Parkinson's disease using electrovestibulography," *Med. Biol. Eng. Comput.,* vol. 50, pp. 483-491, 2012.

[60] B. J. Lithgow, A. L. Garrett, Z. M. Moussavi, C. Gurvich, J. Kulkarni, J. J. Maller and P. B. Fitzgerald, "Major depression and electrovestibulography," *The World Journal of Biological Psychiatry,* pp. 1-17, 2015.

[61] B. J. Lithgow, A. Garrett and D. Heibert, "EVestG™: A measure for meniere's disease," in *Proc. IEEE EMBS,* 2008, pp. 4162-4165.

[62] P. Baldi and S. Brunak, *Bioinformatics: The Machine Learning Approach.* MIT Press, 2001.

[63] R. O. Duda, P. E. Hart and D. G. Stork, *Pattern Classification.* Wiley-Interscience, 2001.

[64] G. Kaur and K. Mahajan, "A Review on Classifiers to Detect Heart Disease," *International Journal of Advances in Science and Technology (IJAST),* vol. 2, 2014.

[65] D. J. Wilkinson, "Stochastic modelling for quantitative description of heterogeneous biological systems," *Nature Reviews Genetics,* vol. 10, pp. 122-133, 2009.

[66] M. Saar-Tsechansky and F. Provost, "Handling missing values when applying classification models," 2007.

[67] C. Setz, J. Schumm, C. Lorenz, B. Arnrich and G. Tröster, "Using ensemble classifier systems for handling missing data in emotion recognition from physiology: One step

towards a practical system," in *3rd International Conference on Affective Computing and Intelligent Interaction and Workshops (ACII)*, 2009, pp. 1-8.

[68] R. Polikar, "Ensemble based systems in decision making," *Circuits and Systems Magazine, IEEE*, vol. 6, pp. 21-45, 2006.

[69] T. C. Hain, "Neurophysiology of Vestibular Compensation," [Online]. Available: http://www.dizziness-and-balance.com/disorders/menieres/menieres.html.

[70] Wikipedia contributors, "*Inner ear*," 21 August 2015, [Online]. Available: https://en.wikipedia.org/w/index.php?title=Inner_ear&oldid=677128382;.

[71] Wikipedia contributors, "Otolithic membrane," 15 February 2011, [online]' Available: https://en.wikipedia.org/wiki/Otolithic_membrane.

[72] C. L. Kumaragamage, "Development and Validation of a Low Noise Signal Acquisition Protocol for Inner Ear Evoked Potentials," M.S. thesis, Biomedical Engineering Program, Univ. of Manitoba, Winnipeg, Manitoba, Canada, 2013.

[73] R. B. Northrop, *Noninvasive Instrumentation and Measurement in Medical Diagnosis.* CRC press, 2001.

[74] Z. S. Nasreddine, N. A. Phillips, V. Bédirian, S. Charbonneau, V. Whitehead, I. Collin, J. L. Cummings and H. Chertkow, "The Montreal Cognitive Assessment, MoCA: a brief screening tool for mild cognitive impairment," *J. Am. Geriatr. Soc.*, vol. 53, pp. 695-699, 2005.

[75] S. A. Montgomery and M. Asberg, "A new depression scale designed to be sensitive to change," *Br. J. Psychiatry*, vol. 134, pp. 382-389, Apr, 1979.

[76] T. Ehtiati, W. Kinsner and Z. Moussavi, "Multifractal characterization of the electromyogram signals in presence of fatigue," in *IEEE Canadian Conference on Electrical and Computer Engineering*, 1998, pp. 866-869.

[77] J. Gnitecki, Z. Moussavi and H. Pasterkamp, "Classification of lung sounds during bronchial provocation using waveform fractal dimensions," in *26th Annual International Conference of the IEEE in Engineering in Medicine and Biology Society (IEMBS)*, 2004, pp. 3844-3847.

[78] T. Higuchi, "Approach to an irregular time series on the basis of the fractal theory," *Physica D*, vol. 31, pp. 277-283, 1988.

[79] W. Kinsner, "A unified approach to fractal dimensions," in *Fourth IEEE Conference on Cognitive Informatics (ICCI)*, 2005, pp. 58-72.

[80] R. Kohavi and G. H. John, "Wrappers for feature subset selection," *Artif. Intell.*, vol. 97, pp. 273-324, 1997.

[81] P. Langley, "Selection of relevant features in machine learning," Defense Technical Information Center, New Orleans, LA., 1994.

[82] J. Cheng and R. Greiner, "Comparing bayesian network classifiers," in *Proceedings of the Fifteenth Conference on Uncertainty in Artificial Intelligence*, 1999, pp. 101-108.

[83] T. R. Golub, D. K. Slonim, P. Tamayo, C. Huard, M. Gaasenbeek, J. P. Mesirov, H. Coller, M. L. Loh, J. R. Downing, M. A. Caligiuri, C. D. Bloomfield and E. S. Lander, "Molecular classification of cancer: class discovery and class prediction by gene expression monitoring," *Science*, vol. 286, pp. 531-537, Oct 15, 1999.

[84] F. Model, P. Adorjan, A. Olek and C. Piepenbrock, "Feature selection for DNA methylation based cancer classification," *Bioinformatics*, vol. 17, pp. 157-64, 2001.

[85] C. H. Ding, "Analysis of gene expression profiles: Class discovery and leaf ordering," in *Proceedings of the Sixth Annual International Conference on Computational Biology*, 2002, pp. 127-136.

[86] K. J. Cherkauer and J. W. Shavlik, "Protein structure prediction: Selecting salient features from large candidate pools." in *Proc. ISMB-93*, 1993, pp. 74-82.

[87] H. Peng, F. Long and C. Ding, "Feature selection based on mutual information criteria of max-dependency, max-relevance, and min-redundancy," *Pattern Analysis and Machine Intelligence, IEEE Transactions On*, vol. 27, pp. 1226-1238, 2005.

[88] H. W. Lilliefors, "On the Kolmogorov-Smirnov test for normality with mean and variance unknown," *Journal of the American Statistical Association*, vol. 62, pp. 399-402, 1967.

[89] R. V. Hogg and J. Ledolter, *Engineering Statistics.* Macmillan Pub Co., 1987.

[90] G. D. Tourassi, E. D. Frederick, M. K. Markey and C. E. Floyd Jr, "Application of the mutual information criterion for feature selection in computer-aided diagnosis," *Med. Phys.*, vol. 28, pp. 2394-2402, 2001.

[91] C. Ding and H. Peng, "Minimum redundancy feature selection from microarray gene expression data," *Journal of Bioinformatics and Computational Biology*, vol. 3, pp. 185-205, 2005.

[92] L. Breiman, "Bagging predictors," *Mach. Learning*, vol. 24, pp. 123-140, 1996.

[93] L. Breiman, "Random forests," *Mach. Learning*, vol. 45, pp. 5-32, 2001.

[94] Y. Freund and R. E. Schapire, "A decision-theoretic generalization of on-line learning and an application to boosting," *Journal of Computer and System Sciences,* vol. 55, pp. 119-139, 1997.

[95] J. Friedman, T. Hastie and R. Tibshirani, "Additive logistic regression: a statistical view of boosting (with discussion and a rejoinder by the authors)," *The Annals of Statistics,* vol. 28, pp. 337-407, 2000.

[96] J. H. Friedman, "Greedy function approximation: a gradient boosting machine," *Annals of Statistics,* pp. 1189-1232, 2001.

[97] G. I. Webb, "Multiboosting: A technique for combining boosting and wagging," *Mach. Learning,* vol. 40, pp. 159-196, 2000.

[98] T. K. Ho, "The random subspace method for constructing decision forests," *Pattern Analysis and Machine Intelligence, IEEE Transactions On,* vol. 20, pp. 832-844, 1998.

[99] X. Wu, V. Kumar, J. R. Quinlan, J. Ghosh, Q. Yang, H. Motoda, G. J. McLachlan, A. Ng, B. Liu and S. Y. Philip, "Top 10 algorithms in data mining," *Knowledge and Information Systems,* vol. 14, pp. 1-37, 2008.

[100] D. Brown, Y. Chihara and Y. Wang, "Changes in utricular function during artificial endolymph injections in guinea pigs," *Hear. Res.,* vol. 304, pp. 70-76, 2013.

[101] Y. Chihara, V. Wang and D. J. Brown, "Evidence for the utricular origin of the vestibular short-latency-evoked potential (VsEP) to bone-conducted vibration in guinea pig," *Experimental Brain Research,* vol. 229, pp. 157-170, 2013.

[102] D. Heibert, B. Lithgow and K. Hourigan, "Computer models of the vestibular head tilt response, and their relationship to EVestG and Meniere's disease," *World Acad. of Sci. , Eng. and Tech.,* vol. 41, pp. 942-955, 2010.

[103] C. A. Smith, H. Davis, B. H. Deatherage and C. F. Gessert, "DC potentials of the membranous labyrinth," *Am. J. Physiol.,* vol. 193, pp. 203-206, 1958.

[104] T. G. Dietterich, "An experimental comparison of three methods for constructing ensembles of decision trees: Bagging, boosting, and randomization," *Mach. Learning,* vol. 40, pp. 139-157, 2000.

[105] P. Melville, N. Shah, L. Mihalkova and R. J. Mooney, "Experiments on ensembles with missing and noisy data," in *Proc. Fifth Int'l Workshop Multiple Classifier Systems,* 2004, pp. 293-302.

[106] I. Gokcen and J. Peng, "Comparing linear discriminant analysis and support vector machines," in *International Conference on Advances in Information Systems,* 2002, pp. 104-113.

[107] H. S. Cohen and K. T. Kimball, "Development of the vestibular disorders activities of daily living scale," *Archives of Otolaryngology–Head & Neck Surgery,* vol. 126, pp. 881-887, 2000.

[108] J. Theiler, "Estimating fractal dimension," *JOSA A,* vol. 7, pp. 1055-1073, 1990.

[109] B. B. Mandelbrot, *The Fractal Geometry of Nature.* Macmillan, 1983.

[110] R. L. Devaney, P. B. Siegel, A. J. Mallinckrodt and S. McKay, *A First Course in Chaotic Dynamical Systems: Theory and Experiment.* MA: Addison-Wesley, 1993.

[111] W. Kinsner, "A unified approach to fractal and multifractal dimensions," *Winnipeg, Manitoba, Canada DEL94-4: University of Manitoba,* Technical Report, 1994.

[112] W. Sun, G. Xu, P. Gong and S. Liang, "Fractal analysis of remotely sensed images: A review of methods and applications," *Int. J. Remote Sens.,* vol. 27, pp. 4963-4990, 2006.

[113] W. Kinsner, "Complexity and its measures in cognitive and other complex systems," in *Cognitive Informatics, 2008. ICCI 2008. 7th IEEE International Conference On,* 2008, pp. 13-29.

[114] C. Gómez, Á Mediavilla, R. Hornero, D. Abásolo and A. Fernández, "Use of the Higuchi's fractal dimension for the analysis of MEG recordings from Alzheimer's disease patients," *Med. Eng. Phys.,* vol. 31, pp. 306-313, 2009.

[115] K. Kith, O. Sourina, V. Kulish and N. M. Khoa, "An algorithm for fractal dimension calculation based on Rényi entropy for short time signal analysis," in *7th International Conference on Information, Communications and Signal Processing (ICICS),* 2009, pp. 1-5.

[116] A. Rényi, "On a new axiomatic theory of probability," *Acta Mathematica Hungarica,* vol. 6, pp. 285-335, 1955.

[117] C. E. Shannon and W. Weaver, *The Mathematical Theory of Communication.* University of Illinois Press, 1959.

[118] P. Grassberger and I. Procaccia, "Estimation of the Kolmogorov entropy from a chaotic signal," *Physical Review A,* vol. 28, pp. 2591, 1983.